AD_____

Award Number:

W81XWH-06-1-0148

TITLE:

Enhancing tumor drug delivery by laser-activated vascular barrier disruption

PRINCIPAL INVESTIGATOR:

Bin Chen, Ph.D.

CONTRACTING ORGANIZATION:

University of the Sciences in Philadelphia
Philadelphia, PA 19104

REPORT DATE:

Dec 2009

TYPE OF REPORT:

Final

PREPARED FOR: U.S. Army Medical Research and Materiel Command
Fort Detrick, Maryland 21702-5012

DISTRIBUTION STATEMENT:

X Approved for public release; distribution unlimited

REPORT DOCUMENTATION PAGE

Form Approved
OMB No. 0704-0188

1. REPORT DATE *(DD-MM-YYYY)*	**2. REPORT TYPE**	**3. DATES COVERED** *(From - To)*
01-12-2009	Final	30 NOV 2005 - 29 NOV 2009

4. TITLE AND SUBTITLE
Enhancing tumor drug delivery by laser-activated vascular barrier disruption

5a. CONTRACT NUMBER

5b. GRANT NUMBER
W81XWH-06-1-0148

5c. PROGRAM ELEMENT NUMBER

6. AUTHOR(S)
Bin Chen, Ph.D.; Chong He, Ph.D.

5d. PROJECT NUMBER

5e. TASK NUMBER

5f. WORK UNIT NUMBER

7. PERFORMING ORGANIZATION NAME(S) AND ADDRESS(ES)
University of the Sciences in Philadelphia
Philadelphia, PA 19104

8. PERFORMING ORGANIZATION REPORT NUMBER

9. SPONSORING / MONITORING AGENCY NAME(S) AND ADDRESS(ES)
U.S. Army Medical Research and Material Command
Fort Detrick, Maryland 21702-5012

10. SPONSOR/MONITOR'S ACRONYM(S)

11. SPONSOR/MONITOR'S REPORT NUMBER(S)

12. DISTRIBUTION / AVAILABILITY STATEMENT
Approved for public release; distribution unlimited

13. SUPPLEMENTARY NOTES

14. ABSTRACT
An obstacle to successful cancer drug therapy is the existence of drug delivery barriers, which causes insufficient drug delivery to the tumor tissue. Because of the inadequate drug delivery, the drug dose has to be increased, which leads to normal tissue toxicity. This delivery problem not only limits the clinical application of existing chemotherapeutics, but also decreases the effectiveness of many new drugs under development for prostate cancer. We found that vascular targeting photodynamic therapy (PDT), a modality involving the combination of a photosensitizer and laser light, is able to disrupt tumor vascular barrier, a significant hindrance to drug delivery. Therefore, tumor accumulation of circulating molecules is significantly enhanced, which has been demonstrated by intravital fluorescence microscopy and whole-body fluorescence imaging techniques. Immunofluorescence staining of endothelial cytoskeleton structure further indicates microtubule depolymerization, stress actin fiber formation and intercellular gap formation. Based on these results, we are using this laser-based therapy to enhance anticancer drug effectiveness. PDT is currently in worldwide multicenter clinical trials for the localized prostate cancer therapy. The available results indicate that PDT employing advanced laser fiber technology and sophisticated light dosimetry is able to treat localized prostate cancer in an effective and safe way. The combination of photosensitization with current chemotherapy or other new drug therapies will further improve its treatment for the localized prostate cancer patients that accounts for more than 90% of total prostate cancer population.

15. SUBJECT TERMS
Photodynamic therapy, verteporfin, tumor vascular targeting, vascular permeability, imaging

16. SECURITY CLASSIFICATION OF:			**17. LIMITATION OF ABSTRACT**	**18. NUMBER OF PAGES**	**19a. NAME OF RESPONSIBLE PERSON**
a. REPORT	**b. ABSTRACT**	**c. THIS PAGE**			USAMRMC
U	U	U	UU	93	**19b. TELEPHONE NUMBER** *(include area code)*

Table of Contents

Introduction

An obstacle to successful cancer drug therapy is the existence of drug delivery barriers, which results in insufficient and heterogeneous drug delivery to the tumor tissue. This drug delivery problem not only limits the clinical application of existing chemotherapeutics, but also decreases the effectiveness of many new drugs under development. Photodynamic therapy (PDT), a modality involving the combination of a photosensitizer and laser light, is an established cancer therapy. We have been focusing on studying PDT as a modality for tumor vascular targeting. Our results demonstrate that vascular-targeting PDT can be used to eradicate tumor tissue, and modify vascular barrier function for an enhanced drug delivery as well. This project has studied in detail how vascular photosensitization permeabilizes blood vessels and the influence of photodynamic vascular targeting on tumor vascular function and drug delivery. We used various imaging modalities including both dynamic live animal/cell imaging that is capable of providing longitudinal information in real time and static ex vivo imaging that is able to reveal biological details at high resolution to address these questions. Our study indicates that vascular-targeting PDT can be designed to enhance tumor drug delivery to improve therapeutic outcome.

Body

Task 1. To investigate the molecular mechanisms by which photosensitization disrupts endothelial barrier function (months 1-12).

(a). Assess the correlation between photosensitization-induced microtubule disassembly and increase in endothelial cell permeability. The purpose of this study is to determine the role of microtubules in photosensitization-induced endothelial barrier function alteration (months 1-4).

We have found that microtubules play an important role in photosensitization-induced endothelial morphological and functional changes. These results have been published in *Clinical Cancer Research* 2006, 10: 917-23.

(b). Elucidate the mechanism by which photosensitization-induced microtubule depolymerization triggers endothelial cell morphological and functional changes.

We have investigated the mechanism involved in PDT-induced endothelial cell morphological and functional changes. Our results indicate that multiple factors contribute to endothelial cell function disruption. We have found that verteporfin-PDT induced the formation of reactive oxygen species and the release of calcium. Calcium release has been shown to cause microtubule depolymerization and induce endothelial cell morphological changes. Most importantly, we found that PDT induced dephosphorylation of myosin light chain kinase (MLCK), but caused phosphorylation of myosin light chain (MLC). MLCK dephosphorylation is related to PDT-induced cell death and MLC phosphorylation is responsible for endothelial cell contraction and barrier dysfunction. Combination of PDT and MLCK inhibitor led to an enhanced effect. A manuscript based on these results is attached in the appendix.

Task 2. To determine the functional change and the structural basis of photosensitization-induced vascular barrier compromise (months 1-24)

(a). Intravital microscopic study of photosensitization-induced vascular functional changes.

We have used intravital fluorescence microscopy to continuously monitor tumor blood flow velocity, vessel diameter and vascular permeability in the orthotopic MatLyLu rat prostate tumors after vascular-targeting PDT using three different doses of photosensitizer verteporfin (0.25, 0.5 and 1.0 mg/kg). These results have been published in *Pharmaceutical Research* 2008, 25: 1873-80. Most importantly, we found that effects of PDT on blood perfusion and vascular permeability followed a reverse dose dependence. A higher dose of verteporfin PDT was more effective in inducing perfusion disruption, but less effective in enhancing vascular permeability and macromolecule accumulation. These results indicate that a lower dose of verteporfin PDT is more favorable for enhancing tumor drug delivery.

(b). Assessment of tumor uptake of fluorescence probes with different sizes.

We have used intravital fluorescence microscopy to compare the tumor accumulation of fluorochrome-labeled dextran molecules with molecular weight of 155 and 2000 kDa after three different doses of photosensitizer verteporfin (0.25, 0.5 and 1.0 mg/kg). We found that PDT using verteporfin was more effective in enhancing the tumor accumulation of a lower molecular weight dextran molecule than a higher molecular weight dextran molecule (*Pharmaceutical Research* 2008, 25: 1873-1880).

Since most chemotherapeutic agents tend to be associated with albumin in circulation, we also used a whole body fluorescence imaging system to monitor TRITC-albumin tumor uptake in real time on live animals. We found that vascular leakage of fluorescence-labeled albumin (TRITC-albumin) was significantly increased after the vascular-targeting PDT, as compared to the control tumor. Interestingly, PDT-induced increase in TRITC-albumin accumulation was especially pronounced in the tumor periphery. To further confirm these macroscopic imaging results, we sacrificed animals at various time points and excised tumor tissues for fluorescence microscopic study. Similar to the whole body tumor images, TRITC-albumin was found to have more accumulation in the tumor periphery. These results have been published in the *International Journal of Cancer* 2008, 123: 695-701. An important finding of this study is to demonstrate the disparity in vascular response to PDT between tumor peripheral and interior blood vessels.

(c). Determine blood vessel structural changes induced by photosensitized vascular permeabilization.

We have performed light and electron microscopy to examine vessel structural changes after PDT. At the light microscopy level, we have found that PDT induced vessel dilation and occlusion at early time points after treatment, which progress to severe vessel degeneration and rapture at late times (*International Journal of Cancer* 2008, 123: 695-701). At the electron microscopy level, we found platelet aggregation, thrombus formation and endothelial cell rupture (**Fig 1**). All these findings demonstrate that PDT damages endothelial cells, which induces vascular dysfunction.

We also performed immunohistochemistry to stain vessel endothelial marker CD31, pericyte marker smooth muscle actin and basement membrane marker Type IV collagen. We found that PDT caused a loss of CD31 staining, again suggesting direct endothelial damage. Interestingly, we found that tumor tissues showed spatial variation in the vessel supporting structure. Central blood vessels generally don't have open lumen and have less coverage of vessel supporting structure (see book chapter in the appendix). This might explain the disparity between interior and peripheral vasculature in vascular response to vascular-targeting PDT.

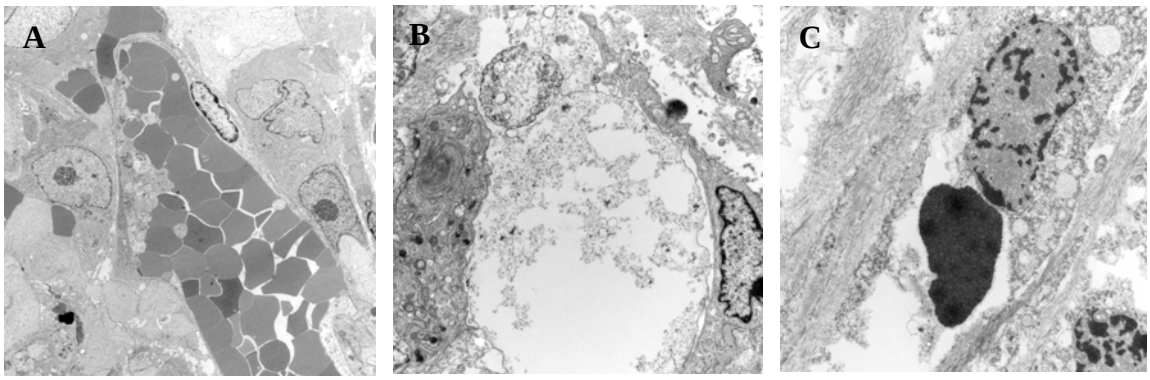

Fig. 1. The electron microscopic photographs showing vascular damage after vascular-targeting PDT. The PC3 human prostate tumors were treated with vascular-targeting PDT (40 J/cm^2 at 15 min after 0.5 mg/kg verteporfin (i.v.)). (A) 1 h after PDT showing platelet aggregation and thrombus formation; (B) 6 h after PDT showing edema, endothelial cell degeneration and vessel rupture; (C) 24 h after PDT showing endothelial cell death, vessel rupture and tumor cell death.

Task 3. To explore the potential of improving tumor drug delivery and therapeutic effect by photosensitized vascular permeabilization (months 25-36).

a. Fluorescence imaging, microscopy & flow cytometry analysis of tumor drug distribution and penetration.

Bevacizumab, a FDA-approved recombinant humanized monoclonal antibody (MW 149 kDa) against VEGF, was used in this study. To visualize the distribution of bevacizumab, we have labeled bevacizumab with Alex Fluor 647 dye using Invitrogen small animal in vivo imaging protein labeling reagents. We found that vascular targeting PDT using verteporfin was able to preferentially enhance the accumulation of bevacizumab at the tumor periphery where tumor recurrence tended to occur. We also found that PDT induced VEGF overexpression at peripheral tumor area. The overexpression of VEGF at tumor periphery might be responsible for peripheral tumor recurrence. Based on these results, we continue to examine the effects of PDT in combination with bevacizumab on tumor regrowth.

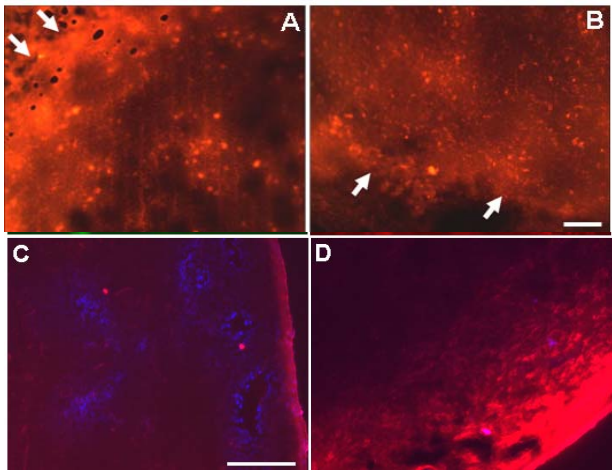

Fig 2 . (A , B) PDT with verteporfin induces VEGF overexpression in tumor peripheral areas. The MatLyLu tumor was treated with verteporfin-PVTT (50 J/cm^2 light treatment at 15 min after 0.25 mg/kg dose of verteporfin). Tumor sections taken at 3 h after treatment were stained for VEGF expression. **(A)** verteporfin-PVTT; **(B)** untreated control. Arrows indicate tumor peripheral areas. Bar, 100 um.

(C, D) Effects of PDT on Alexa 647-bevacizumab distribution. PC-3 tumors were treated with verteporfin-PDT (50 J/cm^2 light treatment at 15 min after 0.5 mg/kg dose of verteporfin). Control tumors received no treatment. Animals were i.v. injected with 50 mg/kg Alexa 647-bevacizumab immediately after treatment. Tumor sections were taken at 24 h after treatments. Red fluorescence shows the distribution of bevacizumab and blue fluorescence indicates functional blood vessels visualized by Hoechst dye. **(C)** Control; **(D)** PDT. Bars, 100 um.

b. Evaluate tumor response following the combination of anticancer agent and verteporfin-photosensitization.

We have evaluated tumor response following the combination of vascular targeting PDT and bevacizumab in the PC-3 human prostate tumor model. As shown in **Fig 3**, the average tumor volume in the group of animals treated with the combination therapy is only about half of the PDT alone group. These results indicate that PDT using verteporfin in combination with bevacizumab leads to an enhanced therapeutic effect.

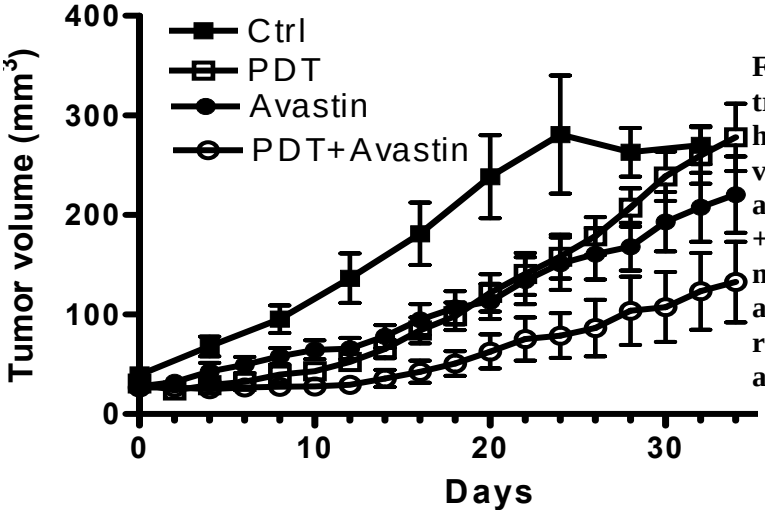

Fig. 3. Tumor regrowth curve after different treatments. For the PDT only group, PC3 human prostate tumors were treated with vascular-targeting PDT (40 J/cm^2 at 15 min after 0.5 mg/kg verteporfin (i.v.)). For the PDT + Ava group, animals were injected with 50 mg/kg Avastin (bevacizumab) immediately after PDT treatment. The control group received no treatment. Each group includes 6-7 animals.

Key research accomplishments

- Photosensitization induces microtubule depolymerization and stress fiber actin formation, leading to endothelial morphological changes and barrier dysfunction.
- Photosensitization induces the formation of reactive oxygen species and calcium release, which induces microtubule depolymerization. Photosensitization causes myosin light chain phosphorylation independent of myosin light chain kinase phosphorylation.
- Vascular-targeting PDT induces time- and dose-dependent decrease in tumor blood flow and increase in vascular permeability.
- PDT-induced vascular barrier dysfunction leads to increased accumulation of circulating molecules in tumor tissues, which can be used to enhance drug delivery to the tumor tissue. Low dose PDT is more effective in enhancing tumor drug delivery than the high dose PDT and PDT-induced drug delivery enhancement is especially pronounced in the tumor periphery.
- PDT is more effective in enhancing the accumulation of macromolecules with a lower molecular weight.
- PDT significantly enhances the distribution of bevacizumab (Avastin) at tumor periphery. Combination of vascular-targeting PDT and antibody drug bevacizumab results in an enhanced anti-tumor effect.

Reportable outcomes

Publications:

Chen B, Pogue BW, Luna J, Hardman R, Hoopes PJ, Hasan T. Tumor vascular permeabilization by vascular-targeting photosensitization: effects, mechanism and therapeutic implications. *Clin Cancer Res.* 2006, 10: 917-23.

Chen B, Pogue BW, Hoopes PJ, Hasan T. Vascular and cellular targeting for photodynamic therapy. *Crit Rev Eukaryot Gene Expr.* 2006, 16: 279-306.

He C, Agharkar P, Chen B. Intravital microscopic analysis of vascular perfusion and macromolecule extravasation after verteporfin-mediated photodynamic therapy. *Pharm Res.* 2008, 25: 1873-80.

Chen B, Crane C, He C, Gondek D, Agharkar P, Savellano M, Hoopes PJ, Pogue BW. Disparity in vascular response to verteporfin-mediated vascular-targeting therapy between prostate tumor interior versus peripheral vasculature. *Int J Cancer.* 2008, 123: 695-701.

He C, Fateye B, Chen B. Combination of vascular targeting PDT with combretastatin A4 phosphate. *Proc of SPIE.* 2009, 7380: 7380321-6.

Agharkar P, Jancina A, Chen B. Myosin light chain kinase as a target of verteporfin-PDT in microvascular endothelial cells.

Book chapter:

Chen B, He C, de Witte P, Hoopes PJ, Hasan T, Pogue BW. "Chapter 9: Vascular Targeting in Photodynamic Therapy" in *Michael R. Hamblin & Pawel Mroz (Editors), Advances in Photodynamic Therapy: Basic, Translational and Clinical, pp 179-91, Norwood, MA: Artech House Inc. 2008.*

Abstracts:

Agharkar P, Chen, B. Elucidating the mechanisms of photodynamic therapy induced endothelial cell morphological and functional change. *The 34th Meeting of the American Society for Photobiology (June 20-25, 2008, Burlingame, CA), page 6.*

He C, Agharkar P, Chen, B. Intravital microscopic analysis of vascular perfusion and macromolecule extravasation after photodynamic vascular targeting therapy. *The 34th Meeting of the American Society for Photobiology (June 20-25, 2008, Burlingame, CA), page 39.*

Chen B, He C, Crane C, Pogue BW. Fluorescence imaging of verteporfin-mediated photodynamic therapy targeting prostate tumor vasculature. *The Department of Defense (DoD) Innovative Minds in Prostate Cancer Today (IMPACT) meeting, Sep 5-8, 2007, Atlanta, Georgia.*

Chen B, He C, Crane C, Pogue BW. Fluorescence imaging of verteporfin-mediated photodynamic therapy targeting prostate tumor vasculature. *Program & Abstracts of 11th World Congress of the International Photodynamic Association (IPA, March 28-31, 2007, Shanghai, China).*

Chen B, Pogue BW, Hoopes PJ, Hasan T. Enhancing tumor drug delivery by laser-activated vascular barrier disruption. *The 11th NCI Prouts Neck Meeting on Prostate Cancer (Nov 2-5, 2006, Prouts Neck, Maine), page 32.*

Chen B, Pogue BW, Hoopes PJ, Hasan T. Photodynamic tumor vascular targeting enhances cancer chemotherapy. *The 90th Optical Society of America (OSA) Annual Meeting (Oct 8-12, 2006, Rochester, NY) Conference Program, page 160.*

Chen B, Pogue BW, Hoopes PJ, Hasan T. Effects and mechanisms of vascular permeabilization by vascular-targeting photodynamic therapy. *Conference Proceedings of the 33rd Meeting of the American Society for Photobiology (Jul 8-12, 2006, Puerto Rico), page 65.*

Conclusions

We have found that photodynamic tumor vascular targeting induced significant vascular morphological and functional changes by targeting endothelial cells. As a result, tumor accumulation of fluorescence molecular probes with different molecular weight is significantly enhanced after photodynamic vascular targeting. The combination of photodynamic tumor vascular targeting and anticancer agent bevacizumab leads to a synergistic therapeutic effect. PDT with appropriate dose can be used to enhance macromolecular anticancer agents to tumor tissues.

Appendices

Chen B, Pogue BW, Luna J, Hardman R, Hoopes PJ, Hasan T. Tumor vascular permeabilization by vascular-targeting photosensitization: effects, mechanism and therapeutic implications. *Clin Cancer Res.* 2006, 10: 917-23.

Chen B, Pogue BW, Hoopes PJ, Hasan T. Vascular and cellular targeting for photodynamic therapy. *Crit Rev Eukaryot Gene Expr.* 2006, 16: 279-306.

He C, Agharkar P, Chen B. Intravital microscopic analysis of vascular perfusion and macromolecule extravasation after verteporfin-mediated photodynamic therapy. *Pharm Res.* 2008, 25: 1873-80.

Chen B, Crane C, He C, Gondek D, Agharkar P, Savellano M, Hoopes PJ, Pogue BW. Disparity in vascular response to verteporfin-mediated vascular-targeting therapy between prostate tumor interior versus peripheral vasculature. *Int J Cancer.* 2008, 123: 695-701.

He C, Fateye B, Chen B. Combination of vascular targeting PDT with combretastatin A4 phosphate. *Proc of*

SPIE. 2009, 7380: 7380321-6.

Agharkar P, Jancina A, Chen B. Myosin light chain kinase as a target of verteporfin-PDT in microvascular endothelial cells.

Chen B, He C, de Witte P, Hoopes PJ, Hasan T, Pogue BW. “Chapter 9: Vascular Targeting in Photodynamic Therapy” in *Michael R. Hamblin & Pawel Mroz (Editors), Advances in Photodynamic Therapy: Basic, Translational and Clinical, pp 179-91, Norwood, MA: Artech House Inc. 2008.*

Tumor Vascular Permeabilization by Vascular-Targeting Photosensitization: Effects, Mechanism, and Therapeutic Implications

Bin Chen,[1,2] Brian W. Pogue,[2,3] Jorge M. Luna,[2] Rulon L. Hardman,[1] P. Jack Hoopes,[1,2] and Tayyaba Hasan[3]

Abstract

Purpose: Loss of vascular barrier function has been observed shortly following vascular-targeting photodynamic therapy. However, the mechanism involved in this event is still not clear, and the therapeutic implications associated with this pathophysiologic change have not been fully explored.

Experimental Design: The effect of vascular-targeting photodynamic therapy on vascular barrier function was examined in both s.c. and orthotopic MatLyLu rat prostate tumor models and endothelial cells *in vitro*, using photosensitizer verteporfin. Vascular permeability to macromolecules (Evans blue-albumin and high molecular weight dextran) was assessed with dye extraction (*ex vivo*) and intravital microscopy (*in vivo*) methods. Intravital microscopy was also used to monitor tumor vascular functional changes after vascular-targeting photodynamic therapy. The effects of photosensitization on monolayer endothelial cell morphology and cytoskeleton structures were studied with immunofluorescence staining.

Results: Vascular-targeting photodynamic therapy induced vascular barrier dysfunction in the MatLyLu tumors. Thus, tumor uptake of macromolecules was significantly increased following photodynamic therapy treatments. In addition to vascular permeability increase, blood cell adherence to vessel wall was observed shortly after treatment, further suggesting the loss of endothelial integrity. Blood cell adhesion led to the formation of thrombi that can occlude blood vessels, causing vascular shutdown. However, viable tumor cells were often detected at tumor periphery after vascular-targeting photodynamic therapy. Endothelial cell barrier dysfunction following photodynamic therapy treatment was also observed *in vitro* by culturing monolayer endothelial cells on Transwell inserts. Immunofluorescence study revealed microtubule depolymerization shortly after photosensitization treatment and stress actin fiber formation thereafter. Consequently, endothelial cells were found to retract, and this endothelial morphologic change led to the formation of intercellular gaps.

Conclusions: Vascular-targeting photodynamic therapy permeabilizes blood vessels through the formation of endothelial intercellular gaps, which are likely induced via endothelial cell microtubule depolymerization following vascular photosensitization. Loss of endothelial barrier function can ultimately lead to tumor vascular shutdown and has significant implications in drug transport and tumor cell metastasis.

Authors' Affiliations: [1]Department of Surgery, Dartmouth Medical School, Lebanon; [2]Thayer School of Engineering, Dartmouth College, Hanover, New Hampshire; and [3]Department of Dermatology, Wellman Center for Photomedicine, Massachusetts General Hospital, Harvard Medical School, Boston, Massachusetts

Received 8/1/05; revised 10/19/05; accepted 11/23/05.

Grant support: National Cancer Institute grant PO1CA84203 and Department of Defense grant W81XWH-04-1-0077.

The costs of publication of this article were defrayed in part by the payment of page charges. This article must therefore be hereby marked *advertisement* in accordance with 18 U.S.C. Section 1734 solely to indicate this fact.

Note: B. Chen is currently at the Department of Pharmaceutical Sciences, Philadelphia College of Pharmacy, University of the Sciences in Philadelphia, 600 South 43rd Street, Philadelphia, PA 19104.

Requests for reprints: Brian W. Pogue, Thayer School of Engineering, 8000, Cummings Hall, Dartmouth College, Hanover, NH 03755. Phone: 215-596-7481; Fax: 215-895-1161; E-mail: pogue@dartmouth.edu.

doi:10.1158/1078-0432.CCR-05-1673

Photodynamic therapy is a modality in which a photosensitizer is administrated systemically or locally and subsequently activated by illumination with visible light, leading to the generation of cytotoxic reactive oxygen species in the presence of oxygen (1). Photodynamic therapy is currently used for the treatment of various types of cancer, including lung, skin, gastrointestinal tract, the head and neck, and urological cancers (2). It has also been used as a treatment for noncancer diseases such as age-related muscular degeneration (AMD), atherosclerosis, and viral or bacterial infections (3).

Verteporfin (the lipid formulation of benzoporphyrin derivative monoacid ring) is a photosensitizer that has been approved for the treatment of AMD (4). Compared with Photofrin (the first photosensitizer with the Food and Drug Administration approval for cancer treatment), the advantages of verteporfin include a strong absorption at longer wavelengths, leading

to deeper tissue penetration and a fast pharmacokinetic behavior *in vivo*, resulting in a reduced skin photosensitivity. Because photosensitizing targets closely depend on the localization of photosensitizers, it is therefore important to determine the temporal and spatial changes of the photosensitizer localization. In the previous studies, we have found that the distribution of verteporfin changes dynamically as a function of time after administration. It is predominantly retained in the tumor vasculature within the first few minutes after i.v. injection (e.g., within 15 minutes) and then systematically extravasates into the tumor interstitial and cellular compartments over longer times (e.g., over a few hours) after administration (5–7). Based on this pharmacokinetic pattern, maximal tumor vascular or cellular targeting can be effectively achieved by illumination at a short or a long time point after drug administration, respectively. Light treatment typically starts at 5 to 15 minutes after administration of verteporfin to selectively target blood vessels. This vascular targeting regimen is currently used for AMD treatment in clinic (4) and experimentally for tumor destruction (5, 6, 8, 9).

Vascular-targeting therapy is a promising strategy in cancer treatment that has received considerable attention in recent years (10, 11). Compared with conventional cancer cell–targeting approaches, targeting tumor vasculature is easier to access, more efficient in cancer cell killing, and has a lower likelihood of developing drug resistance. Although vascular damage has long been known to contribute to the overall photodynamic therapy treatment effect, intentional use of this mechanism based on the photosensitizer pharmacokinetic distribution to maximize clinical effect is a more recent technique, beginning with the implementation of verteporfin for AMD treatment. Following the success of verteporfin, the photodynamic therapy vascular targeting regimen with a short drug-light interval has been used for another photosensitizing agent Tookad, which is currently in clinical trials for prostate cancer treatment (12).

Tumor vasculature is not only a pipeline for the supply of nutrients and removal of metabolic wastes but also a common route for the delivery of anticancer agents to tumor tissues and dissemination of tumor cells to distant organs. The circulatory function of vasculature is largely maintained by the endothelial barrier that tightly controls the substance exchange between blood plasma and interstitial fluids (13). The goal of vascular targeting is to induce vascular shutdown. One of the earliest events following vascular photosensitization is, however, the loss of vascular barrier function (14, 15). Indeed, increase in vascular permeability has been documented after photodynamic therapy treatment with several photosensitizers (14). In AMD patients treated with verteporfin-photodynamic therapy, vascular leakage is observed shortly after treatment and lasts even for days before vessel occlusion (16). Given the critical role of vasculature in tumor cell survival, metastasis, and anticancer drug delivery, it is important to study the effects and mechanisms of verteporfin photosensitization on vascular barrier function. A fundamental understanding of photosensitization-induced vascular permeabilization is necessary for using this modality to target blood vessels for the treatment of cancer, AMD, and other diseases. In this article, we studied tumor vascular barrier function alteration and its mechanisms in response to photodynamic therapy with verteporfin, as used in a vascular-targeting approach.

Materials and Methods

Photosensitizer. Verteporfin (benzoporphyrin derivative in a lipid formulation) was obtained from QLT, Inc., as a gift (Vancouver, Canada). A stock saline solution of verteporfin was reconstituted according to the manufacturer's instructions and stored at 4°C in the dark.

Cell culture. Mouse endothelial cells SVEC4-10 (American Type Culture Collection, Manassas, VA) and R3327-MatLyLu rat prostate cancer cells were maintained in RPMI 1640 with glutamine (Mediatech, Herndon, VA) supplemented with 10% fetal bovine serum (Hyclone, Logan, UT) and 100 units/mL penicillin/streptomycin (Mediatech) at 37°C in a 5% CO_2 incubator.

Animals and tumor model. Male Copenhagen rats (6-8 weeks old) obtained from Charles River Laboratories (Wilmington, MA) were used throughout the study. The R3327-MatLyLu Dunning prostate tumor is an androgen-independent carcinoma, syngeneic to the Copenhagen rats, and highly metastatic to both lymph nodes and lungs (MatLyLu; ref. 17). This Dunning tumor was shown to be similar to human prostate cancer in the response to hormone therapy, chemotherapy, and radiation therapy (18). Cells used in this experiment were no more than 10 passages from the original stock in liquid nitrogen. The s.c. and orthotopic MatLyLu rat prostate cancer models were reproduced as previously described (9). Tumors were used for experiments when reaching a size of 6 to 10 mm in diameter. All animal procedures were done according to a protocol approved by the Dartmouth College Animal Care and Use Committee.

Photodynamic therapy treatments. A diode laser system (Applied Optronics, South Plainfield, NJ) with 690-nm wavelength was used throughout this study for the irradiation of *in vitro* cultured cells and MatLyLu tumors. The light was delivered through an optical fiber (140-μm core diameter). For the *in vitro* study, SVEC4-10 cells were incubated with 200 ng/mL verteporfin for 15 minutes. After removing the drug-containing medium, cells were washed with PBS and exposed to 5 mW/cm^2 intensity of light for 100 or 200 seconds. Light intensity was measured by an optical power meter (Thorlabs, Inc., North Newton, NJ). For photodynamic therapy treatment of MatLyLu tumors, animals were anesthetized with an injection (i.p.) of ketamine (90 mg/kg) and xylazine (9 mg/kg) and placed on a heated blanket throughout the light treatment. The MatLyLu tumors were treated with external light illumination for 1,000 seconds at an incident fluence rate of 50 mW/cm^2. Verteporfin was injected i.v. at a dose of 0.25 mg/kg at 15 minutes or 1.0 mg/kg at 3 hours before light irradiation.

Assessment of vascular permeability to macromolecules in the MatLyLu tumors. Effective vascular permeability in the s.c. MatLyLu tumors was determined as described (19). Immediately after photodynamic therapy treatments (both 15 minutes and 3 hours of drug-light photodynamic therapy), animals were i.v. injected with 10 mg/kg Evans blue (Sigma, St. Louis, MO) and 10 mg/kg FITC-labeled dextran (molecule weight of 2,000 kDa; Sigma). At 0.25, 0.5, 1.0, and 2.0 hours after injection, tumor-bearing animals were euthanized. After systemic perfusion with 50 mL of 0.9% saline to remove macromolecules in the circulation, tumor tissues were excised, minced, and extracted with formamide (1 mL per 100 mg tissue) for 72 hours. The absorbance of Evans blue at 620 nm was measured with a spectrophotometer (Cary 50 Bio, Varian Analytical Instruments, Walnut Creek, CA), and the fluorescence of FITC-dextran was determined with a spectrofluorometer (FluoroMax-3, Jobin Yvon, Inc., Edison, NJ) with 495-nm excitation and 518-nm emission.

Monitoring of tumor vascular function by intravital microscopy. Tumor vascular functional changes induced by vascular-targeting photodynamic therapy regimen (light treatment at 15 minutes after injection of 0.25 mg/kg verteporfin) were examined using a Zeiss fluorescence stereomicroscope (Stemi SV11) in the live animals with orthotopic MatLyLu tumors. Tumor-bearing animals were anesthetized as described above and fixed on the stereomicroscope stage. Orthotopic MatLyLu tumors were surgically exposed and treated with 50 J/cm^2 dose

of light at 15 minutes after i.v. injection of 0.25 mg/kg verteporfin. Immediately after photodynamic therapy treatment, animals were injected with a 2,000-kDa FITC-dextran (10 mg/kg, i.v.). The extravasation of the 2,000-kDa FITC-dextran was imaged using a ×1 objective lens with ×6.6 zoom, and the fluorescence images were captured with an AxioCam CCD camera (Zeiss, Gottingen, Germany) with the filter set of 470 to 490 nm for excitation and 520 to 560 nm for emission. The camera settings were kept constant for the control and photodynamic therapy–treated animals.

To assess the effects of vascular-targeting photodynamic therapy on blood perfusion, rat red blood cells (RBC) were labeled with a fluorescence dye Dil (a carbocyanine dye) as described (20). Briefly, heparinized whole blood was collected from a donor rat. RBCs were isolated from the whole blood by centrifugation and washing with PBS thrice. Then, 1 mL of packed RBCs was incubated with 1 mL of Dil solution (1 mg/mL) at room temperature in dark condition for 30 minutes. After the incubation, RBC suspension was centrifuged and washed with PBS twice to remove the free dye. Then, 200 μL of Dil-labeled RBCs diluted with 800 μL PBS was i.v. injected to the animals before photodynamic therapy treatment. The movement of Dil-labeled RBCs was monitored with the stereomicroscope using a ×1 objective lens plus 6.6 zoom, and the fluorescence images were recorded with the AxioCam CCD camera. The filter set for imaging Dil dye was 530 to 550 nm for excitation and 570 to 610 nm for emission.

Assessment of monolayer endothelial permeability. *In vitro* endothelial permeability was measured by the diffusion of 2,000-kDa FITC-dextran through the endothelial monolayer, as described (21). SVEC-4 endothelial cells were cultured on Transwell inserts (Costar, Cambridge, MA) up to confluence. Cells were incubated with 200 ng/mL verteporfin for 15 minutes and subjected to light treatment (100 or 200 seconds of illumination at 5 mW/cm^2). Immediately after light irradiation, medium containing 1 mg/mL of 2,000-kDa FITC-dextran was loaded on the upper compartment of the Transwell. The amount of FITC-dextran diffused through the endothelial monolayer into the lower compartment was measured by a SynergyHT microplate reader (Bio-Tek Instruments, Winooski, VT) with excitation at 485/20 nm and emission at 525/20 nm.

Immunofluorescence staining of endothelial cytoskeleton. SVEC-4 endothelial cells cultured on glass coverslips were treated with 5 mW/cm^2 light for 200 seconds after incubation with 200 ng/mL verteporfin for 15 minutes. At different time points after treatment, cells were fixed and permeated with cold methanol/acetone (1:1) at −20°C for 30 minutes. Cells were subsequently washed thrice with PBS and blocked for nonspecific binding with 1% bovine serum albumin in PBS for 30 minutes at room temperature. The microtubule was stained with anti-α-tubulin mouse monoclonal antibody (Sigma; 1:500 dilution) for 1 hour at room temperature followed by incubation with Alexa 488–conjugated rabbit anti-mouse secondary antibody (Molecular Probes, Eugene, OR; 1:500 dilution) for 30 minutes. Actin filaments were stained with rhodamine-conjugated phalloidin (Sigma; 1 μg/mL) for 1 hour at room temperature. Cell nulcei were stained with Hoechst dye (Sigma, 5 μmol/L) for 15 minutes. After immunofluorescence staining, cells were imaged with a Zeiss LSM 510 confocal microscopy with appropriate filter setup for different dyes.

Results

Tumor vascular permeability to Evans blue and FITC-dextran (molecular weight, 2,000 kDa) was first assessed in the s.c. MatLyLu tumors. Figure 1 indicates that vascular targeting verteporfin-photodynamic therapy using a 15-minute drug-light interval increases vascular permeability; thus, tumor uptake of macromolecules is significantly increased at 2 hours after injection compared with the control tumor. In contrast, verteporfin-photodynamic therapy using a 3-hour drug-light interval does not significantly increase tumor uptake of the

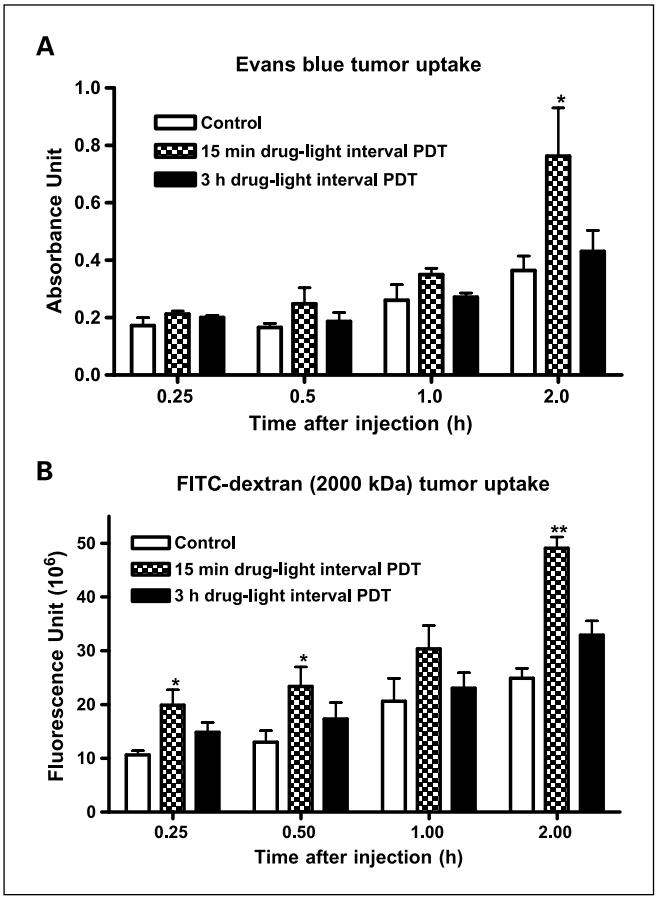

Fig. 1. Verteporfin-photodynamic therapy (*PDT*) increases vascular permeability to macromolecules in the subcutaneous MatLyLu rat prostate tumor model. Tumors were exposed to 50 J/cm^2 dose of light treatment (50 mW/cm^2) at either 15 minutes following 0.25 mg/kg verteporfin injection or 3 hours after 1 mg/kg verteporfin injection. Evans blue (10 mg/kg, *A*) and 2,000-kDa FITC-dextran (10 mg/kg, *B*) were i.v. injected immediately after photodynamic therapy. Tumor uptake of Evans blue and FITC-dextran was measured with spectrophotometry and spectrofluorometry, respectively, at different time points after injection ($n = 3$). *, $P < 0.05$; **, $P < 0.01$, compared with control.

macromolecules. It was noted that vascular-targeting photodynamic therapy could significantly enhance tumor uptake of 2,000-kDa FITC-dextran at 0.25 and 0.5 hour after photodynamic therapy. However, the same treatment was not able to increase Evans blue tumor uptake (Fig. 1).

Vascular permeabilization induced by vascular-targeting photodynamic therapy could also be observed in the orthotopic tumor in real time with intravital microscopy. Immediately after photodynamic therapy treatment, animals were i.v. injected with 2,000-kDa FITC-dextran, and the extravasation of high-molecule dextran was monitored in live animals with a stereo fluorescence microscope. Because blood significantly quenches the fluorescence of FITC through the inner filter effects of hemoglobin (22), only a weak fluorescence signal could be observed within tumor blood vessels (Fig. 2). However, when FITC-dextran leaked out of blood vessels, its fluorescence intensity was greatly enhanced due to the loss of hemoglobin-quenching effect. As shown in Fig. 2, vascular-targeting photodynamic therapy permeabilizes tumor blood vessels, significantly increasing the extravasation of high molecule weight dextran, whereas the leakage of 2,000 kDa

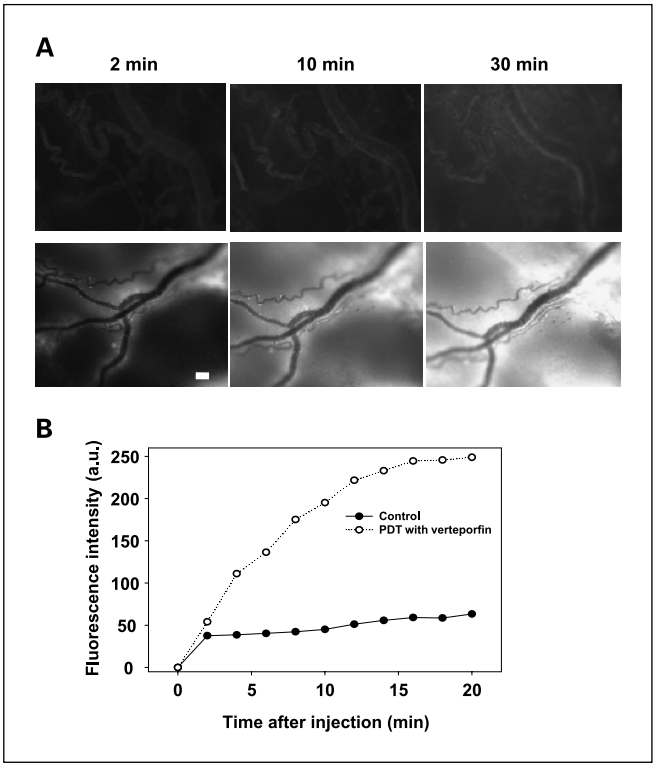

Fig. 2. *A,* intravital microscopic imaging showing the extravasation of 2,000-kDa FITC-dextran out of tumor blood vessels. Orthotopic MatLyLu rat prostate tumors were treated with vascular-targeting photodynamic therapy (*PDT*; i.e., 50 J/cm^2 dose of light; 50 mW/cm^2) at 15 minutes following 0.25 mg/kg verteporfin injection. Control tumors were only injected with 0.25 mg/kg verteporfin without light treatment. Immediately after treatment, animals were injected with 2,000-kDa FITC-dextran (i.v. 10 mg/kg), and tumor blood vessels were imaged with a stereo fluorescence microscope at 2, 10, and 30 minutes thereafter. Top, control tumor; bottom, photodynamic therapy – treated tumor. Bar, 50 μm. *B,* quantitative analysis of 2,000-kDa FITC-dextran extravasation. Total fluorescence intensity was measured with NIH ImageJ software.

in control tumors is limited. Intravital microscope study also revealed the adhesion of fluorescence-labeled RBCs to the vessel wall shortly after vascular-targeting photodynamic therapy (Fig. 3). Blood cell adherence gradually built up and led to the formation of thrombus. Some thrombi were unstable and went into circulation, leaving blood vessels still functional, whereas other thrombi remained at where they were formed and finally occluded the blood vessels. As shown in Fig. 3, an injection of 2,000-kDa FITC-dextran highlights an apparently functional blood vessel at 120 minutes after photodynamic therapy, whereas a nearby vessel occluded by a thrombus showed no fluorescence at all. It is interesting to note that the FITC fluorescence intensity in the blood vessel in this case is much stronger than that in Fig. 2, although the drug dose injected is the same. This might suggest that although still functional at 120 minutes after photodynamic therapy, that blood vessel has low hemoglobin content. A possible explanation for this observation is that photodynamic therapy–induced thrombosis and direct photodynamic damage of RBCs causes some tumor blood vessels flowed with a lower percentage of RBC volume.

Histologic examination of H&E staining tumor sections taken from tumors at 48 hours after vascular-targeting photodynamic therapy indicated extensive vascular disruption and tumor cell death throughout tumor sections (Fig. 4). However, viable tumor cells were commonly detected at tumor periphery. Because of the existence of viable peripheral tumor cells, the vascular-targeting regimen used in this study led to no tumor cure (6).

Endothelial barrier function was also assessed by the diffusion of 2,000-kDa FITC-dextran through the endothelial monolayer cultured on transwell inserts. As shown in Fig. 5, photosensitization with verteporfin (200 ng/mL for 15-minute incubation) significantly increased monolayer endothelial permeability to the macromolecule 2,000-kDa FITC-dextran in a dose-dependent manner, whereas the permeability in the control endothelial cells (with 200 ng/mL verteporfin only, no light) was very limited.

Changes in endothelial cytoskeleton induced by verteporfin-photodynamic therapy were examined with immunofluorescence staining. In the control cells, microtubules extend throughout the cytoplasm to the cell periphery, whereas actin only distributes at the cell periphery (Fig. 6, *top*). This distribution pattern is important for maintaining endothelium integrity (23). Microtubule disassembly was noted shortly after verteporfin-photodynamic therapy followed by the formation of actin stress fibers located in the cell central region (Fig. 6, *middle*). Accompanying the actin stress fibers formation, endothelial cells were observed to retract and display a round morphology, leading to the formation of intercellular gaps (Fig. 6, *bottom*).

Discussion

The goal of tumor vascular targeting is to selectively modulate tumor vascular function for a therapeutic purpose (24). To achieve this goal, therapeutic effectors or cytotoxic agents need to be selectively delivered to the tumor vascular targets. Although there are a variety of potential tumor vascular markers that can be exploited for the selective vascular targeting through conjugating therapeutic agents with tumor vasculature homing molecules, a marker that is absolutely specific for tumor vasculature has not yet been and may never be found (25). Passive targeting of tumor vasculature based upon the temporal confinement of an i.v. injected agent might be practically the most effective approach to targeting tumor blood vessels. This is especially true for photodynamic therapy, where light needs to be applied to activate the photosensitizing compounds that are otherwise not biologically active at all. Photodynamic therapy can be developed as an effective and selective vascular-targeting modality because photosensitizers are exclusively localized within the vasculature shortly after systemic administration and, more importantly, the selectivity of action to the desired site comes through the ability to accurately deliver light provided by current laser fiber technology. Indeed, photodynamic vascular-targeting therapy has already been in clinical applications for AMD and is under clinical investigation for cancer treatments. However, in spite of extensive studies, a detailed scenario of how photodynamic therapy causes vascular shutdown remains unclear. The present study focuses on studying the effects and mechanisms of vascular permeabilization, an early event commonly observed after photodynamic vascular-targeting therapy.

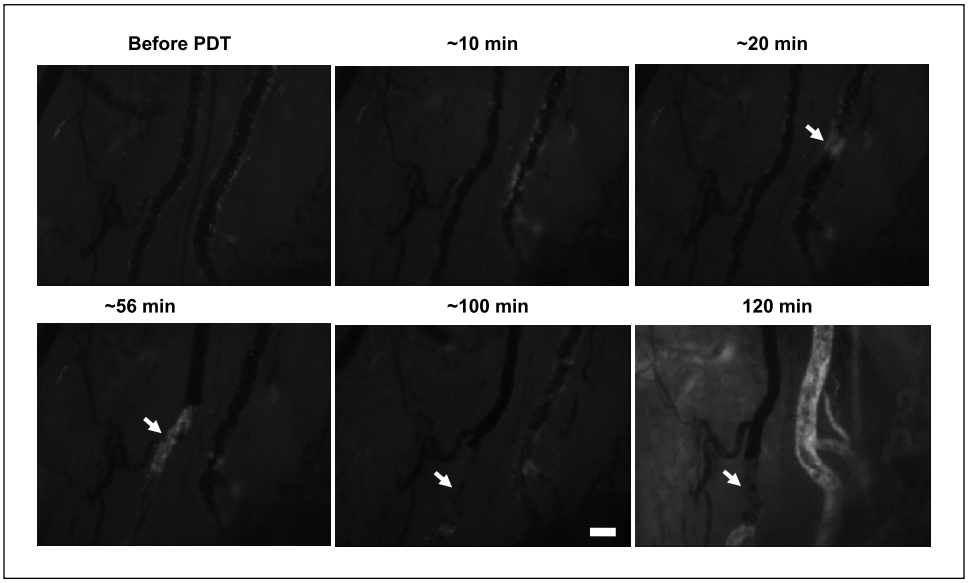

Fig. 3. Intravital microscopic imaging of tumor vascular response to vascular-targeting photodynamic therapy in the orthotopic MatLyLu rat prostate tumor. Rat blood cells were labeled with Dil dye as described in the Materials and Methods and injected to the animals. The orthotopic MatLyLu tumors were exposed to 50 J/cm^2 light (690 nm, at 50 mW/cm^2) at 15 minutes after i.v. injection of 0.25 mg/kg verteporfin. Fluorescence images of tumor blood vessels indicate blood cell adherence and thrombus formation (*arrow*). To examine the vascular function at 120 minutes after photodynamic therapy, the animal was i.v. injected with 10 mg/kg 2,000-kDa FITC-dextran. Fluorescence of FITC was observed in the remaining functional vessels. Bar, 50 μm.

Our present results show that photosensitization with verteporfin significantly increases overall vascular permeability in both s.c. and orthotopic MatLyLu rat prostate tumors. Thus, tumor uptake of macromolecules was increased after the initial photosensitization treatment. This effect seems dependent on the photodynamic therapy conditions and the size of macromolecules. A vascular-targeting photodynamic therapy regimen employing a short drug-light interval induced a stronger effect than the cellular-targeting photodynamic therapy using a long interval (Fig. 1). This is likely because vascular barrier function is maintained by the integrity of endothelial network and specific intravascular photosensitization induced by vascular-targeting photodynamic therapy is able to induce more structural and functional changes on the endothelium. Previous studies also showed that vascular targeting photodynamic therapy employing a short drug-light interval caused more reduction in blood flow (5, 8, 26). It is interesting to note that the increase in tumor uptake of 2,000 kDa dextran was more significant than that of Evans blue. This difference might be related to the size of these two macromolecules. Evans blue strongly binds to albumin in the blood. Its behavior reflects the transport of albumin (19), which is about 67 kDa with a diameter of about 7 nm. This size is similar to the effective pore size of 6 to 7 nm occurring in most normal blood vessels (27), whereas the size of 2,000-kDa dextran is estimated to be about 100 nm (28). Because tumor vessels typically have larger interendothelial junctions than normal blood vessels (29), there might be little hindrance for the transvascular transport of Evans blue-albumin complex. Therefore, further increase in vascular permeability induced by vascular photosensitization may have little influence on the extravasation of albumin that can already across tumor vessel wall. However, it can

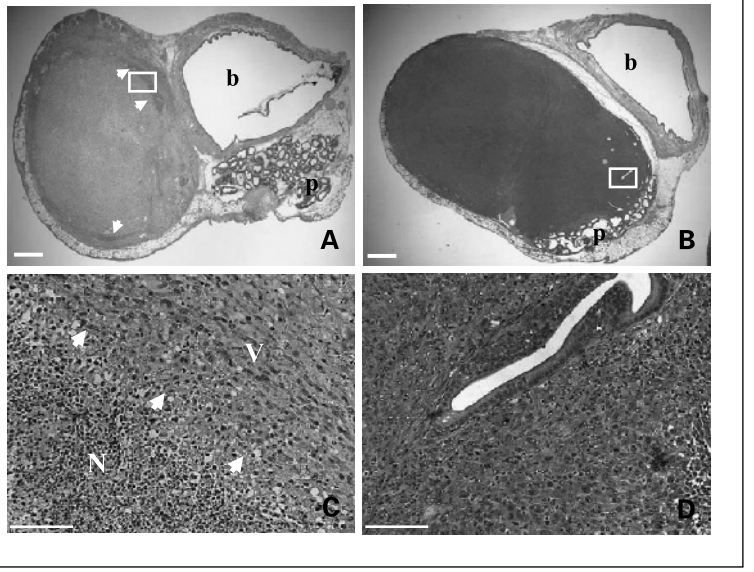

Fig. 4. Histologic changes of orthotopic MatLyLu tumor after photodynamic therapy treatment. The MatLyLu tumors were exposed to 50 J/cm^2 light treatment (690 nm, at 50 mW/cm^2) at 15 minutes after i.v. injection of 0.25 mg/kg verteporfin. Control tumors were only injected with verteporfin without light treatment. Tumor sections were taken at 48 hours after treatments and stained with H&E. Photographs (*A*) and (*C*) were taken from a photodynamic therapy-treated tumor section, and photographs (*B*) and (*D*) were from a control tumor section. Photographs (*A*) and (*B*) were taken at a low magnification, showing a complete tumor section, including the tumor, prostate (*p*), and bladder (*b*). Part of the tumor section (*white box*) in photographs (*A*) and (*B*) is highlighted at a high magnification in photographs (*C*) and (*D*), respectively. Note a clear demarcation (*arrow*) between necrotic tumor area (*N*) and viable tumor area (*V*) at tumor peripheral region. Bar, 1 mm (*A* and *B*) and 100 μm (*C* and *D*).

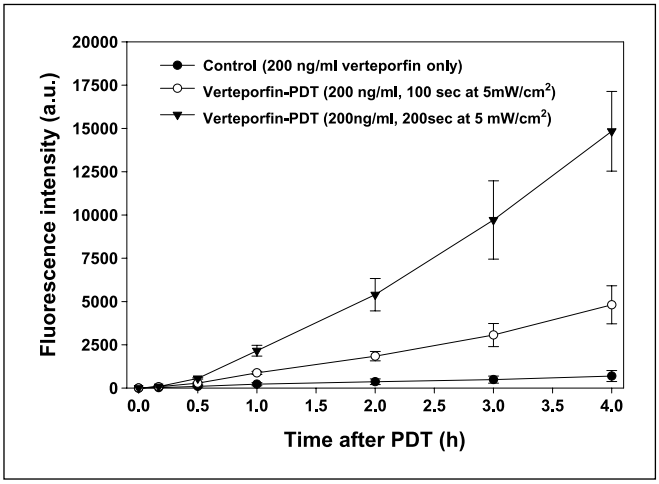

Fig. 5. Photosensitization with verteporfin induces an increase in endothelial monolayer permeability to 2,000-kDa FITC-dextran. Confluent SVEC4-10 endothelial cells cultured on Transwell inserts were exposed to 5 mW/cm^2 light treatment for 100 or 200 seconds after incubation with 200 ng/mL verteporfin in medium for 15 minutes. The amount of FITC-dextran diffused through the endothelial monolayer into the lower compartment was measured by a microplate reader with excitation at 485/20 nm and emission at 525/20 nm. Control cells were only incubated with 200 ng/mL verteporfin without light treatment. PDT, photodynamic therapy.

significantly facilitate the extravasation of larger molecules, such as 2,000-kDa dextran, that are otherwise difficult to transport across the endothelial barrier.

The mechanism of photosensitization-induced vascular permeabilization is still an unresolved issue. Because vascular barrier function critically depends on the endothelial cell integrity, which is maintained by cytoskeletal components, such as filament actin and microtubules (13), we studied the effects of verteporfin photosensitization on endothelial cell morphology, cytoskeleton, and barrier function. Our results show that photosensitization causes endothelial cell microtubule depolymerization and induces the formation of actin stress fibers (Fig. 6). Thus, endothelial cells were found to retract, leading to the formation of intercellular gaps, which result in endothelial barrier dysfunction (Fig. 5). The key question becomes how photosensitization induces the formation of intercellular gaps. Here, we found that microtubule alteration was noted before any apparent changes of actin structures and cell morphology, suggesting that microtubules play a pivotal role in photosensitization-induced endothelial gap formation. Microtubules are a cytoskeletal structure with important function in signal transduction and intracellular transport of membrane-bound organelles (23). Previous study with Photofrin also showed that microtubules were even sensitive to photodynamic therapy dose that produced little cytotoxicity (30). It is likely that direct photodynamic disruption of microtubule network triggers endothelium contraction by inducing actin cytoskeletal changes, such as the formation of actin stress fiber, a filament with contractile property. It has been shown that microtubule disruption can cause endothelial morphologic changes through the activation of Rho protein (31). We are currently investigating the involvement of Rho/Rho kinase pathway in photosensitization-induced endothelial morphologic and functional changes.

Retraction of endothelial cells not only leads to the formation of intercellular gap and therefore causes vascular barrier dysfunction but also exposes basement membrane to circulating blood cells, which triggers blood aggregation cascade and causes blood flow reduction. Our intravital microscopy study showed RBC adherence to vessel wall shortly after vascular-targeting photodynamic therapy (Fig. 3). Blood cell adherence developed into the formation of thrombi. Stable thrombi would decrease blood flow and eventually occlude blood vessels, as shown in Fig. 3. This is in agreement with electron microscopic study showing that tumor blood vessels are often congested with RBCs after photodynamic therapy treatment (32). Exposure of vessel basement membrane as a result of endothelial retraction might be only one of the mechanisms causing thrombi formation. Other mechanisms, such as release of thromboxane from platelets (33) and von Willebrand factor from damaged endothelial cells (34), could also contribute to the thrombosis process.

Because tumor vascular leakiness, on the one hand, governs the delivery of therapeutic agents into the tumor tissue and, on the other hand, facilitates tumor cell intravasation into the circulation (35), tumor vascular permeabilization induced by vascular-targeting photodynamic therapy has profound implications in cancer treatments. A therapeutic benefit of photosensitized vascular permeabilization is that it can be used to improve tumor drug delivery and enhance the therapeutic

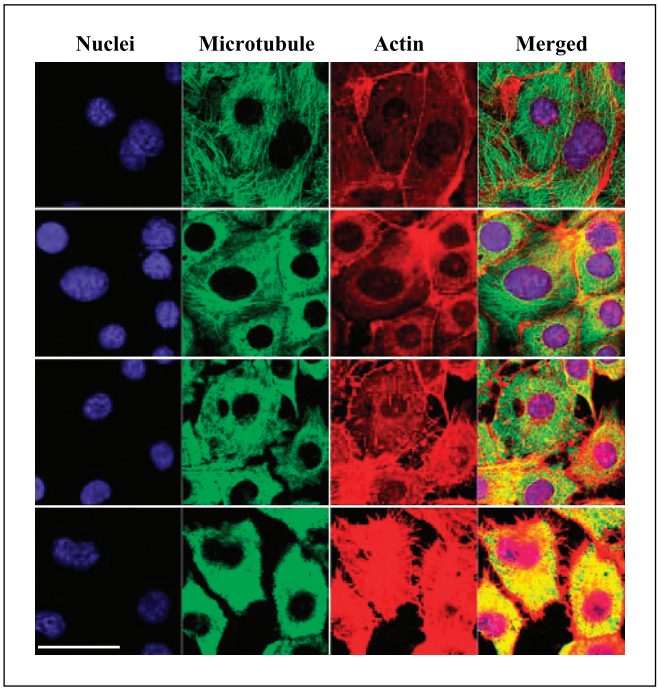

Fig. 6. Photodynamic therapy with verteporfin induces microtubule depolymerization and stress actin fiber formation in SVEC4-10 endothelial cells (with objective lens of ×40). Cells cultured on glass coverslips were treated with 5 mW/cm^2 light for 200 seconds after incubation with 200 ng/mL verteporfin for 15 minutes. Nuclei were stained with Hoechst (*blue*). Microtubule was stained with anti-tubulin antibody followed by incubation with Alexa Fluor 488–labeled secondary antibody (*green*), and filament actin was stained with rhodamine-phalloidin (*red*). Merged images of all three staining (*right*). Top, control; middle top, 5 minutes after photodynamic therapy; middle bottom, 15 minutes after photodynamic therapy; bottom, 30 minutes after photodynamic therapy. Bar, 10 μm.

effect. Indeed, it has been shown that photodynamic therapy regimens with low fluence and fluence rate are able to induce a significant increase in tumor vascular permeability for a sustained period of time (36). Consequently, combination of these photodynamic therapy treatments with liposomal doxorubicin led to an enhanced tumor cure. On the other hand, because tumor vasculature represents an interface between the circulation system and cancer cells, a concern of photodynamic therapy-induced vascular permeabilization is that whether this can potentially induce tumor metastasis by increasing tumor cell intravasation into the circulation. There is evidence showing that sublethal photodynamic therapy damage to tumor cells indeed increases tumor metastasis (37). Although this is considered to be related to the decrease of tumor cell adhesion to the extracellular matrix and the activation of tumor cell survival signal (such as expression of hypoxia-inducible factor-1α and vascular endothelial growth factor) following sublethal photodynamic therapy damage to tumor cells, tumor vascular permeability increase may at least contribute to the metastatic process because sublethal photodynamic therapy itself together with some tumor secreting factors (e.g., vascular endothelial growth factor) all can increase tumor vascular leakiness. Thus, our future efforts will be on exploring the mechanism and therapeutic potential of photodynamic vascular targeting in cancer therapy and anticancer drug delivery, and, importantly, addressing the concern of whether photosensitized vascular permeabilization will increase tumor metastasis.

References

1. Dougherty TJ, Gomer CJ, Henderson BW, et al. Photodynamic therapy. J Natl Cancer Inst 1998;90: 889–905.

2. Dolmans DE, Fukumura D, Jain RK. Photodynamic therapy for cancer. Nat Rev Cancer 2003;3:380–7.

3. Detty MR, Gibson SL, Wagner SJ. Current clinical and preclinical photosensitizers for use in photodynamic therapy. J Med Chem 2004;47:3897–915.

4. Brown SB, Mellish KJ. Verteporfin: a milestone in opthalmology and photodynamic therapy. Expert Opin Pharmacother 2001;2:351–61.

5. Chen B, Pogue BW, Goodwin IA, et al. Blood flow dynamics after photodynamic therapy with verteporfin in the RIF-1 tumor. Radiat Res 2003;160:452–9.

6. Chen B, Pogue BW, Hoopes PJ, Hasan T. Combining vascular and cellular targeting regimens enhances the efficacy of photodynamic therapy. Int J Radiat Oncol Biol Phys 2005;61:1216–26.

7. Zhou X, Pogue BW, Chen B, Hasan T. Analysis of effective molecular diffusion rates for verteporfin in subcutaneous versus orthotopic Dunning prostate tumors. Photochem Photobiol 2004;79:323–31.

8. Fingar VH, Kik PK, Haydon PS, et al. Analysis of acute vascular damage after photodynamic therapy using benzoporphyrin derivative (BPD). Br J Cancer 1999; 79:1702–8.

9. Chen B, Pogue BW, Zhou X, et al. Effect of tumor host microenvironment on photodynamic therapy in a rat prostate tumor model. Clin Cancer Res 2005;11: 720–7.

10. Tozer GM, Bicknell R. Therapeutic targeting of the tumor vasculature. Semin Radiat Oncol 2004;14: 222–32.

11. Tozer GM, Kanthou C, Baguley BC. Disrupting tumour blood vessels. Nat Rev Cancer 2005;5: 423–35.

12. Weersink RA, Bogaards A, Gertner M, et al. Techniques for delivery and monitoring of TOOKAD (WST09)-mediated photodynamic therapy of the prostate: clinical experience and practicalities. J Photochem Photobiol B 2005;79:211–22.

13. Stevens T, Garcia JG, Shasby DM, Bhattacharya J, Malik AB. Mechanisms regulating endothelial cell barrier function. Am J Physiol Lung Cell Mol Physiol 2000;279:L419–22.

14. Fingar VH. Vascular effects of photodynamic therapy. J Clin Laser Med Surg 1996;14:323–8.

15. Henderson BW, Dougherty TJ. How does photodynamic therapy work? Photochem Photobiol 1992;55: 145–57.

16. Michels S, Schmidt-Erfurth U. Sequence of early vascular events after photodynamic therapy. Invest Ophthalmol Vis Sci 2003;44:2147–54.

17. Tennant TR, Kim H, Sokoloff M, Rinker-Schaeffer CW. The Dunning model. Prostate 2000; 43:295–302.

18. Lucia MS, Bostwick DG, Bosland M, et al. Workgroup I: rodent models of prostate cancer. Prostate 1998;36:49–55.

19. Graff BA, Bjornaes I, Rofstad EK. Microvascular permeability of human melanoma xenografts to macromolecules: relationships to tumor volumetric growth rate, tumor angiogenesis, and VEGF expression. Microvasc Res 2001;61:187–98.

20. Unthank JL, Lash JM, Nixon JC, Sidner RA, Bohlen HG. Evaluation of carbocyanine-labeled erythrocytes for microvascular measurements. Microvasc Res 1993;45:193–210.

21. Vouret-Craviari V, Boquet P, Pouyssegur J, Van Obberghen-Schilling E. Regulation of the actin cytoskeleton by thrombin in human endothelial cells: role of Rho proteins in endothelial barrier function. Mol Biol Cell 1998;9:2639–53.

22. Lu W, Schroit AJ. Vascularization of melanoma by mobilization and remodeling of preexisting latent vessels to patency. Cancer Res 2005;65:913–8.

23. Lee TY, Gotlieb AI. Microfilaments and microtubules maintain endothelial integrity. Microsc Res Tech 2003; 60:115–27.

24. Siemann DW, Chaplin DJ, Horsman MR. Vascular-targeting therapies for treatment of malignant disease. Cancer 2004;100:2491–9.

25. Brekken RA, Li C, Kumar S. Strategies for vascular targeting in tumors. Int J Cancer 2002;100:123–30.

26. Kurohane K, Tominaga A, Sato K, North JR, Namba Y, Oku N. Photodynamic therapy targeted to tumor-induced angiogenic vessels. Cancer Lett 2001;167: 49–56.

27. Lum H, Malik AB. Regulation of vascular endothelial barrier function. Am J Physiol 1994;267:L223–41.

28. Yuan H, Gaber MW, McColgan T, Naimark MD, Kiani MF, Merchant TE. Radiation-induced permeability and leukocyte adhesion in the rat blood-brain barrier: modulation with anti-ICAM-1 antibodies. Brain Res 2003;969:59–69.

29. Roberts WG, Palade GE. Neovasculature induced by vascular endothelial growth factor is fenestrated. Cancer Res 1997;57:765–72.

30. Sporn LA, Foster TH. Photofrin and light induces microtubule depolymerization in cultured human endothelial cells. Cancer Res 1992;52:3443–8.

31. Birukova AA, Birukov KG, Smurova K, et al. Novel role of microtubules in thrombin-induced endothelial barrier dysfunction. FASEB J 2004;18:1879–90.

32. Peng Q, Nesland JM. Effects of photodynamic therapy on tumor stroma. Ultrastruct Pathol 2004;28: 333–40.

33. Fingar VH, Wieman TJ, Wiehle SA, Cerrito PB. The role of microvascular damage in photodynamic therapy: the effect of treatment on vessel constriction, permeability, and leukocyte adhesion. Cancer Res 1992; 52:4914–21.

34. Foster TH, Primavera MC, Marder VJ, Hilf R, Sporn LA. Photosensitized release of von Willebrand factor from cultured human endothelial cells. Cancer Res 1991;51:3261–6.

35. McDonald DM, Baluk P. Significance of blood vessel leakiness in cancer. Cancer Res 2002;62:5381–5.

36. Snyder JW, Greco WR, Bellnier DA, Vaughan L, Henderson BW. Photodynamic therapy: a means to enhanced drug delivery to tumors. Cancer Res 2003; 63:8126–31.

37. Momma T, Hamblin MR, Wu HC, Hasan T. Photodynamic therapy of orthotopic prostate cancer with benzoporphyrin derivative: local control and distant metastasis. Cancer Res 1998;58:5425–31.

Critical Reviews™ in Eukaryotic Gene Expression, 16(4):279–305 (2006)

Vascular and Cellular Targeting for Photodynamic Therapy

Bin Chen,[1] Brian W. Pogue,[2,3] P. Jack Hoopes,[2,4] & Tayyaba Hasan[3,]*

[1]Department of Pharmaceutical Sciences, Philadelphia College of Pharmacy, University of the Sciences in Philadelphia, Philadelphia, PA 19104; [2]Thayer School of Engineering, Dartmouth College, Hanover, NH 03755; [3]Wellman Center for Photomedicine, Massachusetts General Hospital, Department of Dermatology, Harvard Medical School, Boston, MA 02114; [4]Department of Surgery, Dartmouth Medical School, Lebanon, NH 03756

* Author to whom all correspondence should be addressed: E-mail: thasan@partners.org

ABSTRACT: Photodynamic therapy (PDT) involves the combination of photosensitizers (PS) with light as a treatment, and has been an established medical practice for about 10 years. Current primary applications of PDT are age-related macular degeneration (AMD) and several types of cancer and precancer. Tumor vasculature and parenchyma cells are both potential targets of PDT damage. The preference of vascular versus cellular targeting is highly dependent upon the relative distribution of photosensitizers in each compartment, which is governed by the photosensitizer pharmacokinetic properties and can be effectively manipulated by the photosensitizer drug administration and light illumination interval (drug-light interval) during PDT treatment, or by the modification of photosensitizer molecular structure. PDT using shorter PS-light intervals mainly targets tumor vasculature by confining photosensitizer localization within blood vessels, whereas if the sensitizer has a reasonably long pharmacokinetic lifetime, then PDT at longer PS-light intervals can induce more tumor cellular damage, because the photosensitizer has then distributed into the tumor cellular compartment. This passive targeting mechanism is regulated by the innate photosensitizer physicochemical properties. In addition to the passive targeting approach, active targeting of various tumor endothelial and cellular markers has been studied extensively. The tumor cellular markers that have been explored for active photodynamic targeting are mainly tumor surface markers, including growth factor receptors, low-density lipoprotein (LDL) receptors, transferrin receptors, folic acid receptors, glucose transporters, integrin receptors, and insulin receptors. In addition to tumor surface proteins, nuclear receptors are targeted, as well. A limited number of studies have been performed to actively target tumor endothelial markers (ED-B domain of fibronectin, VEGF receptor-2, and neuropilin-1). Intracellular targeting is a challenge due to the difficulty in achieving sufficient penetration into the target cell, but significant progress has been made in this area. In this review, we summarize current studies of vascular and cellular targeting of PDT after more than 30 years of intensive efforts.

KEY WORDS: photodynamic therapy (PDT), photosensitizer, vascular targeting, cellular targeting, targeted therapy, drug delivery

I. INTRODUCTION

Photodynamic therapy (PDT) is a treatment modality using light-sensitive drugs (photosensitizers) in combination with nonthermal light activation to achieve selective tissue/cell damage. PDT was initially developed for killing cancer cells. After more than a 30-year effort, Photofrin, a partially purified preparation of haematoporphyrin derivative, became the first photosensitizer approved in the United States, the European Union (EU), and many other countries for the palliative treatment of cancer and precancer diseases. Probably the most successful PDT application is not targeting cancer cells, but targeting the tumor vasculature. PDT with a liposomal photosensitizer verteporfin has received worldwide approval and become the standard of care for neovascularization involved in age-related macular degeneration (AMD). PDT can be de-

1045-4403/06/$35.00

signed to target tumor cells or blood vessels. Its targeting specificity depends on the selective delivery of the photosensitizer and light to the target tissue. Current laser fiber technology allows easily controllable and highly accurate light delivery to almost any tissue in the body, although accurate dosimetry in routine practice still remains somewhat elusive. However, the progress in identifying new photosensitizers, tissue-specific markers, and targeted drug delivery systems (DDS) can significantly enhance the overall ability to selectively deposit a photosensitizer in the target site at appropriate therapeutic levels. In this review, the principle of PDT and current studies involving PDT as a means to specifically target cells and blood vessels is discussed. The application focus is largely on cancer and AMD treatment because these are the two major applications of PDT in current medical practice.

II. OVERVIEW OF PHOTODYNAMIC THERAPY

PDT relies on photophysical principles and uses photochemical reactions to generate biological effectors, such as reactive oxygen species (ROS), which cause oxidative damage to important biological molecules (proteins, lipids, and nucleic acids) in the cell membrane, cytoplasm, and nucleus.[1] It is doubtful that the damage is truly localized in any manner, but rather more likely that it is widespread in the cell and localized mainly by photosensitizer distribution. During this process, three key components—a photosensitizer, light, and oxygen—should be present simultaneously in adequate amounts to produce biological effects. A lack of any of these components will diminish or even completely abolish the effect of PDT on therapeutic outcome.

A. Photophysics and Photochemistry

Upon the absorption of photons of a suitable wavelength, individual monomer photosensitizer molecules are first excited to their short-lived excited singlet state (S_1) (lifetime typically < 100 ns) and then, through intersystem crossing, shift to a lower energy and longer lived excited triplet state (T_1) (lifetime typically > 500 ns).[2] These molecules are chosen or designed to have sufficient magnetic moment to produce a triplet state splitting, which leaves the T_1 level near resonance with the excited state level of molecular oxygen. This situation then allows effective collisional quenching by ground state molecular oxygen (with the ground state already in its triplet state), to transfer energy to create singlet state oxygen. Since only triplet state molecules have a long enough lifetime to react with substrate molecules such as oxygen and generate biological effects, the quantum yield of the excited triplet state is an important criterion in evaluating the biological efficiency of photosensitizers. The triplet quantum yield of most current photosensitizers is high and ranges from about 0.3 to 0.6. The resultant triplet photosensitizer molecules may transfer electrons/hydrogen to nearby biomolecules (Type I reaction), generating free radicals that can further react with oxygen to produce reactive oxygen species (ROS).[1] It is largely believed that the majority of photosensitizers transfer their triplet state energy to oxygen via collisional quenching (Type II reaction), leading to the production of singlet oxygen. Although it is generally accepted that the Type II reaction is the dominant photochemical pathway in photodynamic reactions, as shown in vitro and with indirect studies, it is challenging to directly prove what the exact photochemical origin of the damage truly is.[3] Recent studies have clearly shown that singlet oxygen is produced in vivo and that the production rate is correlated to the damage observed.[4] However, different photosensitizers clearly have varying photochemical pathways, and it is likely that a large cascade of photochemical events is the origin of the resulting damage observed.

B. Photosensitizers

Photosensitizers are chemicals that are able to absorb photons and transfer light energy into the production of ROS, mainly singlet oxygen. Most of the current photosensitizers have porphyrin-related structures, including hematoporphyrin derivatives, phthalocyanines, chlorines, and bacteriochlorins.[5] They can be exogenously administrated compounds or endogenously produced

photosensitive metabolites (e.g., protoporphyrin IX from 5-aminolevulinic acid). To capture photons efficiently, photosensitizing compounds typically have several unsaturated aromatic rings forming large π-bond conjugation structures. Therefore, photosensitizers are generally hydrophobic and form aggregates easily in aqueous media, which not only makes intravenous administration difficult, but also decreases photodynamic efficiency. Generally, when the molecules are in monomer form they are most photophysically active, and when they dimerize or aggregate, their ability to undergo intersystem crossing is severely reduced and largely eliminated. When bound to proteins or lipids in vivo, they are thought to be as close to a monomer form as is feasible. It is challenging to measure the photophysical properties in vivo. However, with diffuse reflectance spectroscopy, some measurements have been performed in tissue, which indicate that the molecules do transition through the triplet state energy level in vivo. To overcome the problem of aggregation during administration, photosensitizers are generally either formulated in various colloidal drug delivery systems, such as liposomes, micelles, and biodegradable nanoparticles, or conjugated with hydrophilic polymers.[6] It is likely that although some level of aggregation might exist, both at the time of administration and in vivo, the fraction of monomerized and singularly bound molecules mediate the effective photodynamic action in vivo.

C. Light

Light is needed to activate the photosensitizer molecules accumulated in the target tissue following administration. Although various lamp light sources can be used for this purpose, a laser light source is generally preferred due to its superior optical properties (collimation, coherence, and monochromicity) and flexibility in manipulation in terms of delivery via small fiber optics.[7] To achieve the highest photosensitizing efficiency, the laser wavelength should match the maximum absorption of the photosensitizer. However, since tissue endogenous molecules (e.g., hemoglobins) have strong absorption at wavelengths below 620 nm and above 900 nm (water), the most penetrating light for PDT is between these two wavelength bounds. Chemicals with long wavelength absorption (>800 nm) tend to have low production of singlet oxygen because the triplet state level is then lying below that of the singlet oxygen energy level, thereby inhibiting collisional quenching of the molecules by oxygen. Most porphyrin-based photosensitizers have two major absorption bands, with the dominant one being a Soret band near 350–450 nm in wavelength and 50–100 nm wide.[8] The molecules with large distributed π-bond structures also have significant Q-band absorption in the red and near-infrared range of wavelengths. The basic porphyrins have a series of Q-bands all the way from 500 nm up to 630 nm, and molecules that have more distributed and asymmetric rings can have enhanced Q-bands in the 660–800 nm range. Chlorins, bacteriochlorins, phthalocyanines, and texaphyrins are all in this category.[5] The 620- to 800-nm-wavelength range is often called the therapeutic window; light penetration is proportional to the incident light wavelength: the longer the wavelength, the deeper the tissue penetration. Therefore, red and far red light is generally used for treating bulk tissues. In certain circumstances, when a superficial treatment is highly desirable, such as in the skin, esophagus, or bladder, research has been undertaken to compare blue light excitation to red light excitation,[9] and it is largely true that the depth of damage can be constrained by the use of blue light, whereas infrared light-activated molecules allow the maximum depth of treatment in PDT.

D. Oxygen

Because PDT uses ROS (mainly singlet oxygen) to induce irreversible cellular damage, oxygen is therefore absolutely necessary for an effective treatment. Numerous in vivo and in vitro studies have demonstrated that lack of oxygen will certainly diminish PDT effect, whereas oxygen enhancement or preservation during treatment will increase PDT efficacy, presumably as a result of enhancement in ROS production.[10–13] Enhancement of oxygen is also beneficial in tumors that are chronically hypoxic, although systematic use of this method of enhanced sensitization is not in

practice. Since ROS have very short lifetimes and limited migration distance, the incited biological effects are largely confined to where they are produced, which is dependent on the localization of the photosensitizers. Thus, since oxygen is pervasive throughout almost all tissues, it is largely the localization of the photosensitizer that determines the areas of damage within the tissue.

III. VASCULAR TARGETING WITH PDT

Similar to normal tissue, tumor growth depends on a functional vascular system for the delivery of oxygen and nutrients and removal of metabolic wastes. However, unlike normal tissue, tumor tissue needs to keep on generating new blood vessels to maintain rapid tumor cell proliferation. Abnormally enhanced neovascularization is a hallmark of pathological conditions, such as cancer, AMD, arthritis, and diabetic retinopathy. Therefore, selectively targeting existing blood vessels (vascular-disrupting therapy) and/or inhibiting the formation of new blood vessels (antiangiogenic therapy) will have tremendous treatment effects.[14] In cancer therapy, the recognition and clinical application of tumor vasculature as a therapeutic target represents a major step in cancer treatment history. Compared to conventional cancer cell-targeting approaches, the advantages of a vascular-targeting strategy includes easier accessibility, more efficient cancer cell-killing ability, and lower chance of developing therapy resistance.[15] PDT has been known for many years to be able to induce strong vascular effects, which contribute significantly to the final treatment outcome.[11] Recent progress further demonstrate that PDT can be developed as a potent and selective vascular-targeting modality with diverse medical applications. To elicit specific photodynamic damage to the vasculature, the photosensitizing agent should be selectively distributed in the vascular compartment, which can be achieved via either passive or active targeting approaches.

A. Passive Vascular-Targeting PDT

Passive photodynamic vascular targeting refers to a vascular-targeting approach based on the accumulation of photosensitizers in the vascular compartment as a result of pharmacological or physicochemical factors. For most exogenous photosensitizers, there is usually a peak plasma concentration immediately after intravenous administration, followed by a fast exponential decay in plasma drug level. The time period when the injected photosensitizer is largely confined in the blood vessels, generally at short time points after administration, provides a temporal therapeutic window for vascular targeting (Fig. 1). Light treatment during this vascular-targeting window, with a high plasma photosensitizer level, leads to potent vascular damage, including damage to blood cells, endothelial cells, and vessel-supporting structures. Photosensitizer physicochemical properties also contribute to the passive vascular-targeting effect. As most photosensitizers are hydrophobic, they need to be associated with plasma proteins to be transported. It has been shown that many photosensitizers bind to low-density lipoproteins (LDL) in the circulation.[16] Neovascular endothelial cells and tumor cells generally have a high expression of LDL receptors resulting from increased cell proliferation. Thus, hydrophilic photosensitizers bound to LDL can be preferentially accumulated into proliferating endothelial cells through the LDL receptor-mediated endocytosis pathway.[17]

As a dominant mechanism underlying current clinical applications of verteporfin and other photosensitizers under clinical trials for AMD, the passive photodynamic vascular-targeting approach can be considered the most successful PDT application, so far. Table 1 summarizes the most studied passive vascular-targeting photosensitizers to date. Being the only photosensitizer that has received approval worldwide for AMD, verteporfin (benzoporphyrin derivative monoacid ring A, Visudyne) is formulated as a unilamellar liposome to aid solubility. It is found that this liposomal formulation also promotes drug redistribution to LDL,[18] leading to cellular uptake via the LDL receptor-mediated endocytosis pathway.[19] The average plasma half-life of verteporfin is 2–5 hours in mice and 5–6 hours in humans.[17] However, to induce significant vascular destruction to choroidal neovascularization (CNV), without major damage to normal surrounding tissue caused by drug extravasation, light is generally delivered at 5–15 minutes after administration in both clinical and preclinical AMD treatments.

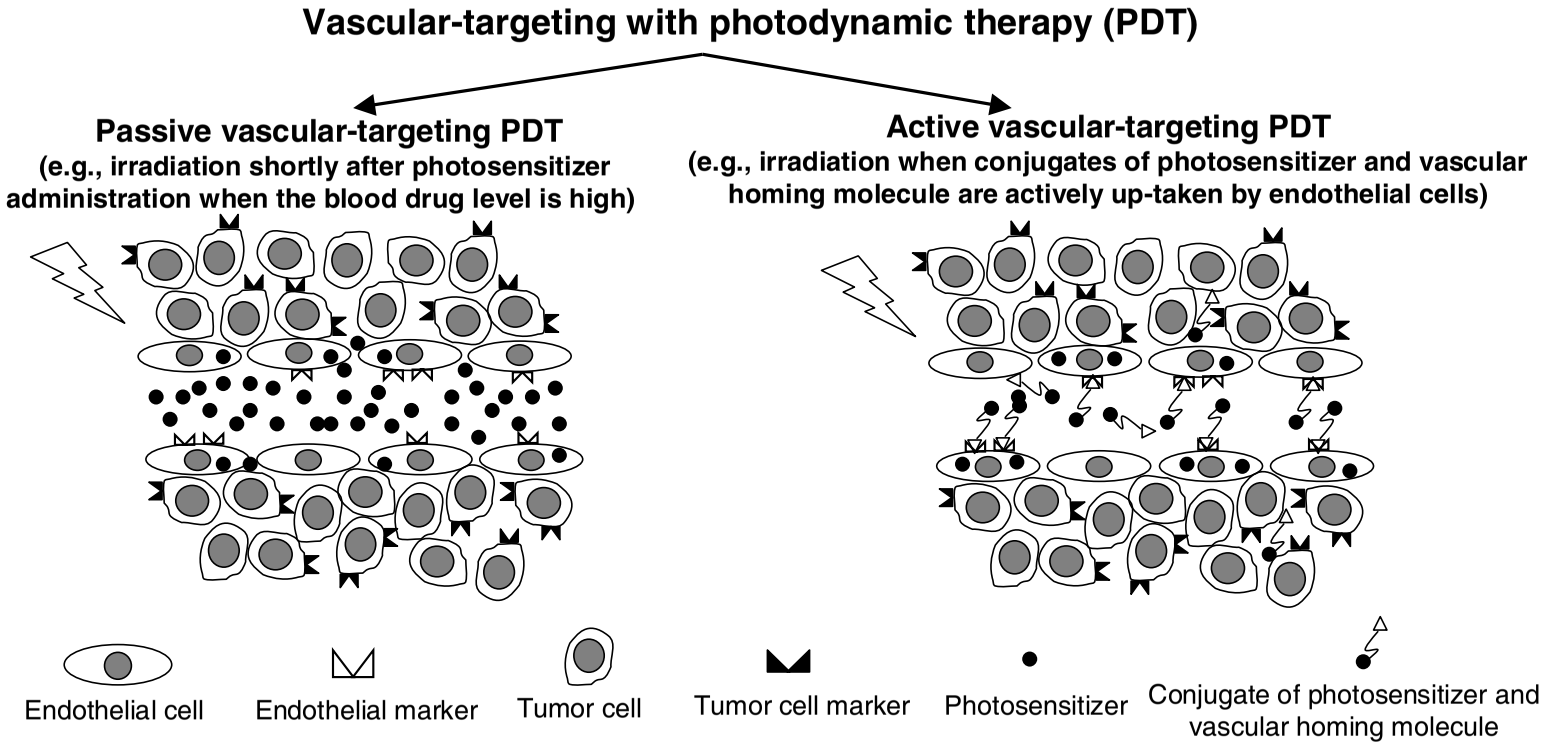

FIGURE 1. Vascular targeting with photodynamic therapy (PDT). Depending on whether a vascular homing molecule is used in the preparation of photosensitizers, vascular-targeting PDT can be divided into passive and active vascular-targeting PDT. In passive vascular-targeting PDT, preferential photosensitizer accumulation in the vascular compartment results from photosensitizer innate pharmacological or physicochemical factors, for example, high blood photosensitizer concentration shortly after photosensitizer i.v. injection. This passive vascular-targeting mechanism is primarily responsible for the clinical application of photosensitizers such as verteporfin and Tookad. In active vascular-targeting PDT, photosensitizer structural modification or targeted drug delivery system formulation with a vascular homing molecule is necessary so that photosensitizing agents can be selectively bound to and retained in the tumor vascular compartment, therefore actively targeting tumor vasculature.

TABLE 1
Common Photosensitizers Used for AMD and Cancer Treatments Based on Passive Vascular-Targeting Mechanisms

Photosensitizers	Formulation	Average plasma $t_{1/2}$	Drug-light interval	Clinical status	Refs.
Verteporfin	Liposome	5–6 h (humans), 2–5 h (mice)	5–15 min	Approved for AMD	17, 22–24
Tin ethyletiopurpurin (SnET2)	Lipid emulsion	NA	10–45 min	Phase III trial	135–137
Lutetium texaphyrin (Lu-Tex)	Aqueous solution	~1 h (humans)	10–45 min	Phase I/II trial	138–141
Mono-L-aspartyl chlorin e6 (NPe6)	Aqueous solution	5–10 h (humans)	5–30 min	Phase I/II trial	142–147
ATX-S10(Na)	Aqueous solution	~45 min (rabbits)	Immediately–5 h	Preclinical	148–151
mTHPC (Foscan)	Lipid emulsion	~30 h (humans), ~7 h (mice)	5–180 min	Approved in EU for cancer	27–29, 152, 153
Tookad	Lipid emulsion	~20 min (humans)	0–30 min	Phase I/II trial	30–34
Hypericin	PEG/water	~1 h (mice)	30 min	Clinical trial in EU	154–157
MV6401	Lipid emulsion	~20 min (mice)	15 min	Preclinical	133, 158

Extending the drug-light interval to more than 50 minutes has been shown to decrease the therapeutic effect.[20] To extend the success of verteporfin, photosensitizers such as tin ethyletiopurpurin (SnET2, Purlytin) and lutetium texaphyrin (Lu-Tex, Optrin) are under clinical trial for AMD, on the basis of the same passive vascular-targeting principle.

In addition to its success in AMD treatment, passive vascular-targeting PDT is showing promise as a cancer treatment as well. Since AMD and cancer share almost the same vascular abnormalities, the photodynamic vascular-targeting modality that has been successful in AMD treatment should also have a role in cancer treatment, for which PDT was originally developed. Accumulative evidence has indicated that passive vascular-targeting PDT can be used for certain types of cancer treatment and is more effective in local tumor control than the traditional tumor cell-targeted PDT using the same photosensitizer and light doses but longer drug-light intervals. For instance, although verteporfin is largely used for AMD, we[21,22] and others[23,24] have shown that it can also be used for targeting neovasculature in tumors. As illustrated in Figure 2, fluorescence microscopic images indicate that verteporfin is predominantly localized within tumor vasculature at 15 minutes after administration. Light irradiation at this time leads to considerable tumor destruction by inducing thrombosis formation and vascular shutdown, and this passive vascular-targeting PDT is more effective in tumor destruction than tumor cellular-targeting PDT using longer drug-light intervals.[22–25]

Another example in this aspect is meso-tetrahydroxyphenylchlorin (mTHPC, Foscan), which has been approved in Europe for the treatment of head and neck cancer. Standard protocol employs a photosensitizer-light interval of about 4 days, so that an optimal tumor-to-normal tissue photosensitizer ratio can be obtained in order to target tumor cells with minimal normal tissue complications. However, experimental data on different tumor models demonstrates that the plasma drug level is a better predictor of tumor response than tumor photosensitizer concentration and that treatments using short drug-light intervals when plasma PS level is high produce much better results.[26–29]

The most advanced tumor vascular-targeting photosensitizer based on the passive targeting principle is palladium-bacteriopheophorbide photosensitizer Tookad (WST09). Tookad is not water soluble and requires a Cremophor-based vehicle to make intravenous administration possible. The plasma half-life of Tookad is only about 20 minutes.[30] With such a fast plasma clearance, it is

necessary to give light almost at the same time or shortly after drug administration to induce an optimal vascular response.[31–34] It has been shown that there is little PDT effect if light is given beyond 30 minutes after Tookad administration.[33] For such an application, intravenous infusion is preferred rather than bolus injection because the plasma drug concentration can be easily controlled by the infusion speed.[32] Currently, Tookad is in a Phase I/II clinical trial for locally recurrent prostate cancer after radiation therapy.

Theoretically, any exogenous photosensitizer can be designed to target blood vessels based on this passive-targeting mechanism, as long as its pharmacokinetic properties enable it to remain sufficiently long enough in circulation. Then, the key is to find the optimal drug-light interval that entails predominant photosensitizer localization to the target vessels. For quite a few photosensitizers, a direct correlation between vascular effects and plasma photosensitizer concentration can be established. Illumination early after intravenous photosensitizer administration generally enhances vascular damage. In some cases, vascular effects induced by PDT at a very short time after photosensitizer injection can be so strong that normal blood vessels are also affected, causing surrounding normal tissue damage. It has been documented that verteporfin-PDT using less than a 5-minute drug-light interval leads to significant choroidal and retinal damage resulting from the occlusion of normal blood vessels.[35,36] PDT dosimetry can play an important role in situations where areas to be treated are delicately situated in close proximity to vital normal tissues. However simply adjusting the photosensitizer and/or light dose or prolonging the drug-light interval (to 15 minutes or more in the case of verteporfin) can make normal blood vessels essentially tolerant to PDT-induced vascular insult, whereas abnormal blood vessels are still sensitive to it, thereby avoiding normal tissue damage.

Passive photodynamic vascular targeting offers a simple means to selectively target blood vessels. This selectivity largely depends on the photosensitizer-light interval and the difference in response to vascular damage as a result of differences in structure and function between nor-

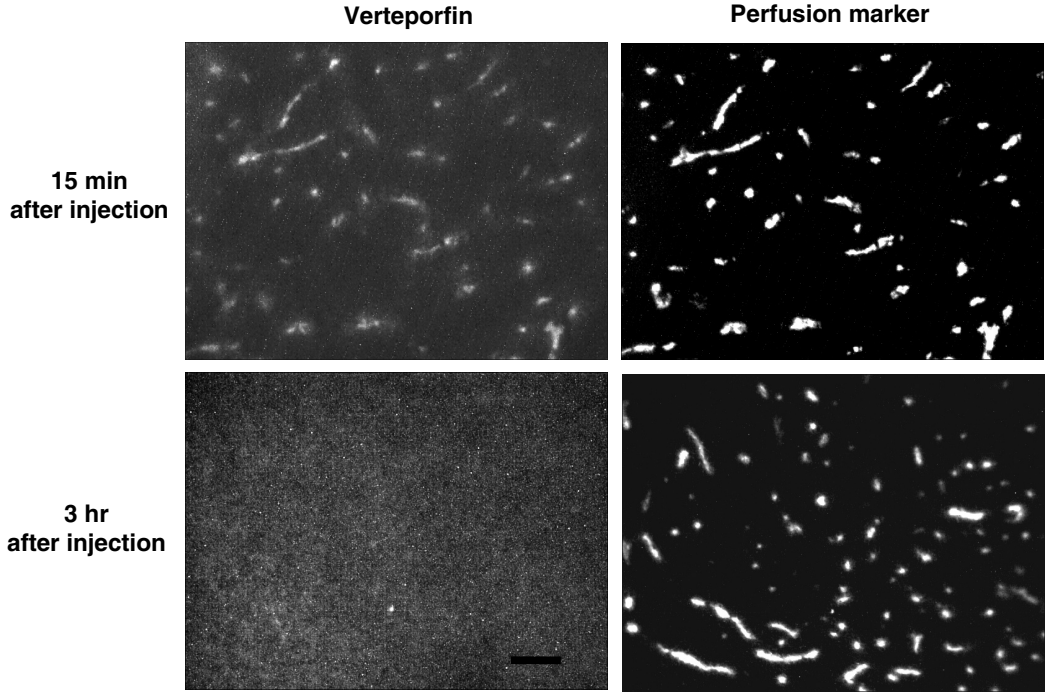

FIGURE 2. Fluorescence images of verteporfin in the subcutaneous MatLyLu rat prostate tumor model at 15 minutes and 3 hours after i.v. injection (1 mg/kg). The perfusion marker $DiOC_7(3)$ (1 mg/kg, i.v.) was injected one minute before tumor excising to visualize the functional vasculature. The same microscopic field was imaged for both verteporfin and $DiOC_7(3)$ by using appropriate filter sets for each dye. Bar, 100 μm.

mal and abnormal neovascular blood vessels. In contrast to normal blood vessels, tumor vessels are leaky and stagnant in function, tortuous and dilated in morphology, and abnormal in structure (irregular pericytes and basement-membrane coverage).[37] As a result, tumor neovasculature has been shown to be more sensitive to photodynamic vascular-targeting therapy.[38] Despite the ability to spare normal blood vessels based on this difference in sensitivity to vascular damage, with a passive vascular-targeting strategy, both normal and abnormal blood vessels are likely exposed to the similar photosensitizer level when light is administered at a short time after drug injection. This suggests that exploration of active photodynamic vascular-targeting approaches, where the photosensitizer could be selectively confined to the neovascular components, would be useful.

B. Active Vascular-Targeting PDT

Active photodynamic vascular-targeting PDT relies on photosensitizer structural modification or a targeted drug delivery system so that the photosensitizing compound can be selectively bound to and retained in the targeted neovasculature components, to elicit a specific vascular effect (Fig. 1). In both cases, a targeting moiety that has a high affinity for neovasculature is directly linked to the photosensitizer molecules or to the photosensitizer delivery systems. The targeting moieties used in targeted drug delivery are peptides, antibodies, or other ligands that recognize molecules selectively expressed on newly formed blood vessels. Despite intensive efforts, a vascular marker that is truly specific to tumor vessels has not been identified.[39] Nevertheless, it has been found that some molecules show higher expression on tumor blood vessels than normal vessels, and these molecules can function as tumor vascular markers to achieve targeted delivery of therapeutic agents to tumor vasculature.

Various tumor vascular markers have been identified on endothelial cells, pericytes, and basement membranes.[40] Endothelial molecular markers are mainly surface membrane proteins overexpressed on tumor endothelial cells, which include growth factor receptors (e.g., VEGFR), integrins ($\alpha_v\beta_3$, $\alpha_v\beta_5$, $\alpha_5\beta_1$), CD105 (endoglin), CD36 (thrombospondin-1 receptor), prostate-specific membrane antigen (PSMA), and tumor endothelial markers (TEMs). Many of these proteins have been used for imaging and targeting tumor neovasculature.[40,41] Although quite a few markers, such as α-smooth muscle actin (α-SMA), platelet-derived growth factor receptor-β (PDGFR-β), and high-molecular-weight melanoma-associated antigen (NG2), have been found on pericytes, the expression of these markers is highly variable on pericytes and often significant on other types of cells as well. Thus, their application in targeted drug delivery remains to be determined. The vascular basement membrane is a self-assembled layer of proteins and proteoglycans formed by endothelial cells and pericytes.[42] Its main components are type IV collagen, fibronectin, laminin, and heparin sulfate proteoglycan. As these components are necessary for angiogenesis and have been shown to be elevated in tumors, the basement membrane is a promising vascular target. For example, tumor fibronectin contains a distinctive extra-domain B (ED-B) that has been exploited for tumor angiogenesis imaging and targeted drug delivery.[43,44]

Active vascular-targeting PDT is emerging as a promising modality for AMD and tumor treatments. Birchler et al. first reported the conjugation of photosensitizer tin (IV) chlorin e_6 with a human antibody fragment (L19) with high affinity for the ED-B domain of fibronectin.[45] In a rabbit cornea angiogenesis model, L19 antibody selectively recognized newly formed blood vessels, but not pre-existing vessels. The conjugate was shown to selectively cause coagulation in corneal neovasculature but not in blood vessels of the surrounding normal tissue when light is delivered 8 hours after administration. At that time point, there was little amount of photosensitizer conjugate (<1%) remaining in the circulation, suggesting that the contribution of passive vascular damage is limited. To target the overexpression of VEGFR on the membranes of angiogenic endothelial cells, Renno et al. conjugated verteporfin (after isolation from a liposomal formulation) to VEGFR-2-binding peptide Ala-Thr-Trp-Leu-Pro-Pro-Arg (ATWLPPR) via a polyvinyl alcohol polymer (PVA) linker.[46] The conjugate displayed similar photophysical properties and photosensitizing activity as verteporfin. PDT us-

ing this targeted verteporfin with a 1 hour drug-light interval was found to be more effective in CNV closure, with less significant damage in normal tissue than standard nontargeted verteporfin in a rat CNV model. If this promising result can be confirmed in the clinical setting, it will greatly improve the effectiveness and safety of current verteporfin therapy for AMD.

Although the ATWLPPR peptide is traditionally considered and used as a VEGFR-2-specific peptide, recent evidence demonstrates that it actually binds to neuropilin-1 (NRP-1) rather than VEGFR-2.[47] NRP-1 is also a type of VEGF receptor and is overexpressed on tumor endothelial cells as well as tumor cells.[48] Tirand et al. recently conjugated a chlorin photosensitizer to the ATWLPPR peptide via a 6-aminohexanoic acid spacer.[49] Their results indicated that ATWLPPR and its photosensitizer conjugate bind exclusively to NRP-1 rather than VEGFR-2. The intracellular concentration of conjugate in the human umbilical vein endothelial cells (HUVECs) was up to 25 times higher than for the free photosensitizer. Furthermore, the addition of ATWLPPR is able to inhibit cellular drug uptake, suggesting a specific receptor-mediated pathway. In agreement with the drug accumulation data, photocytotoxicity of the conjugate was more than 10 times more potent than the free drug in HUVECs. The conjugate seemed stable in the circulation, with an average half-life of 10–13 hours and reached a peak tumor drug level at 1 hour after administration in the U87 human glioma xenograft. Unfortunately, in vivo PDT activity was not reported in the study.

In addition to photosensitizer molecules, photosensitizer delivery systems can also be modified to actively target neovasculature. Ichikawa et al. encapsulated BPD-MA in a polyethylene glycol (PEG)-modified liposome designed to remain in the circulation for a long time and linked it to a peptide (Ala-Pro-Arg-Pro-Gly, APRPG) that binds specifically to angiogenic vessels.[50] Tumor uptake of the APRPG-PEG-modified liposome was about 4-fold higher than the untargeted PEG-liposome 3 hours after administration in a mouse Meth-A sarcoma tumor model. Interestingly, untargeted PEGylated BPD-MA liposomes had little photodynamic activity, presumably due to poor intracellular uptake whereas APRPG-PEG-liposomes showed a significant PDT effect. This result highlights the importance of using vascular homing molecules to achieve intracellular delivery of a photosensitizing agent. Solely increasing tumor drug uptake does not necessarily translate into increase in activity.

Despite these promising results, some key issues are not adequately addressed in these studies. For instance, the plasma stability of these conjugates, the interaction with vascular components, and the pharmacokinetics in plasma and tumor tissue are not well characterized. This information is necessary for determining whether the conjugate is able to specifically target tumor vasculature and what the optimal condition is for targeting tumor vessels. Ideally, the conjugate should have a strong affinity to the neovasculature and fast plasma clearance so that light can be delivered at an optimal time period when only the neovascular structure has significant photosensitizer uptake. Illumination prior to this optimal time period is likely to increase the contribution of nonspecific vascular effect because the photosensitizer plasma concentration remains high. Light treatment beyond after the optimal period might lead to reduced damage to the vascular compartment and increased damage to the parenchyma cells because conjugate molecules may leak into the tissue parenchyma compartment.

IV. TUMOR CELL TARGETING WITH PDT

Tumor cells are obvious and legitimate targets of PDT. A long-cherished goal of any cancer therapy is to kill tumor cells without much involvement of the normal cells. For PDT, selective tumor cell targeting can be achieved by at least two principles. One is the specific light delivery provided by recent developments in various laser light sources and fiber optic delivery devices.[51,52] The other is the targeted delivery of photosensitizers, which is based on the passive or active targeting principle, as illustrated in Figure 3. Additionally, it has been reported that the connective tissue is insensitive to PDT damage, and that normal tissue healing over remaining tissue scaffolds after PDT is quite good.[53–55] These features make PDT a good candidate for tumor cell targeting.

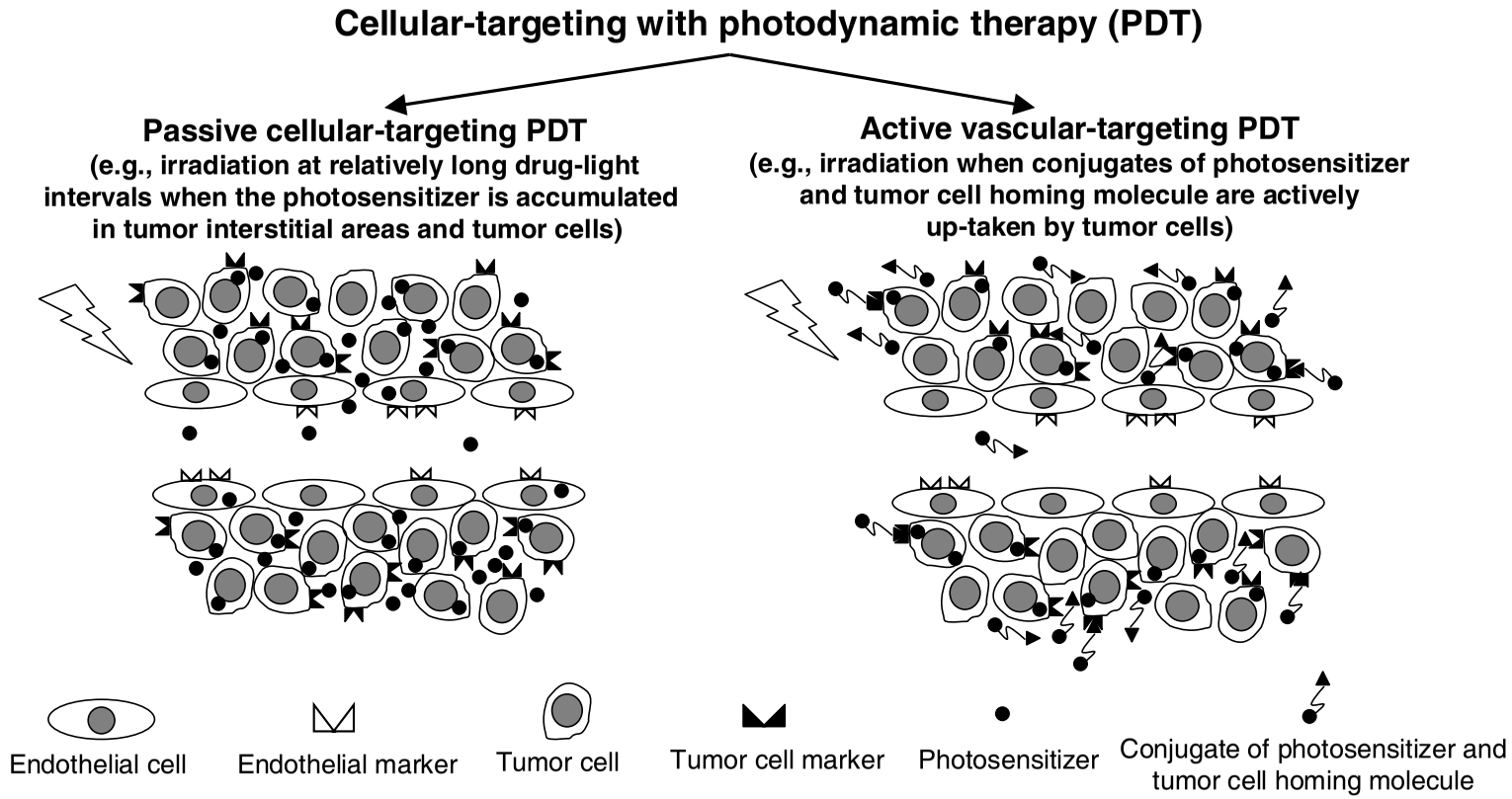

FIGURE 3. Cellular-targeting with photodynamic therapy (PDT). Depending on whether a tumor cellular-targeting molecule is used in the preparation of photosensitizers, cellular-targeting PDT can be divided into passive and active cellular-targeting PDT. Passive cellular-targeting PDT depends on the photosensitizer physicochemical properties and tumor tissue pathophysiological conditions (such as EPR effect) to deliver photosensitizing agents to tumor cells. To allow adequate photosensitizers to accumulate in tumor cellular compartment, light treatment is generally given at hours or days after photosensitizer administration. In active cellular-targeting PDT, photosensitizers or photosensitizer drug delivery systems are usually modified with a tumor cellular-targeting molecule so that only tumor cells expressing the targeting molecules will have significant uptake of photosensitizing agents and be targeted by PDT.

A. Passive Cellular-Targeting PDT

Passive cellular-targeting PDT depends on the photosensitizer physicochemical properties and tumor tissue pathophysiological conditions to deliver photosensitizing agents to tumor cells (Fig. 3). As a matter of fact, most of the past efforts in photosensitizer development rely on finding naturally occurring compounds that appear promising in selective tumor cell damage. Although all of the current photosensitizers do not selectively accumulate in tumor tissues, tumor tissues typically display several times more photosensitizer uptake than the surrounding skin and muscle tissues in most of the preclinical studies.[8] This relative preferential tumor uptake is primarily attributed to photosensitizer physicochemical properties and tumor pathophysiological conditions, which provide favorable conditions for the preferential accumulation of macromolecular drugs in tumor tissues. Unlike normal blood vessels, tumor (angiogenic) blood vessels are generally more permeable to circulating molecules, allowing more drugs to extravasate into the tumor interstitial space. The impaired lymphatic drainage in tumor tissues further retards the clearance of macromolecular drugs from the tumor interstitial area. Through this enhanced permeability and retention (EPR) effect, therapeutic agents are able to accumulate in tumor tissues.[56] To passively target tumor cells based on this EPR effect, the therapeutic agents or formulations should be macromolecules (above 40 kDa) and preferably have long circulation times because tumor drug uptake has been shown to be proportional to the drug circulation time. Although most photosensitizers are small molecules, they are generally bound to plasma proteins in circulation and behave like macromolecules. Thus, preferential photosensitizer tumor accumulation can occur through the EPR effect.

Once photosensitizers are extravasated into the tumor interstitial space, they need to be associated with tumor cell membranes or internalized into tumor cells to generate photocytotoxicity. Photosensitizer physicochemical properties and plasma protein-binding behavior play an important role in determining how and to what extent tumor cells uptake photosensitizers. For example, as most hydrophobic photosensitizers tend to bind to LDL, they may enter the cell via LDL receptor-mediated endocytosis mechanisms.[57] Hydrophobic photosensitizers are more likely to be associated with LDL and lead to an increased intracellular uptake through this pathway.[58] Hydrophobic photosensitizer molecules can also be released from the photosensitizer-plasma protein complex in tumor interstitial areas and passively diffuse into tumor cells.[59] More hydrophilic photosensitizers, such as ATX-S10 and NPe6, are likely to bind to albumin and HDL and be taken up by tumor cells via the nonspecific endocytosis pathway.[60–62]

Intracellular localization of photosensitizers is not as confined as originally thought. They can be co-localized in different cell compartments, such as cell membranes, mitochondria, lysosomes, and endoplasmic reticulum. Thus, tumor cell responses to PDT are complicated and dependent on many factors, such as the photosensitizer, PDT conditions, and the type of tumor cell/model. Almeida et al. have summarized various intracellular signaling pathways following photosensitization treatment.[63] Since the goal of PDT is to induce tumor cell death usually occurring by apoptosis or necrosis, cell death pathways (especially apoptotic cell death) have been extensively studied. PDT can induce tumor cell apoptosis via mitochondria or death receptor-mediated pathways. At high/lethal PDT doses (no limit in photosensitizer concentration, light dose, and oxygen), these cell death signaling pathways will be immediately executed, leading to tumor cell death.[64] However, at low/sublethal PDT doses (usually the case in PDT treatments), tumor cell death will be delayed and dependent on a balance between cell death signaling and PDT-induced cell survival signaling. The cell survival signal can come from the innate cellular protective response toward oxidative damage and apoptotic death signaling (e.g., expression of heat-shock protein, antioxidant enzymes, and antiapoptotic proteins) and response to PDT-induced tissue damage (e.g., expression of hypoxia-inducible factor-1α [HIF-1] and vascular endothelial growth factor [VEGF] in response to tumor hypoxia). Inhibition of these survival signals has been shown to enhance PDT effects, both in vitro[63] and in vivo.[65]

To make passive cellular-targeting PDT effective, light is often given at a relatively long time after photosensitizer injection. The use of

this long drug-light interval is necessary for photosensitizer accumulation in the tumor cellular compartment. As shown in Figure 2, verteporfin has distributed into the tumor tissue at 3 hours after administration, in contrast to the intravascular localization at a 15-minute time point. PDT with long drug-light intervals induces phototoxicity to tumor cells via a passive targeting mechanism. However, passive vascular targeting due to the existence of photosensitizer molecules remaining in tumor vasculature might also contribute to the final PDT outcome. The relative contribution of vascular- versus tumor-cellular effects is dependent upon the distribution of photosensitizing agents in two compartments, which is governed by photosensitizer affinity to each compartment and its pharmacokinetic properties.

B. Active Cellular-Targeting PDT

As passive cellular-targeting PDT, based on innate photosensitizer physicochemical and tumor pathophysiological properties, is often not able to selectively kill tumor cells, active cellular-targeting PDT employing specific modifications of photosensitizers or photosensitizer carrier systems with molecules possessing a high affinity for various specific tumor markers has been actively pursued. Progress in cancer cell and molecular biology has resulted in the discovery of many cellular and molecular targets that can be exploited for targeted drug delivery. Modification of existing photosensitizing agents with tumor cell-targeting molecules intends to restrict photodynamic action to the targeted cells by altering photosensitizer pharmacokinetics and biodistribution. As a result, PDT efficacy is greatly increased, whereas phototoxicity is significantly reduced. Active cellular-targeting PDT has been explored to target not only a variety of surface proteins/peptides and receptors that are overexpressed on the tumor cell membrane, but also tumor cell nuclei, where the uptake of photosensitizers is generally low.

1. Tumor Surface Proteins or Peptides

Mew et al. first introduced the term photoimmunotherapy to describe the use of photosensitizer haematoporphyrin-antibody conjugates designed to specifically target tumor tissues.[66,67] Haematoporphyrin was conjugated directly to antibodies against DBA/2J mouse M-1 myosarcoma or human leukemia-associated antigen (CAMAL) using the carbodiimide procedure. Although the conjugate stability, antigen binding, and biodistribution were not rigorously tested based on current standards, photoimmunoconjugates were indeed shown to induce selective tumor growth inhibition. Promising results of direct photosensitizer and antibody conjugation were also reported by Pogrebniak et al.[68] They conjugated hematoporphyrin to a MAb 45-2D9 recognizing a cell-surface glycoprotein on *ras* oncogene-transformed NIH 3T3 cells and demonstrated both in vitro and in vivo that the photoimmunoconjugate was able to kill tumor cells more selectively and effectively than the free photosensitizer.

The indirect linkage of multiple photosensitizer molecules to antibodies via backbone molecules can produce more reproducible and quantifiable conjugates and, more importantly, retain the binding affinity and biological activity of the antibody and photosensitizer. Chlorin e6 was conjugated to an anti-T-cell monoclonal antibody through dextran or polyglutamic acid (PGA) linker to target human T leukemia cells (HBP-ALL).[69,70] The conjugate with a chlorin/antibody molar ratio of more than 30 still retains about 80% of the antibody-binding affinity and displays the same absorption spectrum and singlet oxygen quantum efficiency as free chlorin e6. Another chlorine photosensitizer, BPD, was covalently linked to antibody MAb 5E8 targeting a cell-surface glycoprotein on human lung squamous cell carcinomas via a polyvinyl alcohol (PVA) linker.[71,72] The BPD-PVA-MAb 5E8 conjugate exhibited more selective and enhanced phototoxicity over free BPD and a control conjugate with an irrelevant antibody in A549 human lung cancer cells. The biodistribution of the conjugate was also studied in A549 xenograft following i.v. injection and compared to free BPD and the control conjugate.[73] Both conjugates have longer circulation and tissue retention than free BPD. Although significant uptake of the BPD-PVA-MAb 5E8 conjugate was observed in the lung, liver, and spleen reticuloendothelial system (RES), it reached the highest tumor-drug concentration

at 14 hours after injection, which is higher than the peak tumor levels of control BPD conjugate and free BPD that occurred at 3 hours after administration. These early studies not only laid the foundation of photoimmunotherapy in cancer cell targeting, but also showed its promise for subsequent cancer therapy development.

The functional carboxyl groups of photosensitizer chlorin e6 can be readily conjugated with targeting molecules. Thus, this type of photosensitizer is often used in the conjugation study. Both chlorin e6 and chlorin e6 monoethylenediamine monoamide (CMA) were conjugated to two antibodies: OC125 recognizing an ovarian carcinoma glycoprotein antigen CA 125 and an anticolon cancer monoclonal antibody 17.1A. Different linkers were used, and the systemic biodistribution and photoactivity of the immunoconjugate were evaluated. An immunoconjugate between CMA and OC125 via polyglutamic acid linkage was demonstrated by ELISA assay to retain significant antigen-binding affinity and specificity.[74] Phototoxicity tested on ascites or pleural fluid cells from patients with ovarian or nonovarian cancers indicated that the conjugate was significantly more cytotoxic to ovarian cancer cells than nonovarian cancer cells. The conjugate was further evaluated in an ascitic ovarian cancer model in the Balb/c nude mice induced by intraperitoneal (i.p.) injection of NIH:OVCAR3 human ovarian cancer cells.[75] Although both the CMA-OC125 immunoconjugate and free CMA reached peak tumor concentrations at 24 hours following i.p. injection, tumor uptake of CMA-OC125 was about 3-fold higher than for the free drug. Tumor levels of the conjugate were, on average, about 6-fold higher than normal tissues, such as skin, blood, and liver, at 23 hours after administration. PDT using the conjugate was effective in killing ascitic tumor cells in a dose-dependent manner, but at high doses induced significant normal tissue damage and even death. A protocol of multiple low-dose PDT treatments turned out to be an effective and safe regimen for reducing tumor burden.[75,76]

A photoimmunoconjugate consisting of chlorin e6 linked via positively charged poly-L-lysine to the $F(ab')_2$ fragment of antibody OC125 was used to study the effect of charge modification on photosensitizer conjugate uptake and phototoxicity.[77] The poly-L-lysine and chlorin e6 complex was first polysuccinylated and then covalently conjugated to the antibody to produce a negatively charged conjugate. Both the positive and negatively charged immunoconjugates still preserved antigen-binding affinity, as suggested by competitive inhibition with the innate antibody in a human ovarian cancer cell line NIH-OVCAR-5. However, the cellular uptake of the positively charged conjugate was much higher than the negatively charged conjugate and free chlorin e6, possibly due to enhanced internalization. In the NIH-OVCAR-5 human ovarian tumor xenograft, the i.p.-administered positively charged immunoconjugate delivered much higher amounts of chlorin e6 to the tumor tissue than the negatively charged immunoconjugate and a nontargeted immunoconjugate prepared with a nonspecific IgG and free chlorin e6.[78] Multiple intraperitoneal PDT performed at 3 hours after photosensitizer administration (i.p.) in the same tumor model demonstrated that tumor-bearing animals tolerated the repeated PDT treatments well, and tumor responses (residual tumor weight and animal survival time) to the positively charged conjugate were much better than responses to the negatively charged or free chlorin e6.[79] The same strategy was employed to target colorectal cancer cells. Two charged photoimmunoconjugates of chlorin e6 and an anticolon cancer monoclonal antibody 17.1A were prepared and found to have selective photocytotoxicity to antigen-positive cells, as compared to the nonspecific IgG conjugate.[80] The positively charged conjugate delivered over 4 times more chlorin e6 to tumor cells than the negatively charged one and was significantly more photoactive than the negatively charged conjugate and free chlorin e6. These results suggest that the positive charge improves endocytosis and subsequent lysosomal degradation of the immunoconjugate.

However, this is not always the case. The same chlorin e6 negatively charged immunoconjugate administered via i.v. injection had a higher tumor accumulation and tumor-to-normal tissue ratio than the positively charged one in a colorectal cancer-induced hepatic tumor model in nude mice.[81] Using an interstitial fiber, hepatic tumors were treated with light at 3 hours after i.v. injection of either negatively charged conjugates

or free chlorin e6, for comparison.[82] PDT with negatively charged immunoconjugates was highly effective in reducing tumor weight and prolonging animal survival, whereas free chlorin e6 PDT was ineffective. These data, seemingly contradictory to the previous results of OC125 conjugates, highlight the importance of target-cell location, histological type, and administration route in affecting photoimmunoconjugate uptake and photoimmunotherapy efficacy.

Several studies have been reported to actively target superficial skin cancers using photosensitizer conjugates. A series of immunoconjugates consisting of photosensitizer tin(IV) chlorin e6 (SnCe6) and antimelanoma antibody MAb 2.1 linked via dextran were prepared to target malignant melanoma cells. The conjugation involved the site-specific modification of the antibody oligosaccharides with a single chain-terminal hydrazide group, which is the coupling point between dextran and the antibody.[83,84] Conjugates with varied photosensitizer-to-antibody molar ratios (up to 18.9) were prepared. A competitive inhibition radioimmunoassay demonstrated that the conjugate retained a good antigen-binding activity, similar to the native antibody. Clonogenic assay showed that the conjugate was selectively phototoxic to the antigen-presenting SK-MEL-2 human malignant melanoma cells. However, it was noted that the quantum yield of singlet oxygen generated by the conjugated SnCe6 was significantly less than that observed with the free drug as a result of reduced triplet yield, which might suggest the formation of aggregates.[85] Chlorin e6 monoethylenediamine monoamide (CMA) was also conjugated to a melanoma-reactive monoclonal antibody IG12.[86] The immunoconjugate was about 9 times more phototoxic toward the targeted OCM431 human uveal melanoma cells than the nontargeted RPMI1846 melanoma cells, whereas the free photosensitizer was more than 2-fold less phototoxic than the conjugates and, importantly, did not possess selective phototoxicity.

Photosensitizer aluminum tetrasulfophthalocyanine ($AlPcS_4$) was covalently coupled to a MAb 35A7 against carcinoembryonic antigen (CEA) via a five-carbon spacer chain.[87] Conjugates with $AlPcS_4$ to mAb 35A7 molar ratios of 5 to 16 were prepared and evaluated for targeting T380 human colon carcinoma xenografts in nude mice. A significant finding of this study was that conjugation with photosensitizer via a five-carbon spacer led to no adverse effect on antibody biological activity, as shown by antigen-binding assay and tumor distribution examination. The conjugates were phototoxic to LoVo colon carcinoma cells. However, in vivo phototoxicity of these conjugates was not reported, making it impossible to evaluate the in vivo activity.

2. Growth Factor Receptors

One of the hallmarks of cancer is uncontrolled cell growth, which can be partially attributed to the overexpression of various growth factor receptors.[88] Among these, the tumorigenic functions of the epidermal growth factor receptor (EGFR) and HER-2 receptor have been most extensively studied and, consequently, actively pursued for therapeutic targeting. It is not surprising to note that many tumor cellular-targeting photosensitizer conjugates are developed to target growth factor receptors, especially EGFR and HER-2 receptor.

Conjugation of EGFR antibody C225 to chlorin e6 yielded a photoimmunoconjugate designed to target EGFR-overexpressing tumor cells in the hamster cheek pouch carcinogenesis model.[89] To diagnose malignancy and monitor treatment response to targeted PDT with chlorin e6-C225, a near-infrared dye Cy5.5 was also conjugated to C225. The results demonstrated that Cy5.5-C225 was able to diagnostically delineate tumor regions and prognostically indicate tumor response to EGFR-targeted PDT. Since EGF is an endogenous ligand of EGFR, Gijsens et al. conjugated EGF and photosensitizer Sn-(IV) chlorin e6 (SnCe6) via three different carriers—dextran (Dex), human serum albumin (HSA), and polyvinylalcohol (PVA)—to target EGFR expressing tumor cells.[90,91] As a comparison, SnCe6 was also conjugated to carrier molecules, only without EGF targeting. Although EGF-PVA-SnCe6 conjugate exhibited a higher photocytotoxicity (IC_{50}: 2.8 microM) than EGF-Dex-SnCe6 (IC_{50}: >10 microM) and free SnCe6 (IC_{50}: >10 microM) in A431 cells, nontargeted PVA-SnCe6 conjugates showed a similar photocyto-

toxicity (IC_{50}: 3.5 microM) to EGF-PVA-SnCe6, suggesting that EGF does not play a major role in conjugate uptake.[90] The EGF-Dex-SnCe6 conjugates have better cellular uptake than EGF-PVA-SnCe6. However, EGF-Dex-SnCe6 only displayed a slight increase in photocytotoxicity over Dex-SnCe6, again indicating a limited EGF receptor-mediated active uptake. The EGF-HSA-SnCe6 conjugates possess the highest cellular uptake and photocytotoxicity (IC_{50}: 63 nM), which can be competitively inhibited by free EGF.[91] These results clearly demonstrate that the efficiency of photoimmunoconjugates strongly depends on the carrier molecules.

EGFR-targeting photosensitizer immunoconjugates were prepared by coupling BPD to an EGFR antibody C225.[92] To increase the conjugate solubility and prevent the formation of aggregates, a small number of antibody lysines (<3 per antibody) were first PEGylated with a 10-kDa branched polyethylene glycol (PEG). BPD, dissolved in a 50% dimethyl sulfoxide-50% aqueous two-solvent system, was covalently linked to the remaining antibody lysines. The resultant conjugates were shown to maintain antigen-binding activity and have low nonspecific macrophage uptake. The BPD-C225 conjugates induced photocytotoxicity in EGFR-overexpressing A-431 cells but had no significant effect on EGFR-negative NR6 cells. Further in vitro photobiological evaluation of this conjugate indicated that BPD-C225 immunoconjugates were more selective, but less effective, than free BPD in killing EGFR-overexpressing cells.[93] The promise of EGFR-targeted photoimmunotherapy based on the conjugation of EGFR antibody and BPD was even extended to in vivo studies. Hemming et al. covalently conjugated an EGFR antibody to BPD via a PVA linker and evaluated its biodistribution and PDT efficacy in the hamster cheek pouch model of squamous cell carcinoma.[94] The EGFR-targeted BPD conjugate demonstrated excellent tumor distribution selectivity. The tumor-to-normal tissue ratio of photosensitizer level was 26 for the BPD-EGFR antibody conjugate and only 2 for free BPD. Tumor response to PDT was consistent with the distribution result. Animals treated with free BPD had a 1-month tumor-free survival of 67%, whereas animals treated with the tumor-specific BPD-EGFR antibody conjugate at one twentieth the total dose of free BPD had an 80% 1-month tumor-free survival. This in vivo study clearly demonstrated that photosensitizer distribution and therapeutic efficacy could be greatly improved through the conjugation to a tumor-specific antibody. The increased efficacy might come from both PDT-induced photocytotoxicity and antibody-induced cytotoxicity.

Both internalizing and noninternalizing antibodies were conjugated to a chlorin photosensitizer mTHPC to determine which conjugate generated better phototoxicity.[95] Photosensitizer mTHPC was first tetracarboxymethylated to increase water solubility and create functional groups for the subsequent conjugation to antibody lysine residues. The modified mTHPC was covalently conjugated to a noninternalizing anti-CD44v6 MAb U36 or an internalizing anti-EGFR MAb 425 to target head and neck squamous cell carcinoma. The conjugates with a mTHPC:MAb molar ratio of up to 4 were shown to be stable, immunoreactive, and photoactive in vitro. In a head and neck carcinoma HNX-OE xenograft, immunoconjugates had better tumor selective distribution than free mTHPC. An important finding of this study was that photosensitizer coupled to an internalizing MAb displayed more phototoxicity than that conjugated to a noninternalizing MAb. Similar results were also reported in studies comparing aluminium tetrasulfophthalocyanine ($AlPcS_4$) immunoconjugates with a noninternalizing MAb 35A7 recognizing carcinoembryonic antigen (CEA) and an internalizing HER2 MAb FSP 77 and 17.1A.[96,97]

This hypothesis was further tested with two hydrophilic photosensitizers.[98,99] The rationale for using hydrophilic photosensitizers is obvious, because this type of photosensitizer generally has low photocytotoxicity due to low cell membrane affinity, and they are good candidates for photoimmunoconjugation because of good water solubility. The question being addressed was whether conjugating hydrophilic photosensitizers to an internalizing MAb would enhance the phototoxicity. Hydrophilic photosensitizer TrisMPyP-φCO_2H[98] or aluminum (III) phthalocyanine tetrasulfonate [$AlPc(SO_3H)_4$][99] was coupled to internalizing antibodies (MAbs U36 and 425) or noninternalizing antibody E48 against a glycosylphosphatidylinositol-anchored surface antigen.

Similar to their previous mTHPC conjugates, new photoimmunoconjugates were stable and showed good immunoreactivity as long as the photosensitizer:MAb ratio was maintained below 4 in both cases. The conjugates with a low photosensitizer:MAb ratio demonstrated selective tumor accumulation in head and neck carcinoma HNX-OE xenografts, although conjugate tumor uptake was always lower than native antibodies. At higher molar ratios, the solubility of conjugates was significantly decreased, which led to a faster plasma clearance and lower tumor uptake. In A431 cells, conjugates with an internalizing antibody (MAb U36 or 425) were significantly more phototoxic than conjugates with a noninternalizing MAb E48 and free photosensitizers, which showed a limited or no photocytotoxicity at all. For instance, $AlPc(SO_3H)_4$-MAb 425 conjugate was about 7500 times more toxic to A431 cells than the free sensitizer (IC_{50}, 0.12 nM vs. 900 nM). However, in a subsequent study involving more cell lines, phototoxicity of $AlPcS_4$-MAb was found to only correlate strongly with the total cell-binding capacity (both internalized and cell-surface bound) and not with the internalization capacity only.[100] Thus, the selection of internalizing or noninternalizing antibody for photoimmunotherapy is not that straightforward. Photosensitizer physicochemical properties, antibody-binding affinity, antigen expression, method of conjugation, and the type of targeting cell are important factors that should be considered.

Almost all the photoimmunoconjugates developed so far are to target a single epitope on the target cells because the monoclonal antibodies used for the conjugation can only bind to and target a single epitope. It was recently shown that the combination of immunoconjugates targeting different epitopes is better than a single immunoconjugate therapy.[101] Photosensitizer pyropheophorbide-a (PPa) was covalently conjugated to either HER55 or HER66, both of which were anti-HER2 monoclonal antibodies. Similar to previous BPD-C225 conjugates constructed in the same manner,[92,93] HER2-targeting immunoconjugates were more selective, but less effective, than the free photosensitizer in killing HER2-overexpressing cells, suggesting quenching of photoimmunoconjugates and possible changes in intracellular localization. Nevertheless, this study clearly demonstrated that multi-epitope targeting with a combination of HER55 and HER66 pyropheophorbide-a conjugates was significantly more effective than single epitope photodynamic targeting with a single anti-HER2 immunoconjugate.

3. LDL Receptors

LDL receptors are a group of cell surface receptors that transport physiological molecules (e.g., cholesterol), drugs, and drug formulations into cells through a receptor-mediated endocytosis pathway.[102] This process involves receptor recognition of a ligand, internalization through clathrin-coated pits, and degradation following fusion with lysosomes. Apolipoprotein B-100 (ApoB-100) on the outer shell of LDL is one of LDL receptor ligands and is responsible for the recognition and binding of LDL to LDL receptors. Although their expressions are somewhat elevated in tumor cells due to increased cell membrane synthesis, this targeting approach is not very specific because LDL receptors are actually expressed on almost all types of cells, especially cells in the liver and adrenal gland. Nevertheless, LDL receptors have been shown to be important in intracellular delivery of hydrophobic photosensitizers, and substantial efforts have focused on modifying photosensitizer structures to increase the interaction between photosensitizer conjugates and LDL receptors so that more drugs can be actively transported into tumor cells.

A seemingly straightforward approach is to covalently conjugate photosensitizer molecules to LDL to actively target LDL receptors. LDL receptor-mediated endocytosis appears to be involved in the cellular uptake of LDL-photosensitizer conjugates. But the extent of active cellular uptake is highly variable, dependent upon the photosensitizer, conjugation chemistry, and the target cells. For example, when haematoporphyrin (HP) is conjugated to LDL, its uptake is increased in the LDL receptor upregulated NIH3T3 cell line and inhibited in the presence of very high levels of free LDL.[103] However, the uptake of HP-LDL conjugate is even more significant in J774.2 macrophages. This result, together with the observation that HP-LDL conjugates form aggregates, suggests that chemical preparation likely affects LDL

ApoB-100 function. Therefore, cells possessing scavenger receptors and/or phagocytic activity mainly take up the conjugate rather than tumor cells expressing LDL receptors. Chlorin e6 (Ce6) was covalently conjugated to LDL via the carbodiimide activation method,[104] where the Ce6-LDL conjugate had a significantly higher (4-5 times) cellular uptake than free Ce6 and Ce6 noncovalently complexed with LDL. Although nonspecific association did occur, an active receptor-mediated uptake pathway was clearly demonstrated by receptor saturation and competitive inhibition experiments. Phototoxicity induced by the Ce6-LDL conjugate was more than 8 times higher than free and LDL-mixed Ce6, which demonstrates the importance of choosing the type of photosensitizer and conjugation method in influencing PDT-targeting capability.

An alternative approach to targeting LDL receptors is to improve photosensitizer incorporation into LDL, which can be achieved chemically by modifying photosensitizer physicochemical properties and/or pharmaceutically formulating photosensitizers in drug delivery systems. Photosensitizer tetrasulfonated aluminum phthalocyanine ($AlPcS_4$) was modified with alkyl chains of various length.[58] Intracellular uptake of the $AlPcS_4$ derivatives depended on the alkyl chain length, where alkylation of $AlPcS_4$ with long chains increased uptake more than short chains: $AlPcS_4$(C16) > $AlPcS_4$(C12) > $AlPcS_4$(C8) > $AlPcS_4$(C4). Human LDL inhibited cellular uptake of alkyl chain conjugates, suggesting an active LDL receptor-mediated pathway. The photocytotoxicities of $AlPcS_4$ derivatives correlated with the intracellular uptake results, demonstrating that modifying photosensitizer molecules with a long hydrophobic chain facilitates conjugate insertion into the lipid core of the LDL particles. Interestingly, Zheng and colleagues reconstructed LDL and used it as an endogenous delivery vehicle to achieve targeted delivery of photosensitizers. They synthesized two photosensitizer conjugates—a pyropheophorbide cholesterol oleate conjugate[105] and a tetra-t-butyl silicon phthalocyanine bearing two oleate moieties at its axial positions[106]—that could be reconstituted into the LDL lipid core with a very high payload (up to several thousand photosensitizer molecules per LDL molecule). Importantly, the reconstituted LDL with such a high photosensitizer payload retained the mean size of native LDL and could be internalized into human hepatoblastoma G2 (HepG2) cells via LDL receptors. As a result, photocytotoxicity of reconstituted LDL loaded with photosensitizers was significantly higher than the free photosensitizers, which presents a unique way to deliver large amounts of photosensitizer molecules to tumor cells.

4. Transferrin Receptors

Transferrin receptors are cell membrane receptors overexpressed on certain cancer cells due to increased cancer cell proliferation.[107] Transferrin (molecular weight, 80,000), being an endogenous ligand to transferrin receptors, is a major protein in the circulation involved in iron transportation. After transferrin binds to the receptor, the transferring iron-receptor complex is internalized and the iron is released intracellularly. Because of its high affinity for the transferrin receptor, transferrin has been used as a ligand to deliver anticancer drugs, including photosensitizers, via receptor-mediated endocytosis.

Haematoporphyrin was conjugated covalently to transferrin using an *N*-hydroxysuccinimide ester linkage.[108] Although the fluorescence of the conjugate was quenched, the conjugate had a similar singlet oxygen quantum yield to the free porphyrin. The uptake of the hematoporphyrin-transferrin conjugate in NIH 3T3 and HT29 cells was somewhat dependent upon receptor-mediated endocytosis, as indicated by partial inhibition by free transferrin and increased uptake following transferring-receptor upregulation. Transferrin was also covalently coupled to chlorin e6 using a procedure involving protein binding to quaternary amino-bearing sephadex prior to chlorin e6 modification to maintain transferrin activity.[109] Although the transferrin-chlorin e6 conjugate had about 70% efficiency of singlet oxygen yield compared to free chlorin e6, it was over 10 times more phototoxic than free chlorin e6 in human MCF7 and rat MTLn3 mammary adenocarcinoma cells.

Hydrophilic photosensitizer $AlPcS_4$ was also encapsulated into transferrin-conjugated PEG liposomes to target transferrin receptor-overexpressing tumor cells.[110] Internalization of trans-

ferrin-$AlPcS_4$ liposomes was shown to involve transferrin receptors, leading to a high intracellular concentration in HeLa cells that overexpress transferrin receptors. As a result, the phototoxicity of the transferrin-$AlPcS_4$ liposome was about 10 times higher than free $AlPcS_4$, whereas a nontargeted $AlPcS_4$ liposome was not phototoxic at all. Further studies revealed that transferrin receptor-overexpressing human AY-27 cancer cells incubated with transferrin-$AlPcS_4$ liposome had more than a 100-fold higher intracellular $AlPcS_4$ concentration than cells incubated with nontargeted liposomes.[111] In an orthotopic AY-27 bladder tumor model, intravesical instillation of the targeted liposome resulted in tumor uptake that was 18 and 78 times higher than normal urothelium and submucosa/muscle, respectively. Although instillation of free $AlPcS_4$ results in nonselective accumulation throughout the whole bladder wall, nontargeted liposome instillation produced no tissue-PS accumulation. The selective uptake of transferrin-$AlPcS_4$ liposome led to a greater phototoxicity to tumor cells, which clearly demonstrates that transferrin-guided photosensitizer conjugates can be used to selectively target transferrin receptor-overexpressing tumors.

This approach, however, does not work for all photosensitzers. An attempt to encapsulate the hydrophobic photosensitizer hypericin within transferrin-conjugated liposomes to target HeLa cells did not significantly improve intracellular hypericin accumulation.[112] A drug-embedding stability study revealed that this hypericin-loaded liposome was not stable. Hypericin, because of its hydrophobic nature, was mainly integrated between lipid bilayers of the liposome and could thus rapidly leak out to redistribute to plasma proteins. In this way, the liposome formulation of hypericin behaved more like the free drug, whereas the more hydrophylic $AlPcS_4$ was stably confined within the liposomal core.

5. Folic Acid Receptor

Folic acid receptors are membrane receptors responsible for the uptake of folic acid, a vitamin essential for *de novo* nucleotide synthesis, via receptor-mediated endocytosis.[113] Folate receptors are only expressed on certain epithelial cells and overexpressed on epithelial malignant cells such as breast, ovary, brain, and lung cancers. Therefore, these receptors can be explored for targeted drug delivery. Two folic acid conjugates were recently prepared using photosensitizer 4-carboxyphenylporphyrine and two different linkers—hexane-1,6-diamine and 2,2′-(ethylenedioxy)-bis-ethylamine.[114] Both conjugates demonstrated a nearly 7-fold higher cellular uptake than the control photosensitizer tetraphenylporphyrin (TPP) after 24 hours incubation with KB nasopharyngeal cells, overexpressing folic acid receptors. Folic acid competitively inhibited tumor cellular uptake by up to 70%, suggesting active transport across the cell membrane via folate receptor-mediated endocytosis. The conjugates also showed photocytotoxicity toward KB cells, whereas the control photosensitizer TPP was not photoactive. These results indicate the feasibility of using folic acid as a targeting molecule to guide photosensitizing agents to target cells.

Folic acid can also be used to modify drug delivery systems to achieve high-payload drug delivery. A pH-sensitive and folic acid receptor-targeted liposome designed to deliver water-soluble photosensitizer chloroaluminum phthalocyanine tetrasulfonate ($[AlPcS_{(4)}]^{(4-)}$) to tumor cells was prepared.[115] This dual-targeting formulation was significantly more phototoxic than free $[AlPcS_{(4)}]^{(4-)}$ and liposomal formulations that were either pH-sensitive or folic acid receptor-targeted only. A novel approach to targeting folic acid receptors using LDL particles was recently reported.[116] As described above, the same group reconstituted endogenous LDL to photodynamically target LDL receptors.[105,106] Because ApoB-100 protein on LDL is responsible for LDL-receptor recognition and binding, it is hypothesized that modifying LDL ApoB-100 will abolish its LDL receptor-binding capacity and, more importantly, be able to reroute the modified LDL to a new target. As a proof of concept, a LDL-based folic acid receptor-targeted nanoparticle was prepared by conjugating folic acid to the Lys residues of ApoB-100 protein, and the photosensitizer tetra-t-butyl-silicon phthalocyanine bisoleate was reconstituted into the LDL lipid core. This novel LDL nanoparticle had a high photosensitizer payload (molar ratio: 300 to 1) and was demonstrated using confocal microscopy and flow

cytometry studies to have significant cellular photosensitizer uptake in folic acid receptor-overexpressing KB cells. Competitive uptake inhibition by free folic acid, combined with a lack of photosensitizer accumulation in folic acid receptor-negative cells (CHO and HT-1080 cell lines) and LDL receptor-overexpressing $HepG_2$ cells, indicates that folic acid conjugation to the Lys side-chain amino groups of ApoB-100 blocks binding to the LDL receptor and reroutes the resulting conjugate to cancer cells via the folic acid pathway.

6. Glucose Transporters

Glucose transporters (GLUTs) are cell membrane proteins responsible for the uptake of glucose by all types of cells. Cancer cells generally overexpress GLUTs due to their increased energy requirements, and the overexpression of GLUTs are associated with tumor metastasis and poor prognosis.[117] GLUT overexpression in human cancers has been explored in tumor positron emission tomography (PET) using 2-fluoro-2-deoxyglucose (^{18}FDG), which is widely used in tumor detection. On the basis of the same principle, a near-infrared fluorescence imaging and photosensitizing agent targeting tumor GLUTs was prepared by conjugating photosensitizer pyropheophorbide with 2-deoxyglucose.[118] The resultant pyropheophorbide 2-deoxyglucosamide (Pyro-2DG) was able to accumulate in tumor cells through GLUTs. Fluorescence-imaging studies demonstrated that Pyro-2DG was selectively retained in the 9L glioma rat tumor. Photoactivation of Pyro-2DG induced selective mitochondrial damage in the tumor tissue. The development of probes with both tumor imaging and targeting functions makes it possible to use a single agent to treat the tumor tissue under the guidance of tumor imaging.

A thio derivative of glucose was conjugated with photosensitizer tetra(pentafluorophenyl) porphyrin, and the resulting conjugate was shown to be actively uptaken by tumor cells via GLUTs and exhibited enhanced photocytotoxicity.[119] Interestingly, glucose conjugation with meta-hydroxyphenyl porphyrin (m-THPP) and meta-hydroxyphenyl chlorin (m-THPC) did not significantly reduce the singlet oxygen yields compared to nonglucosylated photosensitizers,[120] indicating that glucose conjugation of existing photosensitizers could be an effective way to improve tumor cell targeting.

7. Integrin Receptors

Integrins are heterodimeric transmembrane cell-adhesion proteins that promote the attachment and migration of cells to the surrounding extracellular matrix (ECM).[121] They are composed of noncovalently bound α- and β-subunits, the N-terminal domains of which are combined to form a ligand-binding site. Several integrins (e.g., $\alpha_v\beta_3$, $\alpha_v\beta_5$, and $\alpha_5\beta_1$) play important roles in regulating tumor growth, angiogenesis, and metastasis and have been recognized as promising anticancer targets. A phthalocyanine photosensitizer $AlPcS_4$ was covalently conjugated to adenovirus type 2 capsid proteins containing the arginine-glycine-aspartic acid (RGD) motif that is known to have high specificity and affinity to the $\alpha_v\beta_3$ integrin.[122] To minimize the adverse influence of chemical conjugation on the biological activities of the photosensitizer and protein, one or two caproic acid spacer chains were inserted between the photosensitizer and the adenovirus protein. Despite the effort, $AlPcS_4$ and virus protein conjugates were still much lower than the free photosensitizer in singlet oxygen production. Nevertheless, the conjugate with two caproic acid spacer chains was more phototoxic than the conjugate with one caproic acid spacer chain and the free $AlPcS_4$ in human A549 and Hep2 cell lines.

8. Insulin Receptors

The photodynamic targeting of tumor cells can be achieved by targeting the insulin receptor, which is an internalizing cell membrane receptor. Chlorin e6 was covalently coupled to insulin via a BSA carrier.[123–125] The resultant chlorin e6-BSA-insulin conjugate had high-binding affinity for insulin receptors and could be internalized via an active receptor-mediated endocytosis pathway in human hepatoma cell line PLC/PRF/5. Fluores-

cence labeling the conjugate with FITC demonstrated that the conjugate was localized around and within the cell nucleus following endocytosis. The phototoxicity of insulin receptor-targeted sensitizer conjugate was up to 100 times higher than the free chlorin e6, which could be competitively inhibited by receptor ligands.

9. Nuclear Targeting

Because most photosensitizers have low accumulation levels in the cell nucleus, the nucleus is generally not considered as a major target for PDT using common photosensitizers, even though the nucleus is highly sensitive to ROS damage.[126] To obtain nuclear delivery of photosensitizers, Sobolev and colleagues linked variants of the simian virus SV40 large tumor antigen nuclear localization signal (NLS) to the previously mentioned chlorin e6-BSA-insulin conjugate, either by peptide cross-linking to BSA or by encoding the sequence within that of a β-galactosidase fusion-protein carrier.[127,128] The insulin moiety on the conjugate allowed the internalization of conjugate after binding to insulin receptors. Subsequently, the NLS components directed the conjugate to the nucleus. The NLS-chlorin e6-BSA-insulin conjugate dramatically increased the phototoxicity of chlorin e6 in PLC/PRF/5 human hepatoma cells. Chlorin e6 conjugated with β-galactosidase-NLS fusion protein (P10) produced the most phototoxic conjugate, being 2400-fold more cytotoxic than free chlorin e6 and 15-fold more cytotoxic than a NLS-deficient β-galactosidase-(chlorin e6)-insulin construct. This result demonstrates the extraordinary potency of nuclear targeting.

A bacteria-expressed recombinant transporter that can deliver a photosensitizer to a cancer cell nucleus has been reported.[129] It is comprised of four components: α-melanocyte-stimulating hormone (MSH) as an internalizing cell-specific ligand, the NLS from the SV40 large tumor antigen for nuclear drug delivery, an *E. coli* hemoglobin-like protein (HMP) as a carrier, and an endosomolytic polypeptide from diphtheria toxin (DTox) for endosome disruption following internalization. This DTox-HMP-NLS-MSH construct was shown to specifically deliver photosensitizer bacteriochlorin p6 to the nuclei of MSH receptor-positive M3 mouse melanoma cells, but not MSH receptor-negative mouse fibroblast cells. Consequently, the photocytotoxicity of bacteriochlorin p6-DTox-HMP-NLS-MSH was about 230 times higher than that of free bacteriochlorin p6 (IC_{50}: 22 nm versus 4990 nm) in the MSH receptor-overexpressing mouse B16-F1 melanoma cells, whereas it was not phototoxic at all in MSH receptor-negative cells. Interestingly, the construct lacking an endosomolytic moiety DTox or NLS was about 5 and 35 times less effective, respectively, than the complete construct, confirming the importance of nuclear targeting by PDT.

Since steroid hormone receptors are nuclear receptors, conjugating photosensitizers with steroid hormones provides another possibility of targeting the cell nucleus. A conjugate of a C(11)-beta-derivative of estradiol and an asymmetric tetraphenylporphyrin has been synthesized to target estrogen receptor-overexpressing breast tumor cells.[130,131] A radioligand-binding assay indicated that this conjugate was able to bind to estrogen receptors in a dose-dependent manner, even though the binding affinity was about 274 times less than the natural ligand estradiol. Cellular uptake of photosensitizer-estradiol conjugate was significantly higher in the estrogen receptor-positive MCF-7 human breast cancer cells than the receptor-negative HS578t cells and could be competitively inhibited by co-incubation with estradiol. These results indicate that photosensitizer steroid hormone conjugates can be used to target hormone-sensitive cancers, such as breast, ovarian, and prostate cancers.

V. CONCLUSIONS AND FUTURE RESEARCH DIRECTIONS

Clearly, PDT is being actively pursued for targeting either tumor vasculature or cells. Numerous new photosensitizer conjugates have been constructed to target various cellular markers on tumor or endothelial cells. However, few of these new constructs are close to the clinical trial stage. For many photosensitizer conjugates, drug development is unfortunately limited to the stage of in vitro testing. A number of factors related to photosensitizing agents, targeting molecules, and

tumor tissues are responsible for this formidable fact. First, for most hydrophobic photosensitizers, the strong tendency of aggregation makes chemical conjugation and purification difficult. Factors like aggregation of not only photosensitizers but also photosensitizer-targeting molecules and a lack of conjugate stability could certainly compromise drug analysis, pharmacokinetic properties, and biological efficacy. Second, chemical manipulations on targeting molecules (e.g., antibodies, ligands) required for conjugation procedures often result in decreased affinity to their intended tumor marker targets and increased nonspecific interactions, as shown in many previous studies. Third, all the tumor or endothelial cell markers discovered so far are not exclusively expressed on the target cells. They are also expressed on normal cells, although to a lower extent. Moreover, the expression of tumor and endothelial cell markers are neither stable nor homogeneous. These factors will inevitably affect the specificity and efficacy of targeted PDT. Finally, tumor tissues tend to generate various physiological barriers (e.g., heterogeneity in vascular permeability and perfusion, high interstitial pressure), which will further decrease the effectiveness of targeted therapy by limiting the uptake and penetration of targeting molecules.

Being relatively simple in principle and photosensitizer production, passive vascular-targeting PDT using nonconjugated photosensitizers is effective in avoiding some major problems associated with the active targeting PDT mentioned above, and this approach has demonstrated a superior therapeutic advantage in both preclinical and clinical studies. As a result, passive vascular-targeting PDT has been accepted in medical practice, and more regulatory approvals are expected in the near future. The vascular-targeting approach offers several unique advantages in target accessibility and targeting efficiency over the tumor cellular-targeting strategy. With the advent of more and more tumor vascular markers, the active photodynamic vascular-targeting approach, which is currently emerging, will certainly bear fruit in the future.

It may be the case that vascular targeting alone will not be enough to completely eradicate tumor tissue.[15] The combination of tumor vascular and cellular targeting is likely to be a more practical way of achieving tumor control. Several approaches, such as the combined PDT using both vascular-targeting and cellular-targeting photosensitizers,[132] photosensitizer dose fractionation in vascular and cellular compartments,[133] and temporal PDT targeting of tumor cells and vasculature[22] have all been proposed to target both tumor blood vessels and tumor cells for an enhanced therapeutic outcome. With the development of more targeted photosensitizer agents, the possible synergism from the combination of active PDT targeting of tumor vasculature and tumor cells should be explored.

Finally, recent advances in nanotechnology provide a tremendous momentum to construct multifunctional nanophotomedicine platforms.[134] Photosensitizers can be incorporated into various polymeric nanoparticles or nanodevices modified with both tumor imaging and targeting moieties. The resultant nanophotomedicines could serve as both a tumor diagnostic and targeted therapeutic agent. More importantly, these nano drug delivery systems can be specially fabricated to have multiple targeting capabilities and controlled drug release triggered by tumor pathological environment factors (e.g., pH, enzyme activities), magnetic field, and light. The construction of such multifunction and multitargeting nanophotomedicines may allow tumor imaging, targeted tumor therapy, and therapeutic response monitoring in one single entity.

ACKNOWLEDGMENTS

This work was supported by Department of Defense (DOD) Grant W81XWH-06-1-0148 and National Cancer Institute Grant PO1CA84203.

REFERENCES

1. Dougherty TJ, Gomer CJ, Henderson BW, Jori G, Kessel D, Korbelik M, Moan J, Peng Q. Photodynamic therapy. J Natl Cancer Inst. 1998;90:889–905.
2. Schmidt R. Photosensitized generation of singlet oxygen. Photochem Photobiol. 2006;82:1161–77.
3. Moan J, Wold E. Detection of singlet oxygen production by ESR. Nature. 1979;279:450–1.
4. Niedre MJ, Yu CS, Patterson MS, Wilson BC. Singlet oxygen luminescence as an in vivo photodynamic

therapy dose metric: validation in normal mouse skin with topical amino-levulinic acid. Br J Cancer. 2005;92:298–304.
5. Detty MR, Gibson SL, Wagner SJ. Current clinical and preclinical photosensitizers for use in photodynamic therapy. J Med Chem. 2004;47:3897–915.
6. Konan YN, Gurny R, Allemann E. State of the art in the delivery of photosensitizers for photodynamic therapy. J Photochem Photobiol B. 2002;66:89–106.
7. Hsi RA, Rosenthal DI, Glatstein E. Photodynamic therapy in the treatment of cancer: current state of the art. Drugs. 1999;57:725–34.
8. Boyle RW, Dolphin D. Structure and biodistribution relationships of photodynamic sensitizers. Photochem Photobiol. 1996;64:469–85.
9. Nadeau V, O'Dwyer M, Hamdan K, Tait I, Padgett M. In vivo measurement of 5-aminolaevulinic acid-induced protoporphyrin IX photobleaching: a comparison of red and blue light of various intensities. Photodermatol Photoimmunol Photomed. 2004;20: 170–4.
10. Henderson BW, Busch TM, Snyder JW. Fluence rate as a modulator of PDT mechanisms. Lasers Surg Med. 2006;38:489–93.
11. Henderson BW, Dougherty TJ. How does photodynamic therapy work? Photochem Photobiol. 1992;55: 145–57.
12. Foster TH, Hartley DF, Nichols MG, Hilf R. Fluence rate effects in photodynamic therapy of multicell tumor spheroids. Cancer Res. 1993;53:1249–54.
13. Foster TH, Murant RS, Bryant RG, Knox RS, Gibson SL, Hilf R. Oxygen consumption and diffusion effects in photodynamic therapy. Radiat Res. 1991;126: 296–303.
14. Siemann DW, Bibby MC, Dark GG, Dicker AP, Eskens FA, Horsman MR, Marme D, Lorusso PM. Differentiation and definition of vascular-targeted therapies. Clin Cancer Res. 2005;11:416–20.
15. Siemann DW, Chaplin DJ, Horsman MR. Vascular-targeting therapies for treatment of malignant disease. Cancer. 2004;100:2491–9.
16. Sharman WM, van Lier JE, Allen CM. Targeted photodynamic therapy via receptor mediated delivery systems. Adv Drug Deliv Rev. 2004;56:53–76.
17. Schmidt-Erfurth U, Hasan T. Mechanisms of action of photodynamic therapy with verteporfin for the treatment of age-related macular degeneration. Surv Ophthalmol. 2000;45:195–214.
18. Richter AM, Waterfield E, Jain AK, Canaan AJ, Allison BA, Levy JG. Liposomal delivery of a photosensitizer, benzoporphyrin derivative monoacid ring A (BPD), to tumor tissue in a mouse tumor model. Photochem Photobiol. 1993;57:1000–6.
19. Allison BA, Pritchard PH, Levy JG. Evidence for low-density lipoprotein receptor-mediated uptake of benzoporphyrin derivative. Br J Cancer. 1994;69: 833–9.
20. Kramer M, Miller JW, Michaud N, Moulton RS, Hasan T, Flotte TJ, Gragoudas ES. Liposomal benzoporphyrin derivative verteporfin photodynamic therapy. Selective treatment of choroidal neovascularization in monkeys. Ophthalmology. 1996; 103:427–38.
21. Chen B, Pogue BW, Goodwin IA, O'Hara JA, Wilmot CM, Hutchins JE, Hoopes PJ, Hasan T. Blood flow dynamics after photodynamic therapy with verteporfin in the RIF-1 tumor. Radiat Res. 2003; 160:452–9.
22. Chen B, Pogue BW, Hoopes PJ, Hasan T. Combining vascular and cellular targeting regimens enhances the efficacy of photodynamic therapy. Int J Radiat Oncol Biol Phys. 2005;61:1216–26.
23. Fingar VH, Kik PK, Haydon PS, Cerrito PB, Tseng M, Abang E, Wieman TJ. Analysis of acute vascular damage after photodynamic therapy using benzoporphyrin derivative (BPD). Br J Cancer. 1999;79: 1702–8.
24. Kurohane K, Tominaga A, Sato K, North JR, Namba Y, Oku N. Photodynamic therapy targeted to tumor-induced angiogenic vessels. Cancer Lett. 2001;167: 49–56.
25. Chen B, Pogue BW, Luna JM, Hardman RL, Hoopes PJ, Hasan T. Tumor vascular permeabilization by vascular-targeting photosensitization: effects, mechanism, and therapeutic implications. Clin Cancer Res. 2006;12:917–23.
26. Cramers P, Ruevekamp M, Oppelaar H, Dalesio O, Baas P, Stewart FA. Foscan uptake and tissue distribution in relation to photodynamic efficacy. Br J Cancer. 2003;88:283–90.
27. Triesscheijn M, Ruevekamp M, Aalders M, Baas P, Stewart FA. Outcome of mTHPC mediated photodynamic therapy is primarily determined by the vascular response. Photochem Photobiol. 2005;81: 1161–7.
28. Veenhuizen RB, Oppelaar H, Ruevekamp M, Schellens J, Dalesio O, Stewart FA. Does tumor uptake of Foscan determine PDT efficacy? Int J Cancer. 1997;73:236–9.
29. Veenhuizen RB, Ruevekamp MC, Oppelaar H, Helmerhorst TJ, Kenemans P, Stewart FA. Foscan-mediated photodynamic therapy for a peritoneal-cancer model: drug distribution and efficacy studies. Int J Cancer. 1997;73:230–5.
30. Weersink RA, Forbes J, Bisland S, Trachtenberg J, Elhilali M, Brun PH, Wilson BC. Assessment of cutaneous photosensitivity of TOOKAD (WST09) in preclinical animal models and in patients. Photochem Photobiol. 2005;81:106–13.
31. Chen Q, Huang Z, Luck D, Beckers J, Brun PH, Wilson BC, Scherz A, Salomon Y, Hetzel FW. Preclinical studies in normal canine prostate of a novel palladium-bacteriopheophorbide (WST09) photosensitizer for photodynamic therapy of prostate cancers. Photochem Photobiol. 2002;76:438–45.
32. Weersink RA, Bogaards A, Gertner M, Davidson SR, Zhang K, Netchev G, Trachtenberg J, Wilson BC. Techniques for delivery and monitoring of TOOKAD

(WST09)-mediated photodynamic therapy of the prostate: clinical experience and practicalities. J Photochem Photobiol B. 2005;79:211–22.
33. Woodhams JH, MacRobert AJ, Novelli M, Bown SG. Photodynamic therapy with WST09 (Tookad): quantitative studies in normal colon and transplanted tumours. Int J Cancer. 2006;118:477–82.
34. Koudinova NV, Pinthus JH, Brandis A, Brenner O, Bendel P, Ramon J, Eshhar Z, Scherz A, Salomon Y. Photodynamic therapy with Pd-Bacteriopheophorbide (TOOKAD): successful in vivo treatment of human prostatic small cell carcinoma xenografts. Int J Cancer. 2003;104:782–9.
35. Reinke MH, Canakis C, Husain D, Michaud N, Flotte TJ, Gragoudas ES, Miller JW. Verteporfin photodynamic therapy retreatment of normal retina and choroid in the cynomolgus monkey. Ophthalmology. 1999;106:1915–23.
36. Miller JW, Schmidt-Erfurth U, Sickenberg M, Pournaras CJ, Laqua H, Barbazetto I, Zografos L, Piguet B, Donati G, Lane AM, Birngruber R, van den Berg H, Strong A, Manjuris U, Gray T, Fsadni M, Bressler NM, Gragoudas ES. Photodynamic therapy with verteporfin for choroidal neovascularization caused by age-related macular degeneration: results of a single treatment in a phase 1 and 2 study. Arch Ophthalmol. 1999;117:1161–73.
37. Jain RK. Normalization of tumor vasculature: an emerging concept in antiangiogenic therapy. Science. 2005;307:58–62.
38. Borle F, Radu A, Fontolliet C, van den Bergh H, Monnier P, Wagnieres G. Selectivity of the photosensitiser Tookad for photodynamic therapy evaluated in the Syrian golden hamster cheek pouch tumour model. Br J Cancer. 2003;89:2320–6.
39. Baluk P, Hashizume H, McDonald DM. Cellular abnormalities of blood vessels as targets in cancer. Curr Opin Genet Dev. 2005;15:102–11.
40. McDonald DM, Choyke PL. Imaging of angiogenesis: from microscope to clinic. Nat Med. 2003;9:713–25.
41. Szala S. Two-domain vascular disruptive agents in cancer therapy. Curr Cancer Drug Targets. 2004;4: 501–9.
42. Kalluri R. Basement membranes: structure, assembly and role in tumour angiogenesis. Nat Rev Cancer. 2003;3:422–33.
43. Borsi L, Balza E, Carnemolla B, Sassi F, Castellani P, Berndt A, Kosmehl H, Biro A, Siri A, Orecchia P, Grassi J, Neri D, Zardi L. Selective targeted delivery of TNFalpha to tumor blood vessels. Blood. 2003; 102:4384–92.
44. Santimaria M, Moscatelli G, Viale GL, Giovannoni L, Neri G, Viti F, Leprini A, Borsi L, Castellani P, Zardi L, Neri D, Riva P. Immunoscintigraphic detection of the ED-B domain of fibronectin, a marker of angiogenesis, in patients with cancer. Clin Cancer Res. 2003;9:571–9.
45. Birchler M, Viti F, Zardi L, Spiess B, Neri D. Selective targeting and photocoagulation of ocular angiogenesis mediated by a phage-derived human antibody fragment. Nat Biotechnol. 1999;17:984–8.
46. Renno RZ, Terada Y, Haddadin MJ, Michaud NA, Gragoudas ES, Miller JW. Selective photodynamic therapy by targeted verteporfin delivery to experimental choroidal neovascularization mediated by a homing peptide to vascular endothelial growth factor receptor-2. Arch Ophthalmol. 2004;122:1002–11.
47. Perret GY, Starzec A, Hauet N, Vergote J, Le Pecheur M, Vassy R, Leger G, Verbeke KA, Bormans G, Nicolas P, Verbruggen AM, Moretti JL. In vitro evaluation and biodistribution of a 99mTc-labeled anti-VEGF peptide targeting neuropilin-1. Nucl Med Biol. 2004;31:575–81.
48. Chen C, Li M, Chai H, Yang H, Fisher WE, Yao Q. Roles of neuropilins in neuronal development, angiogenesis, and cancers. World J Surg. 2005;29:271–5.
49. Tirand L, Frochot C, Vanderesse R, Thomas N, Trinquet E, Pinel S, Viriot ML, Guillemin F, Barberi-Heyob M. A peptide competing with VEGF165 binding on neuropilin-1 mediates targeting of a chlorin-type photosensitizer and potentiates its photodynamic activity in human endothelial cells. J Control Release. 2006;111:153–64.
50. Ichikawa K, Hikita T, Maeda N, Yonezawa S, Takeuchi Y, Asai T, Namba Y, Oku N. Antiangiogenic photodynamic therapy (PDT) by using long-circulating liposomes modified with peptide specific to angiogenic vessels. Biochim Biophys Acta. 2005;1669: 69–74.
51. Fried NM. Therapeutic applications of lasers in urology: an update. Expert Rev Med Devices. 2006; 3:81–94.
52. Panjehpour M, Overholt BF, Haydek JM. Light sources and delivery devices for photodynamic therapy in the gastrointestinal tract. Gastrointest Endosc Clin N Am. 2000;10:513–32.
53. Haylett AK, Higley K, Chiu M, Shackley DC, Moore JV. Collagen secretion after photodynamic therapy versus scar-inducing anti-cancer modalities: an in vitro study. Photochem Photobiol Sci. 2002;1:673–7.
54. Chang SC, Buonaccorsi G, MacRobert A, Bown SG. Interstitial and transurethral photodynamic therapy of the canine prostate using meso-tetra-(m-hydroxyphenyl) chlorin. Int J Cancer. 1996;67:555–62.
55. Hopper C. Photodynamic therapy: a clinical reality in the treatment of cancer. Lancet Oncol. 2000;1:212–9.
56. Maeda H. The enhanced permeability and retention (EPR) effect in tumor vasculature: the key role of tumor-selective macromolecular drug targeting. Adv Enzyme Regul. 2001;41:189–207.
57. Jori G, Reddi E. The role of lipoproteins in the delivery of tumour-targeting photosensitizers. Int J Biochem. 1993;25:1369–75.
58. Allen CM, Langlois R, Sharman WM, La Madeleine C, Van Lier JE. Photodynamic properties of amphiphilic derivatives of aluminum tetrasulfophthalocyanine. Photochem Photobiol. 2002;76:208–16.
59. Van de Putte M, Roskams T, Vandenheede JR,

Agostinis P, de Witte PA. Elucidation of the tumoritropic principle of hypericin. Br J Cancer. 2005;92: 1406–13.
60. Sheyhedin I, Aizawa K, Araake M, Kumasaka H, Okunaka T, Kato H. The effects of serum on cellular uptake and phototoxicity of mono-L-aspartyl chlorin e6 (NPe6) in vitro. Photochem Photobiol. 1998;68: 110–4.
61. Mori M, Kuroda T, Obana A, Sakata I, Hirano T, Nakajima S, Hikida M, Kumagai T. In vitro plasma protein binding and cellular uptake of ATX-S10(Na), a hydrophilic chlorin photosensitizer. Jpn J Cancer Res. 2000;91:845–52.
62. Kessel D, Whitcomb KL, Schulz V. Lipoprotein-mediated distribution of N-aspartyl chlorin-E6 in the mouse. Photochem Photobiol. 1992;56:51–6.
63. Almeida RD, Manadas BJ, Carvalho AP, Duarte CB. Intracellular signaling mechanisms in photodynamic therapy. Biochim Biophys Acta. 2004;1704:59–86.
64. Piette J, Volanti C, Vantieghem A, Matroule JY, Habraken Y, Agostinis P. Cell death and growth arrest in response to photodynamic therapy with membrane-bound photosensitizers. Biochem Pharmacol. 2003;66: 1651–9.
65. Ferrario A, Fisher AM, Rucker N, Gomer CJ. Celecoxib and NS-398 enhance photodynamic therapy by increasing in vitro apoptosis and decreasing in vivo inflammatory and angiogenic factors. Cancer Res. 2005;65:9473–8.
66. Mew D, Wat CK, Towers GH, Levy JG. Photoimmunotherapy: treatment of animal tumors with tumor-specific monoclonal antibody-hematoporphyrin conjugates. J Immunol. 1983;130:1473–7.
67. Mew D, Lum V, Wat CK, Towers GH, Sun CH, Walter RJ, Wright W, Berns MW, Levy JG. Ability of specific monoclonal antibodies and conventional antisera conjugated to hematoporphyrin to label and kill selected cell lines subsequent to light activation. Cancer Res. 1985;45:4380–6.
68. Pogrebniak HW, Matthews W, Black C, Russo A, Mitchell JB, Smith P, Roth JA, Pass HI. Targetted phototherapy with sensitizer-monoclonal antibody conjugate and light. Surg Oncol. 1993;2:31–42.
69. Oseroff AR, Ohuoha D, Hasan T, Bommer JC, Yarmush ML. Antibody-targeted photolysis: selective photodestruction of human T-cell leukemia cells using monoclonal antibody-chlorin e6 conjugates. Proc Natl Acad Sci U S A. 1986;83:8744–8.
70. Oseroff AR, Ara G, Ohuoha D, Aprille J, Bommer JC, Yarmush ML, Foley J, Cincotta L. Strategies for selective cancer photochemotherapy: antibody-targeted and selective carcinoma cell photolysis. Photochem Photobiol. 1987;46:83–96.
71. Jiang FN, Jiang S, Liu D, Richter A, Levy JG. Development of technology for linking photosensitizers to a model monoclonal antibody. J Immunol Methods. 1990;134:139–49.
72. Jiang FN, Liu DJ, Neyndorff H, Chester M, Jiang SY, Levy JG. Photodynamic killing of human squamous cell carcinoma cells using a monoclonal antibody-photosensitizer conjugate. J Natl Cancer Inst. 1991;83:1218–25.
73. Jiang FN, Richter AM, Jain AK, Levy JG, Smits C. Biodistribution of a benzoporphyrin derivative-monoclonal antibody conjugate in A549-tumor-bearing nude mice. Biotechnol Ther. 1993;4:43–61.
74. Goff BA, Bamberg M, Hasan T. Photoimmunotherapy of human ovarian carcinoma cells ex vivo. Cancer Res. 1991;51:4762–7.
75. Goff BA, Hermanto U, Rumbaugh J, Blake J, Bamberg M, Hasan T. Photoimmunotherapy and biodistribution with an OC125-chlorin immunoconjugate in an in vivo murine ovarian cancer model. Br J Cancer. 1994;70:474–80.
76. Goff BA, Blake J, Bamberg MP, Hasan T. Treatment of ovarian cancer with photodynamic therapy and immunoconjugates in a murine ovarian cancer model. Br J Cancer. 1996;74:1194–8.
77. Hamblin MR, Miller JL, Hasan T. Effect of charge on the interaction of site-specific photoimmunoconjugates with human ovarian cancer cells. Cancer Res. 1996;56:5205–10.
78. Duska LR, Hamblin MR, Bamberg MP, Hasan T. Biodistribution of charged F(ab')2 photoimmunoconjugates in a xenograft model of ovarian cancer. Br J Cancer. 1997;75:837–44.
79. Molpus KL, Hamblin MR, Rizvi I, Hasan T. Intraperitoneal photoimmunotherapy of ovarian carcinoma xenografts in nude mice using charged photoimmunoconjugates. Gynecol Oncol. 2000;76:397–404.
80. Del Governatore M, Hamblin MR, Piccinini EE, Ugolini G, Hasan T. Targeted photodestruction of human colon cancer cells using charged 17.1A chlorin e6 immunoconjugates. Br J Cancer. 2000;82:56–64.
81. Hamblin MR, Del Governatore M, Rizvi I, Hasan T. Biodistribution of charged 17.1A photoimmunoconjugates in a murine model of hepatic metastasis of colorectal cancer. Br J Cancer. 2000;83:1544–51.
82. Del Governatore M, Hamblin MR, Shea CR, Rizvi I, Molpus KG, Tanabe KK, Hasan T. Experimental photoimmunotherapy of hepatic metastases of colorectal cancer with a 17.1A chlorin(e6) immunoconjugate. Cancer Res. 2000;60:4200–5.
83. Rakestraw SL, Tompkins RG, Yarmush ML. Antibody-targeted photolysis: in vitro studies with Sn(IV) chlorin e6 covalently bound to monoclonal antibodies using a modified dextran carrier. Proc Natl Acad Sci U S A. 1990;87:4217–21.
84. Rakestraw SL, Tompkins RG, Yarmush ML. Preparation and characterization of immunoconjugates for antibody-targeted photolysis. Bioconjug Chem. 1990; 1:212–21.
85. Rakestraw SL, Ford WE, Tompkins RG, Rodgers MA, Thorpe WP, Yarmush ML. Antibody-targeted photolysis: in vitro immunological, photophysical, and cytotoxic properties of monoclonal antibody-dextran-Sn(IV) chlorin e6 immunoconjugates. Biotechnol Prog. 1992;8:30–9.

86. Hu LK, Hasan T, Gragoudas ES, Young LH. Photoimmunotherapy of human uveal melanoma cells. Exp Eye Res. 1995;61:385–91.
87. Carcenac M, Larroque C, Langlois R, van Lier JE, Artus JC, Pelegrin A. Preparation, phototoxicity and biodistribution studies of anti-carcinoembryonic antigen monoclonal antibody-phthalocyanine conjugates. Photochem Photobiol. 1999;70:930–6.
88. Hanahan D, Weinberg RA. The hallmarks of cancer. Cell. 2000;100:57–70.
89. Soukos NS, Hamblin MR, Keel S, Fabian RL, Deutsch TF, Hasan T. Epidermal growth factor receptor-targeted immunophotodiagnosis and photoimmunotherapy of oral precancer in vivo. Cancer Res. 2001;61:4490–6.
90. Gijsens A, De Witte P. Photocytotoxic action of EGF-PVA-Sn(IV)chlorin e6 and EGF-dextran-Sn(IV)chlorin e6 internalizable conjugates on A431 cells. Int J Oncol. 1998;13:1171–7.
91. Gijsens A, Missiaen L, Merlevede W, de Witte P. Epidermal growth factor-mediated targeting of chlorin e6 selectively potentiates its photodynamic activity. Cancer Res. 2000;60:2197–202.
92. Savellano MD, Hasan T. Targeting cells that overexpress the epidermal growth factor receptor with polyethylene glycolated BPD verteporfin photosensitizer immunoconjugates. Photochem Photobiol. 2003;77:431–9.
93. Savellano MD, Hasan T. Photochemical targeting of epidermal growth factor receptor: a mechanistic study. Clin Cancer Res. 2005;11:1658–68.
94. Hemming AW, Davis NL, Dubois B, Quenville NF, Finley RJ. Photodynamic therapy of squamous cell carcinoma. An evaluation of a new photosensitizing agent, benzoporphyrin derivative and new photoimmunoconjugate. Surg Oncol. 1993;2:187–96.
95. Vrouenraets MB, Visser GW, Stewart FA, Stigter M, Oppelaar H, Postmus PE, Snow GB, van Dongen GA. Development of meta-tetrahydroxyphenylchlorin-monoclonal antibody conjugates for photoimmunotherapy. Cancer Res. 1999;59:1505–13.
96. Carcenac M, Dorvillius M, Garambois V, Glaussel F, Larroque C, Langlois R, Hynes NE, van Lier JE, Pelegrin A. Internalisation enhances photo-induced cytotoxicity of monoclonal antibody-phthalocyanine conjugates. Br J Cancer. 2001;85:1787–93.
97. Hudson R, Carcenac M, Smith K, Madden L, Clarke OJ, Pelegrin A, Greenman J, Boyle RW. The development and characterisation of porphyrin isothiocyanate-monoclonal antibody conjugates for photoimmunotherapy. Br J Cancer. 2005;92:1442–9.
98. Vrouenraets MB, Visser GW, Loup C, Meunier B, Stigter M, Oppelaar H, Stewart FA, Snow GB, van Dongen GA. Targeting of a hydrophilic photosensitizer by use of internalizing monoclonal antibodies: a new possibility for use in photodynamic therapy. Int J Cancer. 2000;88:108–14.
99. Vrouenraets MB, Visser GW, Stigter M, Oppelaar H, Snow GB, van Dongen GA. Targeting of aluminum (III) phthalocyanine tetrasulfonate by use of internalizing monoclonal antibodies: improved efficacy in photodynamic therapy. Cancer Res. 2001;61:1970–5.
100. Vrouenraets MB, Visser GW, Stigter M, Oppelaar H, Snow GB, van Dongen GA. Comparison of aluminium (III) phthalocyanine tetrasulfonate- and meta-tetrahydroxyphenylchlorin-monoclonal antibody conjugates for their efficacy in photodynamic therapy in vitro. Int J Cancer. 2002;98:793–8.
101. Savellano MD, Pogue BW, Hoopes PJ, Vitetta ES, Paulsen KD. Multiepitope HER2 targeting enhances photoimmunotherapy of HER2-overexpressing cancer cells with pyropheophorbide-a immunoconjugates. Cancer Res. 2005;65:6371–9.
102. Chung NS, Wasan KM. Potential role of the low-density lipoprotein receptor family as mediators of cellular drug uptake. Adv Drug Deliv Rev. 2004;56:1315–34.
103. Hamblin MR, Newman EL. Photosensitizer targeting in photodynamic therapy. II. Conjugates of haematoporphyrin with serum lipoproteins. J Photochem Photobiol B. 1994;26:147–57.
104. Schmidt-Erfurth U, Diddens H, Birngruber R, Hasan T. Photodynamic targeting of human retinoblastoma cells using covalent low-density lipoprotein conjugates. Br J Cancer. 1997;75:54–61.
105. Zheng G, Li H, Zhang M, Lund-Katz S, Chance B, Glickson JD. Low-density lipoprotein reconstituted by pyropheophorbide cholesteryl oleate as target-specific photosensitizer. Bioconjug Chem. 2002;13:392–6.
106. Li H, Marotta DE, Kim S, Busch TM, Wileyto EP, Zheng G. High payload delivery of optical imaging and photodynamic therapy agents to tumors using phthalocyanine-reconstituted low-density lipoprotein nanoparticles. J Biomed Opt. 2005;10:41203.
107. Singh M. Transferrin as a targeting ligand for liposomes and anticancer drugs. Curr Pharm Des. 1999;5:443–51.
108. Hamblin MR, Newman EL. Photosensitizer targeting in photodynamic therapy. I. Conjugates of haematoporphyrin with albumin and transferrin. J Photochem Photobiol B. 1994;26:45–56.
109. Cavanaugh PG. Synthesis of chlorin e6-transferrin and demonstration of its light-dependent in vitro breast cancer cell killing ability. Breast Cancer Res Treat. 2002;72:117–30.
110. Gijsens A, Derycke A, Missiaen L, De Vos D, Huwyler J, Eberle A, de Witte P. Targeting of the photocytotoxic compound AlPcS4 to Hela cells by transferrin conjugated PEG-liposomes. Int J Cancer. 2002;101:78–85.
111. Derycke AS, Kamuhabwa A, Gijsens A, Roskams T, De Vos D, Kasran A, Huwyler J, Missiaen L, de Witte PA. Transferrin-conjugated liposome targeting of photosensitizer AlPcS4 to rat bladder carcinoma cells. J Natl Cancer Inst. 2004;96:1620–30.
112. Derycke AS, De Witte PA. Transferrin-mediated

targeting of hypericin embedded in sterically stabilized PEG-liposomes. Int J Oncol. 2002;20:181–7.
113. Lu Y, Low PS. Folate-mediated delivery of macromolecular anticancer therapeutic agents. Adv Drug Deliv Rev. 2002;54:675–93.
114. Schneider R, Schmitt F, Frochot C, Fort Y, Lourette N, Guillemin F, Muller JF, Barberi-Heyob M. Design, synthesis, and biological evaluation of folic acid targeted tetraphenylporphyrin as novel photosensitizers for selective photodynamic therapy. Bioorg Med Chem. 2005;13:2799–808.
115. Qualls MM, Thompson DH. Chloroaluminum phthalocyanine tetrasulfonate delivered via acid-labile diplasmenylcholine-folate liposomes: intracellular localization and synergistic phototoxicity. Int J Cancer. 2001;93:384–92.
116. Zheng G, Chen J, Li H, Glickson JD. Rerouting lipoprotein nanoparticles to selected alternate receptors for the targeted delivery of cancer diagnostic and therapeutic agents. Proc Natl Acad Sci U S A. 2005;102:17757–62.
117. Medina RA, Owen GI. Glucose transporters: expression, regulation and cancer. Biol Res. 2002;35:9–26.
118. Zhang M, Zhang Z, Blessington D, Li H, Busch TM, Madrak V, Miles J, Chance B, Glickson JD, Zheng G. Pyropheophorbide 2-deoxyglucosamide: a new photosensitizer targeting glucose transporters. Bioconjug Chem. 2003;14:709–14.
119. Chen X, Hui L, Foster DA, Drain CM. Efficient synthesis and photodynamic activity of porphyrin-saccharide conjugates: targeting and incapacitating cancer cells. Biochemistry. 2004;43:10918–29.
120. Bautista-Sanchez A, Kasselouri A, Desroches MC, Blais J, Maillard P, de Oliveira DM, Tedesco AC, Prognon P, Delaire J. Photophysical properties of glucoconjugated chlorins and porphyrins and their associations with cyclodextrins. J Photochem Photobiol B. 2005;81:154–62.
121. Jin H, Varner J. Integrins: roles in cancer development and as treatment targets. Br J Cancer. 2004;90:561–5.
122. Allen CM, Sharman WM, La Madeleine C, Weber JM, Langlois R, Ouellet R, van Lier JE. Photodynamic therapy: tumor targeting with adenoviral proteins. Photochem Photobiol. 1999;70:512–23.
123. Sobolev AS, Akhlynina TV, Yachmenev SV, Rosenkranz AA, Severin ES. Internalizable insulin-BSA-chlorin E6 conjugate is a more effective photosensitizer than chlorin E6 alone. Biochem Int. 1992;26:445–50.
124. Akhlynina TV, Rosenkranz AA, Jans DA, Gulak PV, Serebryakova NV, Sobolev AS. The use of internalizable derivatives of chlorin E6 for increasing its photosensitizing activity. Photochem Photobiol. 1993;58:45–8.
125. Akhlynina TV, Rosenkranz AA, Jans DA, Sobolev AS. Insulin-mediated intracellular targeting enhances the photodynamic activity of chlorin e6. Cancer Res. 1995;55:1014–9.
126. Rosenkranz AA, Jans DA, Sobolev AS. Targeted intracellular delivery of photosensitizers to enhance photodynamic efficiency. Immunol Cell Biol. 2000;78:452–64.
127. Akhlynina TV, Jans DA, Rosenkranz AA, Statsyuk NV, Balashova IY, Toth G, Pavo I, Rubin AB, Sobolev AS. Nuclear targeting of chlorin e6 enhances its photosensitizing activity. J Biol Chem. 1997;272:20328–31.
128. Akhlynina TV, Jans DA, Statsyuk NV, Balashova IY, Toth G, Pavo I, Rosenkranz AA, Naroditsky BS, Sobolev AS. Adenoviruses synergize with nuclear localization signals to enhance nuclear delivery and photodynamic action of internalizable conjugates containing chlorin e6. Int J Cancer. 1999;81:734–40.
129. Rosenkranz AA, Lunin VG, Gulak PV, Sergienko OV, Shumiantseva MA, Voronina OL, Gilyazova DG, John AP, Kofner AA, Mironov AF, Jans DA, Sobolev AS. Recombinant modular transporters for cell-specific nuclear delivery of locally acting drugs enhance photosensitizer activity. FASEB J. 2003;17:1121–3.
130. James DA, Swamy N, Paz N, Hanson RN, Ray R. Synthesis and estrogen receptor binding affinity of a porphyrin-estradiol conjugate for targeted photodynamic therapy of cancer. Bioorg Med Chem Lett. 1999;9:2379–84.
131. Swamy N, James DA, Mohr SC, Hanson RN, Ray R. An estradiol-porphyrin conjugate selectively localizes into estrogen receptor-positive breast cancer cells. Bioorg Med Chem. 2002;10:3237–43.
132. Peng Q, Warloe T, Moan J, Godal A, Apricena F, Giercksky KE, Nesland JM. Antitumor effect of 5-aminolevulinic acid-mediated photodynamic therapy can be enhanced by the use of a low dose of photofrin in human tumor xenografts. Cancer Res. 2001;61:5824–32.
133. Dolmans DE, Kadambi A, Hill JS, Flores KR, Gerber JN, Walker JP, Borel Rinkes IH, Jain RK, Fukumura D. Targeting tumor vasculature and cancer cells in orthotopic breast tumor by fractionated photosensitizer dosing photodynamic therapy. Cancer Res. 2002;62:4289–94.
134. Moghimi SM, Hunter AC, Murray JC. Nanomedicine: current status and future prospects. FASEB J. 2005;19:311–30.
135. Moshfeghi DM, Peyman GA, Moshfeghi AA, Khoobehi B, Primbs GB, Crean DH. Ocular vascular thrombosis following tin ethyl etiopurpurin (SnET2) photodynamic therapy: time dependencies. Ophthalmic Surg Lasers. 1998;29:663–8.
136. Primbs GB, Casey R, Wamser K, Snyder WJ, Crean DH. Photodynamic therapy for corneal neovascularization. Ophthalmic Surg Lasers. 1998;29:832–8.
137. Peyman GA, Moshfeghi DM, Moshfeghi A, Khoobehi B, Doiron DR, Primbs GB, Crean DH. Photodynamic therapy for choriocapillaris using tin ethyl etiopurpurin (SnET2). Ophthalmic Surg Lasers. 1997;28:409–17.
138. Criswell MH, Ciulla TA, Lowseth LA, Small W, Danis RP, Carson DL. Anastomotic vessels remain

viable after photodynamic therapy in primate models of choroidal neovascularization. Invest Ophthalmol Vis Sci. 2005;46:2168–74.
139. Woodburn KW, Fan Q, Miles DR, Kessel D, Luo Y, Young SW. Localization and efficacy analysis of the phototherapeutic lutetium texaphyrin (PCI-0123) in the murine EMT6 sarcoma model. Photochem Photobiol. 1997;65:410–5.
140. Blumenkranz MS, Woodburn KW, Qing F, Verdooner S, Kessel D, Miller R. Lutetium texaphyrin (Lu-Tex): a potential new agent for ocular fundus angiography and photodynamic therapy. Am J Ophthalmol. 2000;129:353–62.
141. Miles D, Mody TD, Hatcher LI, Fiene J, Stiles M, Lin PP, Lee JW. Quantitation of motexafin lutetium in human plasma by liquid chromatography-tandem mass spectrometry and inductively coupled plasma-atomic emission spectroscopy. AAPS PharmSci. 2003;5:E23.
142. Gomer CJ, Ferrario A. Tissue distribution and photosensitizing properties of mono-L-aspartyl chlorin e6 in a mouse tumor model. Cancer Res. 1990;50: 3985–90.
143. Saito K, Mikuniya N, Aizawa K. Effects of photodynamic therapy using mono-L-aspartyl chlorin e6 on vessels and its contribution to the antitumor effect. Jpn J Cancer Res. 2000;91:560–5.
144. Nakashizuka T, Mori K, Hayashi N, Anzail K, Kanail K, Yoneya S, Moshfeghi DM, Peyman GA. Retreatment effect of NPe6 photodynamic therapy on the normal primate macula. Retina. 2001;21:493–8.
145. Peyman GA, Kazi AA, Moshfeghi D, Unal M, Khoobehi B, Yoneya S, Mori K, Rivera I. Threshold and retreatment parameters of NPe6 photodynamic therapy in retinal and choroidal vessels. Ophthalmic Surg Lasers. 2000;31:323–7.
146. Mori K, Yoneya S, Anzail K, Kabasawa S, Sodeyama T, Peyman GA, Moshfeghi DM. Photodynamic therapy of experimental choroidal neovascularization with a hydrophilic photosensitizer: mono-L-aspartyl chlorin e6. Retina. 2001;21:499–508.
147. Chan AL, Juarez M, Allen R, Volz W, Albertson T. Pharmacokinetics and clinical effects of mono-L-aspartyl chlorin e6 (NPe6) photodynamic therapy in adult patients with primary or secondary cancer of the skin and mucosal surfaces. Photodermatol Photoimmunol Photomed. 2005;21:72–8.
148. Harada M, Woodhams J, MacRobert AJ, Feneley MR, Kato H, Bown SG. The vascular response to photodynamic therapy with ATX-S10Na(II) in the normal rat colon. J Photochem Photobiol B. 2005; 79:223–30.
149. Obana A, Gohto Y, Kaneda K, Nakajima S, Takemura T, Miki T. Selective occlusion of choroidal neovascularization by photodynamic therapy with a water-soluble photosensitizer, ATX-S10. Lasers Surg Med. 1999;24:209–22.
150. Gohto Y, Obana A, Kanai M, Nagata S, Nakajima S, Miki T. Treatment parameters for selective occlusion of experimental corneal neovascularization by photodynamic therapy using a water soluble photosensitizer, ATX-S10(Na). Exp Eye Res. 2001;72:13–22.
151. Gohto Y, Obana A, Kanai M, Nagata S, Miki T, Nakajima S. Photodynamic therapy for corneal neovascularization using topically administered ATX-S10 (Na). Ophthalmic Surg Lasers. 2000;31:55–60.
152. Glanzmann T, Hadjur C, Zellweger M, Grosiean P, Forrer M, Ballini JP, Monnier P, van den Bergh H, Lim CK, Wagnieres G. Pharmacokinetics of tetra(m-hydroxyphenyl)chlorin in human plasma and individualized light dosimetry in photodynamic therapy. Photochem Photobiol. 1998;67:596–602.
153. Jones HJ, Vernon DI, Brown SB. Photodynamic therapy effect of m-THPC (Foscan) in vivo: correlation with pharmacokinetics. Br J Cancer. 2003;89:398–404.
154. Chen B, Roskams T, de Witte PA. Antivascular tumor eradication by hypericin-mediated photodynamic therapy. Photochem Photobiol. 2002;76:509–13.
155. Chen B, Roskams T, Xu Y, Agostinis P, de Witte PA. Photodynamic therapy with hypericin induces vascular damage and apoptosis in the RIF-1 mouse tumor model. Int J Cancer. 2002;98:284–90.
156. Chen B, Xu Y, Roskams T, Delaey E, Agostinis P, Vandenheede JR, de Witte P. Efficacy of antitumoral photodynamic therapy with hypericin: relationship between biodistribution and photodynamic effects in the RIF-1 mouse tumor model. Int J Cancer. 2001;93:275–82.
157. Chen B, Zupko I, de Witte PA. Photodynamic therapy with hypericin in a mouse P388 tumor model: vascular effects determine the efficacy. Int J Oncol. 2001;18:737–42.
158. Dolmans DE, Fukumura D, Jain RK. Photodynamic therapy for cancer. Nat Rev Cancer. 2003;3:380–7.

Pharmaceutical Research, Vol. 25, No. 8, August 2008 (© 2008)
DOI: 10.1007/s11095-008-9604-5

Research Paper

Intravital Microscopic Analysis of Vascular Perfusion and Macromolecule Extravasation after Photodynamic Vascular Targeting Therapy

Chong He,[1] Priyanka Agharkar,[1] and Bin Chen[1,2,3]

Received February 25, 2008; accepted April 16, 2008; published online April 30, 2008

Purpose. Photodynamic therapy (PDT), involving the combination of a photosensitizer and light, is being evaluated as a vascular disrupting therapy and drug delivery enhancement modality based on its effects on vascular perfusion and barrier function. Since tumor vasculature is the common route for the delivery of both blood and therapeutic agents, it is important to compare the effects of PDT on blood perfusion and substance transport.
Materials and Methods. Tumor blood cell velocity and the extravasation of high molecular weight dextran molecules were continuously monitored by intravital fluorescence microscopy for up to 60 min after PDT using three doses of verteporfin in the MatLyLu prostate tumor model.
Results. PDT induced tumor perfusion disruption via thrombus formation. PDT using a higher dose of verteporfin was more effective in inhibiting blood perfusion while a lower dose verteporfin-PDT was more potent in enhancing dextran extravasation. The increase in dextran extravasation induced by PDT was dependent upon dextran molecular weight. A lower molecular weight dextran obtained a higher tumor accumulation after PDT than a higher molecular weight dextran.
Conclusions. PDT with verteporfin had different effects on tumor vascular perfusion *versus* the extravasation of macromolecules. Optimal PDT conditions should be adjusted based on the therapeutic application.

KEY WORDS: benzoporphyrin derivative (BPD); blood flow; drug delivery; photodynamic therapy (PDT); photosensitizer; vascular permeability; vascular targeting.

INTRODUCTION

Tumor vasculature represents an important target for cancer therapy due to the dependence of tumor cells on a functional blood supply for cell growth, and blood-borne therapeutic agents to get access to tumor tissues (1). On the one hand, tumor blood vessels can be targeted by antiangiogenic and vascular disrupting agents to inhibit tumor progression (2). On the other hand, tumor vascular function can be modified to enhance the delivery of anticancer agents to tumor tissues because tumor vasculature is one of the major physiological barriers for sufficient delivery of therapeutic agents to tumor tissues, especially for macromolecular agents (3). Thus, strategies aimed at specifically disrupting the endothelial barrier integrity are being developed to improve delivery of therapeutic agents to the tumor tissues (4).

Photodynamic therapy (PDT) is an established cancer treatment modality, which involves the combination of a photosensitizing compound, light with a wavelength matching the absorption of photosensitizer, and oxygen molecules (5). Upon absorption of light, photosensitizer molecules are activated from the ground state to the triplet state, which then react with oxygen and produce highly reactive singlet oxygen. The mechanism of PDT is complicated, involving a combined effect of photocytotoxicity, vascular damage and immune reactions (6). Photodynamic vascular targeting therapy aims to selectively target tumor vasculature for therapeutic purposes. In this case, laser light is usually delivered to tumor tissues shortly after systematic administration of a photosensitizer when the drug is predominately localized within blood vessels (7). Preferential photosensitization of vascular components leads to vessel functional changes. This vascular-targeting modality has been approved for the treatment of age-related macular degeneration and is currently under clinical trial for prostate cancer treatment (7).

It was recently reported that PDT can be used to facilitate the delivery of macromolecular agents to tumor tissues via induced vascular leakage (8). We demonstrated in the MatLyLu rat prostate tumor model that vascular-targeting PDT with photosensitizer verteporfin significantly increases vascular permeability and tumor accumulation of circulating molecules (9). However, the same treatment was also found to cause vascular shutdown by inducing thrombus formation, resulting in extensive tumor necrosis. Because tumor vasculature is the common route for the delivery of both blood and therapeutic agents, it is important to understand how

[1] Department of Pharmaceutical Sciences, Philadelphia College of Pharmacy, University of the Sciences in Philadelphia, 600 South 43rd Street, Philadelphia, Pennsylvania 19104, USA.
[2] Department of Radiation Oncology, University of Pennsylvania, Philadelphia, Pennsylvania 19104, USA.
[3] To whom correspondence should be addressed. (e-mail: b.chen@usp.edu)

differently vascular-targeting PDT affects tumor perfusion and vascular barrier functions. Such knowledge is crucial to apply this modality for tumor targeting and anticancer drug delivery enhancement. By permitting high resolution imaging of vessel structure and function in live animals, intravital microscopy offers a powerful tool to study vascular morphology and function (10). Here we used this system to examine changes of vessel perfusion and barrier function after verteporfin-PDT targeting tumor blood vessels in an orthotopic rat prostate tumor model.

MATERIALS AND METHODS

Orthotopic Prostate Tumor Model. The orthotopic R3327-MatLyLu Dunning rat prostate tumor model was used in this study. The MatLyLu tumor is an androgen-independent prostate carcinoma, syngeneic to the male Copenhagen rats, and highly metastatic to lymph nodes and lungs (MatLyLu) (11). The MatLyLu cells were maintained in the RPMI-1640 with glutamine (Mediatech, Herndon, VA) supplemented with 10% fetal bovine serum (HyClone, Logan, UT) and 100 units/ml penicillin-streptomycin (Mediatech) at 37°C in a 5% CO_2 incubator. The orthotopic tumors were induced by injecting 1×10^5 tumor cells in the ventral lobe of prostate in the Copenhagen rats (6–8 weeks old, Charles River Laboratories, Wilmington, MA), as described previously (12). Tumors were used for experiments at 7–8 days after implantation with a size of 8–10 mm in diameter. All animal procedures were carried out according to the NIH Principles of Laboratory Animal Care and approved by the Institutional Animal Care and Use Committee (IACUC).

Photosensitizer. Verteporfin (benzoporphyrin derivative (BPD) monoacid ring A in a lipid-formulation) was obtained from QLT Inc. (Vancouver, Canada) as a gift. A stock saline solution of verteporfin was reconstituted according to the manufacturer's instruction and stored at 4°C in the dark. Stock solution of BPD was diluted right before injection.

PDT Treatments. A diode laser system (High Power Devices Inc., North Brunswick, NJ) with 690 nm wavelength was used for the irradiation of MatLyLu tumors. The laser was coupled to an optical fiber with 600 μm core diameter for light delivery. A microlens was connected to the end of fiber to achieve homogeneous irradiation of a 12 mm-diameter spot. The MatLyLu tumors were surgically exposed to illumination with an irradiance of 50 mW/cm^2 for 1,000 s, resulting in a total light dose of 50 J/cm^2. Light intensity was measured with an optical power meter (Thorlabs Inc, North Newton, NJ). Animals were anesthetized with injection (i.p.) of a mixture of ketamine (90 mg/kg) and xylazine (9 mg/kg) during treatment. Three different doses of verteporfin (0.25, 0.5 and 1.0 mg/kg) were examined, which was always i.v. injected at 15 min prior to light irradiation. We have shown in the previous study that verteporfin is primarily localized in the tumor vasculature at this time (13).

Intravital Fluorescence Microscopy. Immediately after PDT treatment, tumor-bearing animals were i.v. injected with 20 mg/kg of Hoechst, 5 mg/kg of fluorescein isothiocyanate-labeled dextran with a molecular weight of 2,000 kilo Dalton (2,000 kDa FITC-dextran), and 10 mg/kg of tetramethylrhodamine isothiocyanate-labeled dextran with a molecular weight of 155 kilo Dalton (155 kDa TRITC-dextran). These three fluorescence dyes (all from Sigma-Aldrich Corp, St. Louis, MO) were bolus injected as a mixture. The anesthetized animals were then placed in a prone position on the microscope stage and the MatLyLu tumors were imaged with a Leica DMI 6000B inverted fluorescence microscope. A microscopic field including clearly visible blood vessels was selected and imaged every 5 min for up to 60 min after injection. A 20× long working distance objective was used to image tumor tissues and different channel fluorescence images were captured with a Hamamatsu ORCA-AG CCD monochrome camera. The multi-channel image acquisition with appropriate filter setup was controlled by SimplePCI software (Compix Inc, Cranberry, PA). All the following image analyses were performed with the SimplePCI and NIH ImageJ software packages.

Analysis of Blood Cell Velocity. Blood cell flow velocity was measured based on the Hoechst channel (excitation: 360/40 nm; emission: 470/40 nm) images, which were captured at a speed of 17 frames per second for 3 s every 5 min after PDT. Hoechst dye stained the nuclei of circulating blood cells. Blood cell flow velocity was calculated by measuring the distance of Hoechst-positive cells traveled between two consecutive images divided by the time interval between these two images. Because the morphological differences between arteriols and venules in tumor tissues are often not distinct, vessels were chosen for velocity measurements solely based on the vessel size. In each animal, blood cell velocity values at different time points after PDT were normalized to the first point value, i.e. 5 min after PDT, to obtain the relative change after treatment. The percentage changes of each animal in the same group were pooled to generate an overall response curve.

Analysis of Blood Vessel Diameter and Fluorochrome-Labeled Dextran Extravasation. The FITC channel (excitation: 480/40 nm; emission: 527/30 nm) and TRITC channel (excitation: 546/12 nm; emission: 600/40 nm) images were captured every 5 min for up to 60 min after PDT with fixed camera settings. Images in each channel were properly oriented and stacked to ensure that measurements were taken at approximately the same location. Blood vessel diameter was measured based on the FITC-dextran images.

To measure the extravasation of fluorochrome-labeled dextrans in tumor tissues, regions of interest (ROIs) with diameter of 10 μm were selected on the FITC channel images. The same ROIs were also marked at same locations on the matched TRITC images. Although close to nearby blood vessels, these ROIs were chosen in areas without visible blood vessels. The average fluorescence intensity in ROIs was measured on the FITC and TRITC images taken at different times after PDT. All intensity values in each ROI were normalized to its first point value, i.e. 5 min after PDT, to obtain percentage changes as a function of time after treatment. Data of ROIs in the same group were pooled to generate the overall response curve. The area under curve (AUC) of each ROI intensity change curve was calculated to

represent the accumulation of fluorochrome-labeled dextran in tumor tissues over the 60 min period.

Statistical Analysis. Blood cell flow velocity, vessel diameter and fluorescence intensity data were first analyzed using repeated measures analysis of variance (ANOVA) with Tukey's post test to examine statistical differences among measurements taken at various time points during the 60 min period after treatment. One-way ANOVA test with Tukey's post test was then used to determine statistical differences between various treatment groups and the control group. Statistical significance was accepted at $p<0.05$. All statistical analyses were carried out using GraphPad Prism software (GraphPad, San Diego, CA).

RESULTS

Thrombus formation and blood flow stasis were two significant observations after PDT treatments. PDT with 0.25 mg/kg dose of verteporfin mainly induced the formation of emboli (unstable thrombi). Although reduction in blood flow was clearly visible, most blood vessels were still functional at the end of 60 min after this PDT treatment possibly due to the dislodging of unstable clots. As shown in Fig. 1, thrombus formation was observed as early as 5 min after 0.5 mg/kg dose of verteporfin-PDT. The development of thrombus caused vessel lumen narrowing and stagnant blood flow, resulting in complete perfusion arrest at 50 min after treatment.

Changes in blood cell flow velocity and vessel diameter were continuously measured for a period of 60 min after treatments and the data were shown in Fig. 2. There was a slight increase in blood cell velocity in control tumors, but this change was not statistically significant ($p>0.05$, Fig. 2A). PDT with 0.25 mg/kg dose of verteporfin induced up to 50% reduction in blood cell velocity after treatment ($p<0.01$). However, among eight blood vessels analyzed, six were still functional at the end of 60 min after PDT. Significant decrease in blood cell velocity was also observed in tumors treated with 0.5 mg/kg dose of verteporfin PDT ($p<0.01$). After a short rebound, blood cell velocity continued to decline to nearly complete perfusion arrest at 60 min after treatment. Only 2 out of 14 vessels analyzed were still functional at the end of observation. PDT with 1.0 mg/kg dose of verteporfin caused complete blood flow arrest within 20 min and no recovery was observed up to 60 min after PDT ($p<0.01$). Similar to control tumors, no significant change in vessel diameter was detected in tumors treated with either 0.25 or 0.5 mg/kg dose of verteporfin PDT ($p>0.05$, Fig. 2B). PDT with 1.0 mg/kg dose of verteporfin induced an initial vessel constriction followed by vessel dilation at late times. However, none of these changes were statistically significant compared to the 5 min time point ($p>0.05$).

Blood vessels analyzed in this study ranged from 0 to 1817.6 μm/s in blood cell velocity and from 8.3 to 83.1 μm in vessel diameter. There was no correlation between blood cell velocity and vessel diameter in control and all three PDT groups at any time point ($p>0.05$). As PDT with 0.5 mg/kg dose of verteporfin caused vascular shutdown in 12 out of 14 blood vessels observed within 60 min after PDT, we analyzed the relationship among vessel diameter, blood cell velocity and the time taken to reach zero blood flow. Figure 3 indicates no significant correlation between vessel diameter and blood cell velocity ($p=0.819$). Also there was no correlation between vessel diameter and the time taken to zero blood flow ($p=0.246$). However, a strong correlation was found between the initial blood cell velocity and the time taken to reach zero blood cell velocity ($p=0.007$).

Fluorescence images of 2,000 kDa FITC-dextran and 155 kDa TRITC-dextran were shown in Fig. 4 to illustrate the extravasation of macromolecules after treatments. Average fluorescence intensities of 2,000 kDa FITC-dextran and 155 kDa TRITC-dextran in ROIs were measured and shown

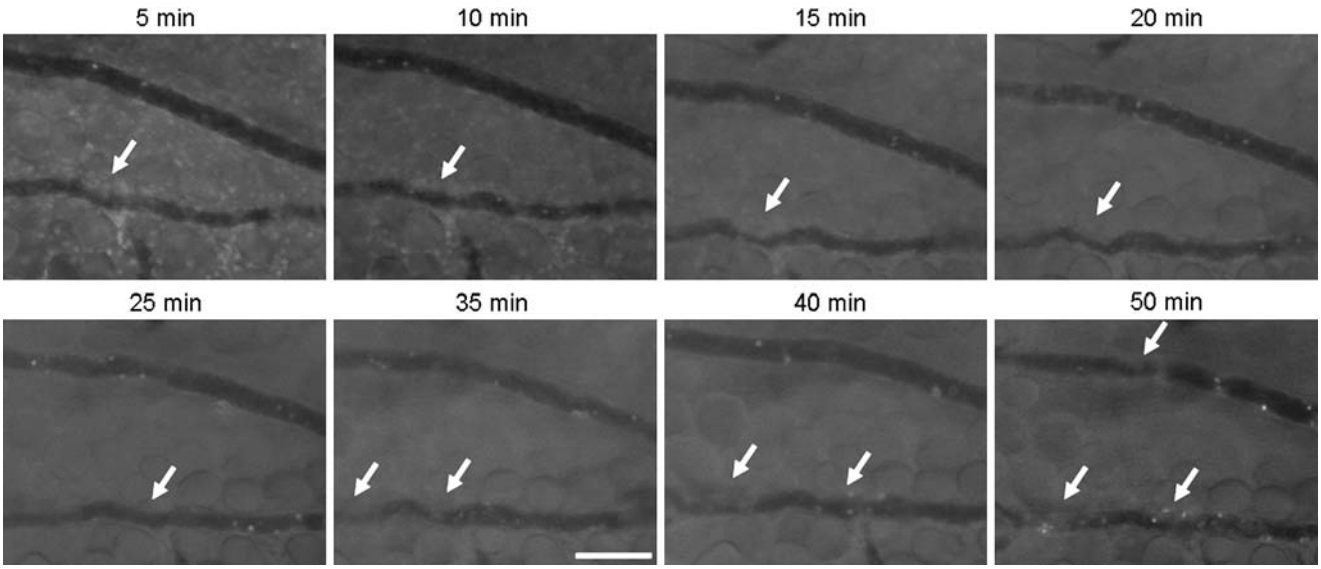

Fig. 1. Thrombus formation after PDT with verteporfin. The MatLyLu tumors were treated with 50 J/cm^2 light dose at 15 min after i.v. injection of 0.5 mg/kg dose of verteporfin. Tumor blood vessels were continuously imaged by intravital fluorescence microscopy showing the formation of thrombi (indicated by *arrows*) that caused progressive vessel lumen obstruction and ultimately vascular shutdown at 50 min after treatment. Bar=100 um.

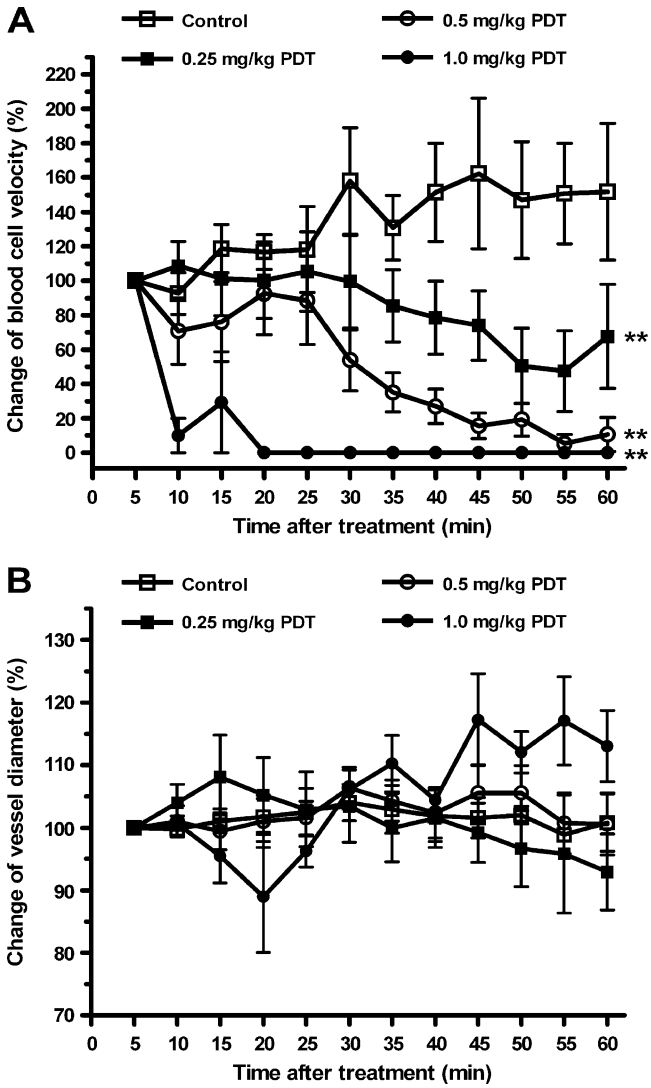

Fig. 2. Effects of PDT with verteporfin on blood cell velocity (**A**) and blood vessel diameter (**B**). The MatLyLu tumors were treated with 50 J/cm^2 light dose at 15 min after i.v. injection of 0.25, 0.5 or 1.0 mg/kg doses of verteporfin. Control tumors received no treatment. Blood cell velocity and vessel diameter were continuously measured every 5 min for up to 60 min after treatment by intravital fluorescence microscopy. Each data point represents the mean of 4–12 blood vessels and is expressed as a percentage of the 5 min point value. Bars indicate the standard error. Compared to the control, $^{**}p<0.01$.

in Fig. 5. The extravasation of 2,000 kDa FITC-dextran (Fig. 5A) and 155 kDa TRITC-dextran (Fig. 5B) led to significant increase in fluorescence intensity in untreated control tumors ($p<0.05$). Compared to untreated control tumors, PDT with 0.25 mg/kg dose of verteporfin significantly enhanced the extravasation of 2,000 kDa FITC-dextran in tumor tissues ($p<0.01$) while PDT with both 0.5 and 1.0 mg/kg doses of verteporfin had no significant effect on FITC-dextran extravasation ($p>0.05$). Both 0.25 and 0.5 mg/kg doses of verteporfin-PDT caused significant increase in the extravasation of 155 kDa TRITC-dextran compared to control tumors ($p<0.01$). But there was no significant difference between 0.25 and 0.5 mg/kg dose PDT treatments in affecting 155 kDa TRITC-dextran extravasation ($p>0.05$). PDT with 1.0 mg/kg dose of verteporfin induced an initial decrease in the fluorescence of 155 kDa TRITC-dextran. It is not clear what caused this decrease in the TRITC fluorescence, which was not observed in the corresponding FITC channel. The fluorescence of 155 kDa TRITC-dextran recovered after the initial decrease. Overall no significant difference was found between 1.0 mg/kg verteporfin-PDT and untreated control tumors in the TRITC-dextran extravasation over the 60 min period ($p>0.05$).

The AUC of fluorescence intensity–time curve was calculated to estimate tumor uptake of fluorochrome-labeled dextrans during the 60 min period (Fig. 6). Among three different doses of PDT treatments, only PDT with 0.25 mg/kg dose of verteporfin caused significant increase in tumor accumulation of 2,000 kDa FITC-dextran compared to control tumors ($p<0.05$). However, both 0.25 and 0.5 mg/kg doses of PDT significantly enhanced tumor accumulation of 155 kDa TRITC-dextran. Tumor uptake of 155 kDa TRITC-dextran was significantly higher than that of 2,000 kDa FITC-dextran after either 0.25 or 0.5 mg/kg PDT treatment ($p<0.01$). The 1.0 mg/kg dose PDT appeared to induce a decrease in tumor uptake of 155 kDa TRITC-dextran compared to control tumors, but this was not statistically significant ($p>0.05$).

DISCUSSION

Since tumor vasculature serves to provide blood supply to tumor tissues and regulate substance exchange between blood and tumor interstitial fluid (1), it is important to understand how a tumor vascular disrupting therapy affects these two key vascular functions. In the present study, we used intravital microscopy to analyze changes in tumor vascular perfusion and macromolecule extravasation after verteporfin-mediated photodynamic vascular targeting therapy in the orthotopic MatLyLu rat prostate tumor model. Based on our previous study that PDT with 0.25 mg/kg dose of verteporfin increases macromolecule extravasation and

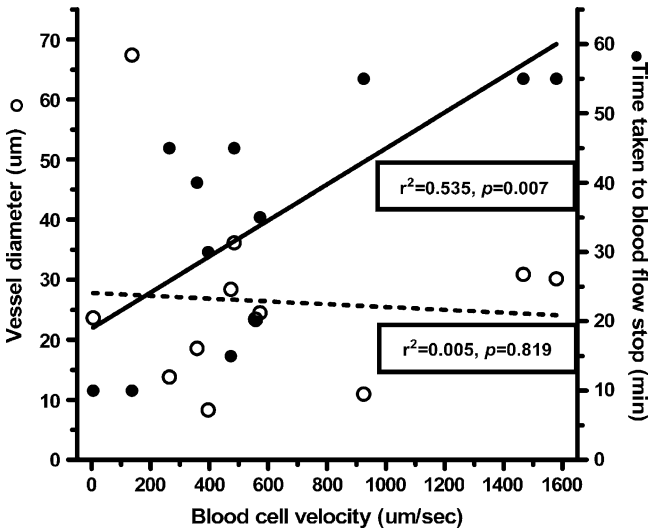

Fig. 3. Relationship between blood cell velocity and the time taken to reach zero blood flow after PDT with verteporfin. A significant correlation was found between the initial blood cell velocity and the time taken to zero blood cell velocity ($p=0.007$) after PDT with 0.5 mg/kg dose of verteporfin. The correlation between vessel diameter and blood cell velocity was not significant ($p=0.819$).

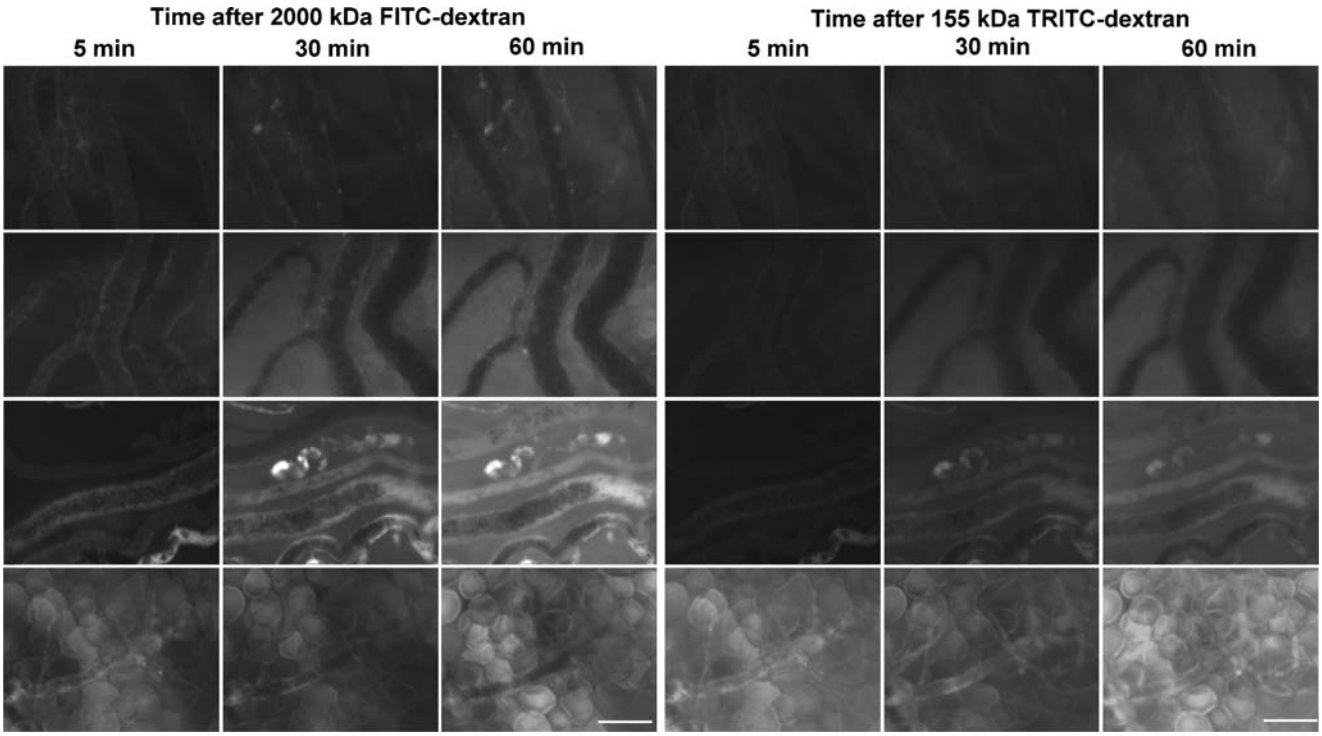

Fig. 4. Fluorescence images of 2,000 kDa FITC-dextran and 155 kDa TRITC-dextran at 5, 30 and 60 min after treatments. The MatLyLu tumors were treated with 50 J/cm^2 light dose at 15 min after i.v. injection of 0.25, 0.5 or 1.0 mg/kg doses of verteporfin. Control tumors received no treatment. Animals were i.v. injected with 2,000 kDa FITC-dextran and 155 kDa TRITC-dextran immediately after treatment and tumors were imaged with intravital fluorescence microcopy. *Top panel* control; *second panel* 0.25 mg/kg verteporfin-PDT; *third panel* 0.5 mg/kg verteporfin-PDT; *fourth panel* 1.0 mg/kg verteporfin-PDT. Bar=100 um.

induces tumor necrosis (9), we chose to examine two higher verteporfin doses (0.5 and 1.0 mg/kg) together with 0.25 mg/kg dose in this study. Our results demonstrate that PDT with verteporfin caused significant reduction in blood perfusion and an increase in the extravasation of dextran molecules. But the effects of PDT on blood perfusion and substance extravasation followed a reverse dose-dependence.

As expected, PDT with a higher dose of verteporfin was more effective in inducing blood flow reduction than a lower dose of verteporfin-PDT (Fig. 2). Similar to the previous studies (9,14,15), thrombus formation was found to contribute to PDT-induced vascular perfusion disruption. Stable thrombi formed inside vessel lumen caused blood flow reduction and even complete vascular occlusion. Even though vessel constriction was indeed observed in some blood vessels, vessel constriction in overall did not appear to play a major role in verteporfin-mediated vascular disruption, which has been reported to be involved in PDT with another photosensitizer Photofrin (16). Figure 2 indicates that no significant vessel size change was found after all three different doses of PDT treatments. This simply suggests the complexity of vessel response to PDT because, depending on the release of vasoactive substances with opposite effects on vessel size and spontaneous vessel response to tissue hypoxia, temperature and other microenvironment factors, both vessel constriction and dilation can happen at different time after verteporfin-PDT. These results are in agreement with those of Fingar *et al.* who reported that PDT with verteporfin had no significant effect on vessel diameter in a rat chondrosarcoma tumor model (15).

The mechanism underlying thrombus formation induced by photodynamic vascular targeting therapy is complicated and not yet clear. Reactive oxygen species generated intravascularly after PDT likely cause damage to multiple targets such as red blood cells, platelets and endothelial cells, which in turn leads to the activation of haemostatic cascades and results in thrombus formation (17,18). Endothelial damage plays an important role in initiating this cascade. As shown in the previous study, we have found a rapid endothelial cell microtubule depolymerization and endothelial cell contraction following verteporfin-PDT (9). Since endothelial cells form an interface between the blood and underneath tissue, these endothelial morphological changes lead to the exposure of tissue extracellular matrix to circulating blood, which causes blood cell adherence to the damaged endothelial cells via activating platelets and polymorphonuclear leukocytes (19,20). This might explain intravital microscopic observations that thrombi induced by verteporfin-PDT often started from endothelial sites and gradually increased in size, ultimately leading to blood vessel occlusion (Fig. 1).

Tumor blood vessels exhibited heterogeneity in response to PDT-induced perfusion disruption (21). By examining the response of each individual vessel to PDT, it is possible to identify the determinants that contribute to vascular response heterogeneity, which may help to find ways to enhance vascular response to PDT. Our data indicate that blood flow velocity was an important parameter in determining vascular response to PDT. Vessels with higher flow velocity were more resistant to PDT-induced vascular shutdown (Fig. 3). This is likely because high flow velocity was not conducive to

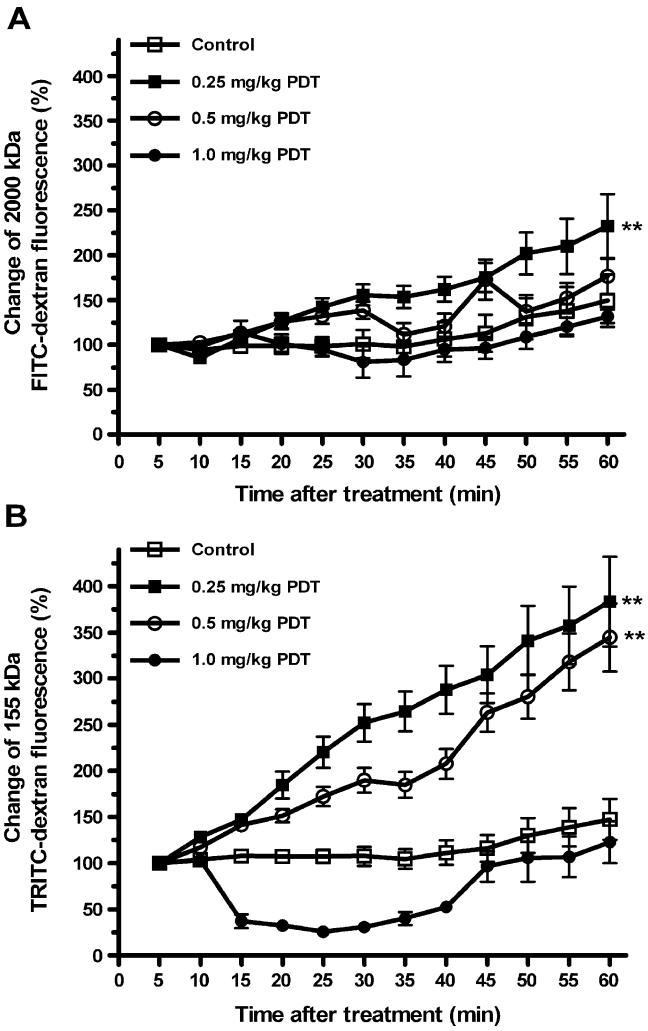

Fig. 5. Effects of PDT with verteporfin on the extravasation of 2,000 kDa FITC-dextran (**A**) and 155 kDa TRITC-dextran (**B**). The MatLyLu tumors were treated with 50 J/cm^2 light dose at 15 min after i.v. injection of 0.25, 0.5 or 1.0 mg/kg doses of verteporfin. Control tumors received no treatment. Animals were i.v. injected with 2,000 kDa FITC-dextran and 155 kDa TRITC-dextran immediately after treatment and tumors were imaged with intravital fluorescence microcopy. Fluorescence intensities of dextran molecules in the ROIs were continuously measured every 5 min for up to 60 min after treatment. Each data point represents the mean of 4–29 ROIs and is expressed as a percentage of the 5 min point value. *Bars* indicate the standard error. Compared to the control, $^{**}p<0.01$.

thrombus formation and able to push some already formed thrombi into circulation, which resumes blood perfusion function. Emboli were indeed commonly observed in blood vessels treated with a low dose of PDT and in vessels with fast blood flow in this study. A previous study demonstrates that tumor areas with low oxygen partial pressure (pO_2) have more rapid decrease in pO_2 level after verteporfin-PDT than areas with high pO_2 (22). Since it is very possible that tumor areas with low pO_2 also have low blood flow, the faster drop of tumor pO_2 in low pO_2 tumor areas than in high pO_2 tumor areas after PDT is likely because PDT induces a more rapid vascular shutdown in slow-flow vessels than in high-flow vessels. These results suggest that photodynamic vascular targeting therapy needs to be improved for targeting blood vessels with high blood flow. On the other hand, because tumor blood vessels generally have slower flow rate than normal vessels (23), this finding might explain why tumor vessels are more sensitive to vascular targeting PDT than normal vessels, which has been observed in the previous study (24).

Since vascular barrier is dependent upon endothelial tight junctions (25), another consequence of PDT-induced endothelial cell morphological change is the formation of inter-endothelial cell gaps, which disrupts vascular barrier. As shown in the present study, the extravasation and accumulation of high molecular weight dextran in tumor tissues were significantly increased as a result of vascular permeability increase after verteporfin-PDT. However, compared to the PDT effect on tumor perfusion, the effect of verteporfin-PDT on dextran delivery followed a reverse dose dependence. PDT with a lower dose of verteporfin was more effective in enhancing the extravasation and accumulation of dextran molecules in tumor tissues than a higher dose of verteporfin-PDT. This inverse dose dependence is likely due to the fact that PDT with a higher dose of verteporfin (e.g. 1.0 mg/kg) induced rapid vascular shutdown (Fig. 2), which prevented dextran molecules from being delivered to tumor tissues, while a lower dose verteporfin-PDT (e.g. 0.25 or 0.5 mg/kg) was able to maintain blood perfusion for sometime, which allowed continuous extravasation and accumulation of dextran molecules into the tumor tissue. These results suggest the importance of maintaining tumor perfusion in drug delivery enhancement by using a vascular targeted modality.

Our data also demonstrate that the enhancement of dextran delivery induced by verteporfin-PDT was dependent upon dextran molecular weight. Dextran with a lower molecular weight (155 kDa) exhibited a higher tumor extravasation and uptake than a higher molecular weight dextran (2,000 kDa) after both 0.25 and 0.5 mg/kg doses of PDT treatments. Since it has been known that tumor vascular permeability (26) and the transport of molecules in tumor interstitial area (27) decrease with the increase of molecular weight, the limited enhancement seen in the delivery of 2,000 kDa dextran was likely because it has a lower vascular permeability and slower diffusion in tumor interstitial area than the 155 kDa dextran.

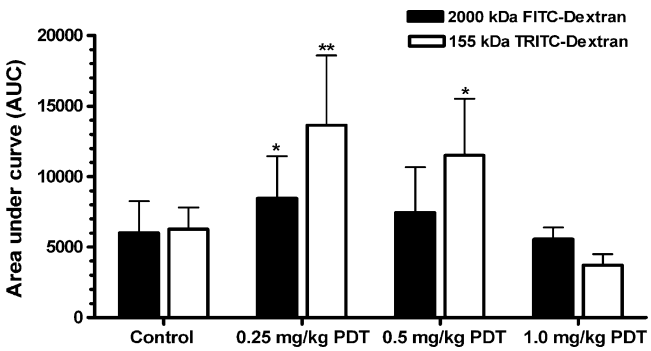

Fig. 6. Effects of PDT with verteporfin on the accumulation of 2,000 kDa FITC-dextran and 155 kDa TRITC-dextran in tumor tissues. The AUC of fluorescence intensity-time curve, as described in the legend of Fig. 5, was calculated to represent the tumor accumulation of dextran molecules. Compared to the control, $^{*}p<0.05$, $^{**}p<0.01$.

This study implies that, although photodynamic vascular targeting therapy with verteporfin may be used for both tumor destruction and drug delivery enhancement, optimal PDT conditions should be tailored to different therapeutic applications. PDT with a higher dose of verteporfin (e.g. 1.0 mg/kg) might be more appropriate for tumor eradication as a rapid and extensive vascular shutdown might be able to maximize tumor cell killing by oxygen and nutrients deprivation. We have found that PDT with 0.25 mg/kg dose of verteporfin causes substantial tumor necrosis. It remains to be determined whether PDT with a higher dose of verteporfin will lead to more tumor necrosis. For primarily enhancing the delivery of other therapeutic agents, PDT with a lower dose of verteporfin (e.g. 0.25 mg/kg) is likely preferred because it can obtain optimal drug tumor accumulation by maintaining tumor perfusion after treatment, as shown in the present and previous (9) study. PDT has been proposed to enhance the delivery of anticancer agent (8). Strategies such as illumination with low light doses and low dose rates (8) or in combination with anti-coagulants (28) also work through preserving tumor perfusion to obtain an enhanced drug delivery to tumor tissues. However, for most cancer combination therapies, PDT with an intermediate dose of verteporfin (e.g. 0.5 mg/kg) is likely to be a practical choice because this treatment can cause considerable tumor perfusion disruption and some effect of drug delivery enhancement, as demonstrated in the present study. Combination of intermediate dose PDT with anticancer drug therapy is more likely to achieve synergistic effect.

In conclusion, we found that photodynamic vascular targeting with verteporfin disrupted tumor perfusion by inducing thrombus formation, and enhanced tumor accumulation of high molecular weight dextrans by increasing vascular permeability. However, effects of PDT on blood perfusion and accumulation of dextran molecules followed a reverse dose dependence. A higher dose of verteporfin PDT was more effective in inducing perfusion disruption, but less effective in enhancing dextran accumulation. A lower dose of verteporfin PDT was favorable for drug delivery enhancement by maintaining tumor perfusion. Dextran with a lower molecular weight (155 kDa) obtained a higher tumor accumulation than a higher molecular weight dextran (2,000 kDa). These findings are important for optimizing PDT conditions as a vascular disrupting therapy or a modality for drug delivery enhancement.

ACKNOWLEDGEMENTS

This work is supported by Department of Defense (DOD) Grant W81XWH-06-1-0148 and Lindback Foundation. The authors would like to gratefully acknowledge Dr. Brian Pogue for reading the manuscript and QLT Inc. for providing photosensitizer verteporfin.

REFERENCES

1. C. Bouzin and O. Feron. Targeting tumor stroma and exploiting mature tumor vasculature to improve anti-cancer drug delivery. *Drug Resist. Updat.* **10**:109–20 (2007).
2. D. W. Siemann, M. C. Bibby, G. G. Dark, A. P. Dicker, F. A. Eskens, M. R. Horsman, D. Marme, and P. M. Lorusso. Differentiation and definition of vascular-targeted therapies. *Clin. Cancer Res*. **11**:416–20 (2005).
3. F. Yuan. Transvascular drug delivery in solid tumors. *Semin. Radiat. Oncol*. **8**:164–75 (1998).
4. G. P. van Nieuw Amerongen and V. W. van Hinsbergh. Targets for pharmacological intervention of endothelial hyperpermeability and barrier function. *Vasc. Pharmacol*. **39**:257–72 (2002).
5. T. J. Dougherty, C. J. Gomer, B. W. Henderson, G. Jori, D. Kessel, M. Korbelik, J. Moan, and Q. Peng. Photodynamic therapy. *J. Natl. Cancer Inst*. **90**:889–905 (1998).
6. D. E. Dolmans, D. Fukumura, and R. K. Jain. Photodynamic therapy for cancer. *Nat. Rev. Cancer.* **3**:380–7 (2003).
7. B. Chen, B. W. Pogue, P. J. Hoopes, and T. Hasan. Vascular and cellular targeting for photodynamic therapy. *Crit. Rev. Eukaryot Gene Expr.* **16**:279–305 (2006).
8. J. W. Snyder, W. R. Greco, D. A. Bellnier, L. Vaughan, and B. W. Henderson. Photodynamic therapy: a means to enhanced drug delivery to tumors. *Cancer Res*. **63**:8126–31 (2003).
9. B. Chen, B. W. Pogue, J. M. Luna, R. L. Hardman, P. J. Hoopes, and T. Hasan. Tumor vascular permeabilization by vascular-targeting photosensitization: effects, mechanism, and therapeutic implications. *Clin. Cancer Res*. **12**:917–23 (2006).
10. R. K. Jain, L. L. Munn, and D. Fukumura. Dissecting tumour pathophysiology using intravital microscopy. *Nat. Rev. Cancer* **2**:266–76 (2002).
11. T. R. Tennant, H. Kim, M. Sokoloff, and C. W. Rinker-Schaeffer. The Dunning model. *Prostate* **43**:295–302 (2000).
12. B. Chen, B. W. Pogue, X. Zhou, J. A. O'Hara, N. Solban, E. Demidenko, P. J. Hoopes, and T. Hasan. Effect of tumor host microenvironment on photodynamic therapy in a rat prostate tumor model. *Clin. Cancer Res*. **11**:720–7 (2005).
13. B. Chen, B. W. Pogue, P. J. Hoopes, and T. Hasan. Combining vascular and cellular targeting regimens enhances the efficacy of photodynamic therapy. *Int. J. Radiat. Oncol. Biol. Phys*. **61**:1216–26 (2005).
14. U. Schmidt-Erfurth and T. Hasan. Mechanisms of action of photodynamic therapy with verteporfin for the treatment of age-related macular degeneration. *Surv. Ophthalmol*. **45**:195–214 (2000).
15. V. H. Fingar, P. K. Kik, P. S. Haydon, P. B. Cerrito, M. Tseng, E. Abang, and T. J. Wieman. Analysis of acute vascular damage after photodynamic therapy using benzoporphyrin derivative (BPD). *Br. J. Cancer.* **79**:1702–8 (1999).
16. V. H. Fingar, T. J. Wieman, S. A. Wiehle, and P. B. Cerrito. The role of microvascular damage in photodynamic therapy: the effect of treatment on vessel constriction, permeability, and leukocyte adhesion. *Cancer Res*. **52**:4914–21 (1992).
17. V. H. Fingar. Vascular effects of photodynamic therapy. *J. Clin. Laser Med. Surg*. **14**:323–8 (1996).
18. B. Krammer. Vascular effects of photodynamic therapy. *Anticancer Res*. **21**:4271–7 (2001).
19. W. J. de Vree, M. C. Essers, H. S. de Bruijn, W. M. Star, J. F. Koster, and W. Sluiter. Evidence for an important role of neutrophils in the efficacy of photodynamic therapy *in vivo*. *Cancer Res*. **56**:2908–11 (1996).
20. W. J. de Vree, A. N. Fontijne-Dorsman, J. F. Koster, and W. Sluiter. Photodynamic treatment of human endothelial cells promotes the adherence of neutrophils *in vitro*. *Br. J. Cancer.* **73**:1335–40 (1996).
21. T. M. Busch. Local physiological changes during photodynamic therapy. *Lasers Surg. Med*. **38**:494–9 (2006).
22. B. W. Pogue, R. D. Braun, J. L. Lanzen, C. Erickson, and M. W. Dewhirst. Analysis of the heterogeneity of pO2 dynamics during photodynamic therapy with verteporfin. *Photochem. Photobiol.* **74**:700–6 (2001).
23. D. Fukumura and R. K. Jain. Tumor microenvironment abnormalities: causes, consequences, and strategies to normalize. *J. Cell Biochem*. **101**:937–49 (2007).
24. F. Borle, A. Radu, C. Fontolliet, H. van den Bergh, P. Monnier, and G. Wagnieres. Selectivity of the photosensitiser Tookad for photodynamic therapy evaluated in the Syrian golden hamster cheek pouch tumour model. *Br. J. Cancer.* **89**:2320–6 (2003).
25. G. Bazzoni. Endothelial tight junctions: permeable barriers of the vessel wall. *Thromb Haemost*. **95**:36–42 (2006).

26. M. R. Dreher, W. Liu, C. R. Michelich, M. W. Dewhirst, F. Yuan, and A. Chilkoti. Tumor vascular permeability, accumulation, and penetration of macromolecular drug carriers. *J. Natl. Cancer Inst.* **98**:335–44 (2006).
27. A. Pluen, Y. Boucher, S. Ramanujan, T. D. McKee, T. Gohongi, E. di Tomaso, E. B. Brown, Y. Izumi, R. B. Campbell, D. A. Berk, and R. K. Jain. Role of tumor–host interactions in interstitial diffusion of macromolecules: cranial *vs.* subcutaneous tumors. *Proc. Natl. Acad. Sci. U S A*. **98**:4628–33 (2001).
28. E. Debefve, B. Pegaz, J. P. Ballini, Y. N. Konan, and H. van den Bergh. Combination therapy using aspirin-enhanced photodynamic selective drug delivery. *Vasc. Pharmacol.* **46**:171–80 (2007).

Int. J. Cancer: **123,** 695–701 (2008)

Disparity between prostate tumor interior *versus* peripheral vasculature in response to verteporfin-mediated vascular-targeting therapy

Bin Chen[1,2]*, Curtis Crane[3], Chong He[1], David Gondek[4], Priyanka Agharkar[1], Mark D. Savellano[3,5], P. Jack Hoopes[3,5] and Brian W. Pogue[3,5,6]

[1]*Department of Pharmaceutical Sciences, Philadelphia College of Pharmacy, University of the Sciences in Philadelphia, Philadelphia, PA*
[2]*Department of Radiation Oncology, University of Pennsylvania, Philadelphia, PA*
[3]*Department of Surgery, Dartmouth Medical School, Lebanon, NH*
[4]*Department of Immunology, Dartmouth Medical School, Lebanon, NH*
[5]*Thayer School of Engineering, Dartmouth College, Hanover, NH*
[6]*Wellman Center for Photomedicine, Massachusetts General Hospital, Department of Dermatology, Harvard Medical School, Boston, MA*

Photodynamic therapy (PDT) is a light-based cancer treatment modality. Here we employed both *in vivo* and *ex vivo* fluorescence imaging to visualize vascular response and tumor cell survival after verteporfin-mediated PDT designed to target tumor vasculature. EGFP-MatLyLu prostate tumor cells, transduced with EGFP using lentivirus vectors, were implanted in athymic nude mice. Immediately after PDT with different doses of verteporfin, tumor-bearing animals were injected with a fluorochrome-labeled albumin. The extravasation of fluorescent albumin along with tumor EGFP fluorescence was monitored noninvasively with a whole-body fluorescence imaging system. *Ex vivo* fluorescence microscopy was performed on frozen sections of tumor tissues taken at different times after treatment. Both *in vivo* and *ex vivo* imaging demonstrated that vascular-targeting PDT with verteporfin significantly increased the extravasation of fluorochrome-labeled albumin in the tumor tissue, especially in the tumor periphery. Although PDT induced substantial vascular shutdown in interior blood vessels, some peripheral tumor vessels were able to maintain perfusion function up to 24 hr after treatment. As a result, viable tumor cells were typically detected in the tumor periphery in spite of extensive tumor cell death. Our results demonstrate that vascular-targeting PDT with verteporfin causes a dose- and time-dependent increase in vascular permeability and decrease in blood perfusion. However, compared to the interior blood vessels, peripheral tumor blood vessels were found less sensitive to PDT-induced vascular shutdown, which was associated with subsequent tumor recurrence in the tumor periphery.

Key words: photodynamic therapy (PDT); verteporfin; vascular targeting; fluorescence imaging; vascular permeability; tumor perfusion; enhanced green fluorescence protein (EGFP); prostate tumor model

Photodynamic therapy (PDT) induces tumor destruction through a photochemical reaction involving a photosensitizer, light of a specific wavelength matching the absorption of the photosensitizer and molecular oxygen.[1] Singlet oxygen, a product of this photochemical reaction, causes oxidative damage to target cells and tissues and is the primary reactive oxygen species responsible for the biological effects of PDT.[2] Although direct tumor cytotoxicity and immune responses are involved as well, damage to the tumor vasculature has been shown to contribute significantly to the overall PDT effect of most photosensitizers.[3]

Verteporfin (the lipid-formulation of benzoporphyrin derivative monoacid ring A) is a photosensitizer that is currently approved for the treatment of age-related macular degeneration (AMD).[4] We have shown previously that the dynamic distribution of verteporfin is predominantly intravascular at 15 min after intravenous injection and becomes mainly extravascular at 3 hr after injection.[5] Based on this pharmacokinetic property, preferential tumor vascular targeting can be achieved by illumination at 15 min after verteporfin administration. We have been exploring this passive vascular targeting principle for the treatment of prostate tumors. Intravital fluorescence microscopy studies in the MatLyLu rat prostate tumor model has demonstrated that vascular-targeting PDT with verteporfin induces vascular permeability increase and thrombus formation, which ends in vascular shutdown and tumor necrosis.[6] These results indicate that vascular-targeting PDT using verteporfin can be used for the management of localized prostate cancer.

Because vascular damage is the dominant effect of PDT, especially in the case of vascular-targeting PDT, it is important to study in detail how photosensitization modifies vascular functions. Most studies on PDT-induced tumor vascular changes have been done on excised tumor specimens after sacrificing the animals. Although they have been valuable in revealing microscopic details, such studies are only able to provide snap-shot information on each individual animal. To obtain longitudinal information in a single animal, noninvasive imaging techniques are necessary to examine vessel functional changes after PDT. Imaging modalities such as laser Doppler perfusion imaging,[7,8] diffuse correlation spectroscopy,[9] laser speckle imaging,[10,11] optical coherence tomography[12] and ultrasonography[13] have all been shown to be useful techniques for monitoring tumor blood flow dynamics noninvasively after PDT. Moreover, noninvasive imaging using contrast agents allows one to follow perfusion changes and also provides real-time information regarding vascular permeability. For instance, angiography with fluorescent dyes such as fluorescein or indocyanine green is routinely used to examine vessel leakage and occlusion in AMD patients treated with PDT.[14] Changes in tumor perfusion and vascular permeability after PDT have also been studied with contrast-enhanced MRI.[15,16]

Because of its high sensitivity and versatility, *in vivo* fluorescence imaging is able to provide both macroscopic and microscopic longitudinal data in individual animals, which cannot be obtained in other ways.[17–19] In this study, we used an *in vivo* whole-body fluorescence imaging system to monitor vascular response and tumor cell survival in an EGFP-expressing prostate tumor model following treatment with verteporfin-PDT. Moreover, we compared the *in vivo* tumor imaging results with the *ex vivo* fluorescence microscopy of frozen tumor sections. Our results indicate that the vascular response to vascular-targeting PDT is clearly different between tumor interior vessels and peripheral blood vessels.

Grant sponsor: Department of Defense (DOD) Prostate Cancer Research; Grant number: W81XWH-06-1-0148; Grant sponsor: Lindback Foundation.

***Correspondence to:** Department of Pharmaceutical Sciences, Philadelphia College of Pharmacy, University of the Sciences in Philadelphia, 600 South 43rd Street, Philadelphia, PA 19104, USA Fax: 215-895-1161. E-mail: b.chen@usip.edu

Received 14 December 2007; Accepted after revision 1 February 2008
DOI 10.1002/ijc.23538
Published online 22 May 2008 in Wiley InterScience (www.interscience.wiley.com).

Material and methods

Production and titer of lentivirus

Lentiviral production was performed as previously described.[20] Briefly, we cotransfected pWPT-EGFP and third-generation packaging vectors into 293FT cells (Invitrogen Life Technologies) and collected culture supernatants after 48 and 72 hr of incubation in a 37°C and 5% CO_2 incubator. We recovered virus by ultracentrifugation (1.5 hr at 25,000 rpm) in a Beckman SW28 rotor and resuspended the virus pellet in 25 μl of Opt-MEM media (Invitrogen Life Technologies). Viral titers were determined by infecting 293FT cells with serial dilutions of concentrated lentivirus followed by flow cytometry analysis 48 hr later. Typical viral preparations yielded 5×10^8 transducing units/ml.

Tumor cells and lentiviral transduction

R3327-MatLyLu rat prostate cancer cells were maintained in the RPMI-1640 medium with glutamine (Mediatech, Herndon, VA) supplemented with 10% fetal bovine serum (HyClone, Logan, UT) and 100 units/ml penicillin–streptomycin (Mediatech) at 37°C in a 5% CO_2 incubator. For lentiviral transduction, the MatLyLu cells were infected with a multiplicity of infection of 50 and allowed to incubate overnight. Polybrene (8 μg/ml, Sigma) was used to facilitate lentiviral transduction. Supernatant was then removed after infection and replaced with complete RPMI-1640 growth medium. EGFP-transduced MatLyLu cells were examined with a fluorescence microscope at 48 hr after transduction. EGFP-MatLyLu cells were harvested, serial diluted and seeded in a 96-well plate with cell density of 1 cell per well. After incubation for 7 days at 37°C and 5% CO_2 atmosphere, the clone exhibiting the highest EGFP fluorescence intensity was selected and expanded for subsequent experiments.

Animals and tumor models

Male NCr athymic nude mice (4–5 weeks old, National Cancer Institute, Frederick, MD) were used throughout the study. Tumors were induced by subcutaneous injection of about 1×10^5 EGFP-MatLyLu tumor cells in the thigh region of mice. Tumors were used for experiments when they reached a size of 5–7 mm in diameter. All animal procedures were carried out according to a protocol approved by the Institutional Animal Care and Use Committee (IACUC).

Photosensitizer

Verteporfin (benzoporphyrin derivative (BPD) in a lipid-formulation) was obtained from QLT (Vancouver, Canada) as a gift. A stock saline solution of verteporfin was reconstituted according to the manufacturer's instructions and stored at 4°C in the dark.

PDT treatments

A diode laser system (High Power Devices, North Brunswick, NJ) at 690-nm wavelength was used for the irradiation of EGFP-MatLyLu tumors. The laser was coupled to an optical fiber with 600 μm core diameter and expanded to generate an 11-mm diameter illumination spot through a collimator. Animals were anesthetized with injection (i.p.) of a mixture of ketamine (90 mg/kg) and xylazine (9 mg/kg) and tumors were exposed to light with an irradiance of 50 mW/cm^2. Light intensity was measured with an optical power meter (Thorlabs, North Newton, NJ). Verteporfin was injected (i.v.) 15 min prior to light irradiation at a dose of 0.25 mg/kg.

Noninvasive tumor fluorescence imaging and image analysis

Tumor-bearing animals were i.v. injected with 20 mg/kg albumin labeled with tetramethylrhodamine isothiocyanate (TRITC-albumin, Sigma) immediately after PDT. EGFP-MatLyLu tumors were imaged with a noninvasive whole body fluorescence imaging system for the EGFP and TRITC signal before and at various times after treatment. The setup of this home-built broad beam imaging system has been described in detail in our previous paper.[21] Briefly, the system includes a filtered white light source for excitation and a SensiCamQE high performance digital CCD camera (The Cook Corp, Auburn Hills, MI) to capture fluorescence emission passing through an emission filter. We used a 470/20 nm excitation filter and a 520/20 nm emission filter for imaging tumor EGFP fluorescence and a 535/20 nm excitation filter and 590-nm long-pass emission filter for imaging the TRITC fluorescence. Camera settings were kept constant for the control and PDT-treated animals throughout the imaging process. Animals were anesthetized by inhalation of 1.5% isofluorane and imaged first for EGFP and then TRITC fluorescence without moving the animals. The EGFP and TRITC images were pseudocolored and superimposed to generate composite images.

A 2.5-mm diameter region of interest (ROI) was centered over tumor or tumor-adjacent normal tissue areas, and the average EGFP and TRITC fluorescence intensities in the ROI were quantified with NIH ImageJ software. The fluorescence intensity in tumor or tumor-adjacent tissues after PDT was normalized to its own pretreatment value in each animal, and the data from different animals in each group were pooled to generate response curves. To determine the TRITC-albumin distribution in relation to tumor EGFP fluorescence, a straight line was drawn through the tumor tissue on composite images and the corresponding green (EGFP) and red (TRITC) intensities were measured along the line.

Tumor tissue fluorescence microscopy

Tumor-bearing animals were i.v. injected with 20 mg/kg Hoechst (Sigma) as a vascular perfusion marker at different time points after treatment. Animals were euthanized within 1 min after injection and tumor tissues were excised and snap-frozen in isopentane precooled with liquid nitrogen. Frozen tumor sections with thickness of 10 μm were cut and examined under a Leica DMI6000B fluorescence microscope with appropriate filter sets for Hoechst (excitation: 360/40 nm; emission: 470/40 nm) and TRITC (excitation: 546/12 nm; emission: 600/40 nm).

Tumor volume measurement and tumor histology

Three-dimensional tumor sizes were measured regularly after treatment by caliper, and the tumor volume was calculated using the formula $\pi/6 \times$ tumor length $\times$ tumor width $\times$ tumor height. Animals were euthanized at various time points after treatment. Tumor tissues were excised and fixed in 4% formalin solution. Fixed tumor tissues were dehydrated and then embedded in paraffin. Tissue sections with thickness of 5 μm were cut and stained with H&E.

Statistical analysis

Students' 2-tailed *t*-test was used to calculate statistical differences between 2 groups and the significance was accepted at $p < 0.05$. Statistical analysis was carried out using GraphPad software (GraphPad, San Diego, CA).

Results

The extravasation of TRITC-albumin, as indicated by the increase in TRITC fluorescence, was imaged noninvasively with a whole-body fluorescence imaging system. Figure 1 shows the TRITC fluorescence images (red) merged with tumor EGFP fluorescence images (green) at different time points after vascular-targeting PDT with verteporfin. PDT caused an overall increase in the TRITC fluorescence and this was more pronounced in the peritumor area. PDT-induced TRITC-albumin extravasation appeared to be dose dependent because the 50 J/cm^2 light dose PDT caused a greater increase in the TRITC fluorescence compared to the 25 J/cm^2 light dose treatment.

The average TRITC fluorescence intensity in tumor and tumor-adjacent normal tissue ROIs was quantified with NIH ImageJ software. It was observed that the average TRITC fluorescence in

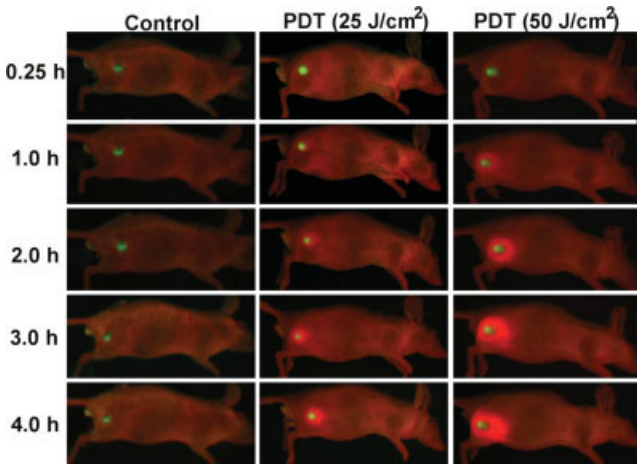

FIGURE 1 – *In vivo* fluorescence images of the TRITC-albumin extravasation and tumor EGFP fluorescence. The EGFP-MatLyLu tumors were illuminated with 25 or 50 J/cm^2 light at 15 min after i.v. injection of 0.25 mg/kg dose of verteporfin. Immediately after treatment, tumor-bearing animals were i.v. injected with 20 mg/kg TRITC-albumin and imaged at different times after injection with a whole-body fluorescence imaging system as described in the materials and methods. Control tumors received no treatment. The images shown are the merged image of TRITC (red) and EGFP (green) fluorescence images. [Color figure can be viewed in the online issue, which is available at www.interscience.wiley.com.]

tumor areas was about 20% lower than tumor-adjacent normal tissue areas presumably because higher blood volume in tumor tissues causes more TRITC fluorescence quenching than in normal tissues.[19] Both 25 and 50 J/cm^2 PDT treatments significantly increased the TRITC fluorescence intensity in tumor (Fig. 2*a*, $p < 0.05$) and tumor-adjacent tissues (Fig. 2*b*, $p < 0.05$). Fluorescence intensity increase started from 1-hr post-PDT treatments and reached a plateau at about 4 hr thereafter while untreated control tumors exhibited little change in fluorescence intensity over the same period of time. In both tumor and tumor-adjacent tissues, PDT with 50 J/cm^2 light dose induced a greater increase in the TRITC fluorescence intensity than the 25 J/cm^2 light dose ($p < 0.01$). The 25 J/cm^2 light dose PDT caused a similar increase (maximally about 1.5-fold increase) in the TRITC fluorescence intensity in both tumor and tumor-adjacent tissues ($p > 0.05$). The 50 J/cm^2 PDT caused significantly higher TRITC fluorescence increase in tumor-adjacent tissues (about 3-fold increase at peak) compared to tumor tissues (about 2-fold increase at peak, $p < 0.05$).

Changes in the average EGFP fluorescence intensity in tumor tissues were also quantified and are shown in Figure 2*c*. Both 25 and 50 J/cm^2 PDT treatments caused a significant decrease in tumor EGFP fluorescence at 1 hr after treatment ($p < 0.05$). After the initial decrease, there was no further decrease in tumor EGFP fluorescence intensity. Control tumors showed little change in the EGFP fluorescence during this 5-hr period.

Analysis of TRITC and corresponding EGFP intensity profiles indicated that the TRITC fluorescence intensity in tumor peripheral area was higher than in tumor interior area at 4 hr after injection of TRITC-albumin (Fig. 3). However, an opposite pattern was found in tumor EGFP intensity profiles with the higher intensity values detected in the tumor center. Both 25 and 50 J/cm^2 PDT treatments caused an overall increase in the TRITC intensity and decrease in tumor EGFP intensity. The increase in the TRITC intensity was found to be higher in the tumor periphery than in the tumor center.

To verify the whole-body fluorescence imaging results, we euthanized animals at 1, 4 and 24 hr after 50 J/cm^2 PDT treatment and excised tumor tissues for fluorescence microscopy. Hoechst dye was i.v. injected shortly before euthanizing animals to highlight functional blood vessels. As shown in Figure 4, tumor staining of Hoechst dye decreased significantly after vascular-targeting PDT with 50 J/cm^2 light dose compared to the control tumor, indicating a decrease in functional blood vessels. Moreover, functional

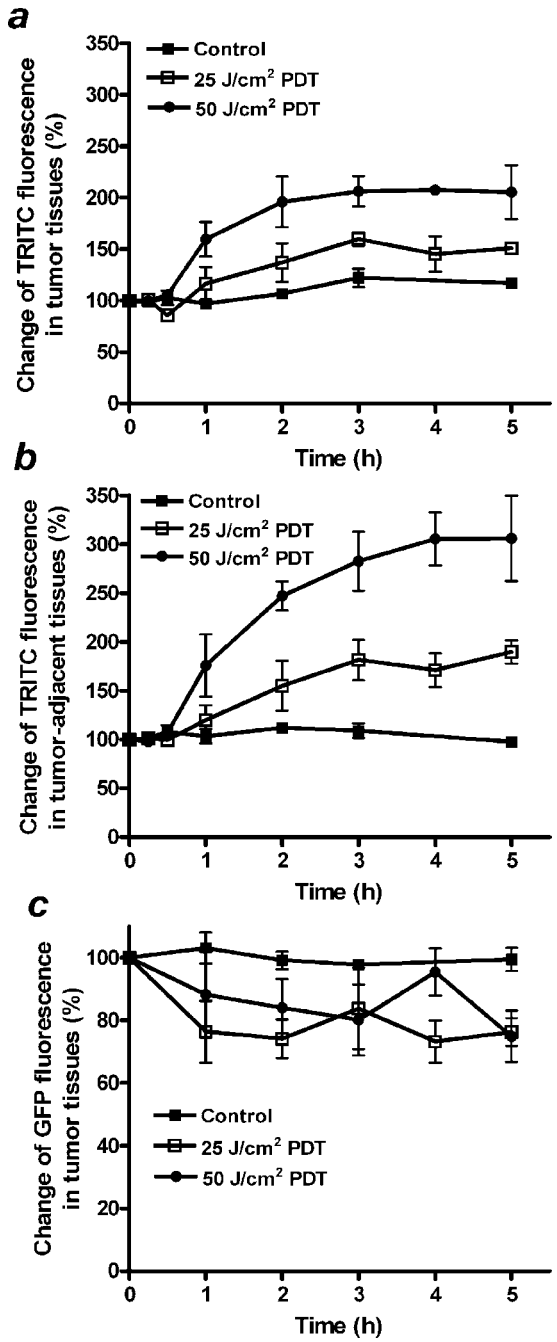

FIGURE 2 – *In vivo* fluorescence image analysis showing (*a*) changes of the TRITC-albumin fluorescence intensity in tumor tissues, (*b*) changes of the TRITC-albumin fluorescence intensity in tumor-adjacent tissues, and (*c*) changes of tumor EGFP fluorescence intensity after treatment. The EGFP-MatLyLu tumors were treated with vascular-targeting PDT and imaged with a whole-body fluorescence imaging system. The TRITC and EGFP fluorescence intensities were measured in a circular 2.5 mm diameter ROI placed over the tumor or tumor-adjacent area on the fluorescence images. The fluorescence intensity values after treatment in each animal were normalized to their own pretreatment values, which are displayed as 100% at 0 time point. Each group included 3 or 4 animals. Error bars represent the standard deviation.

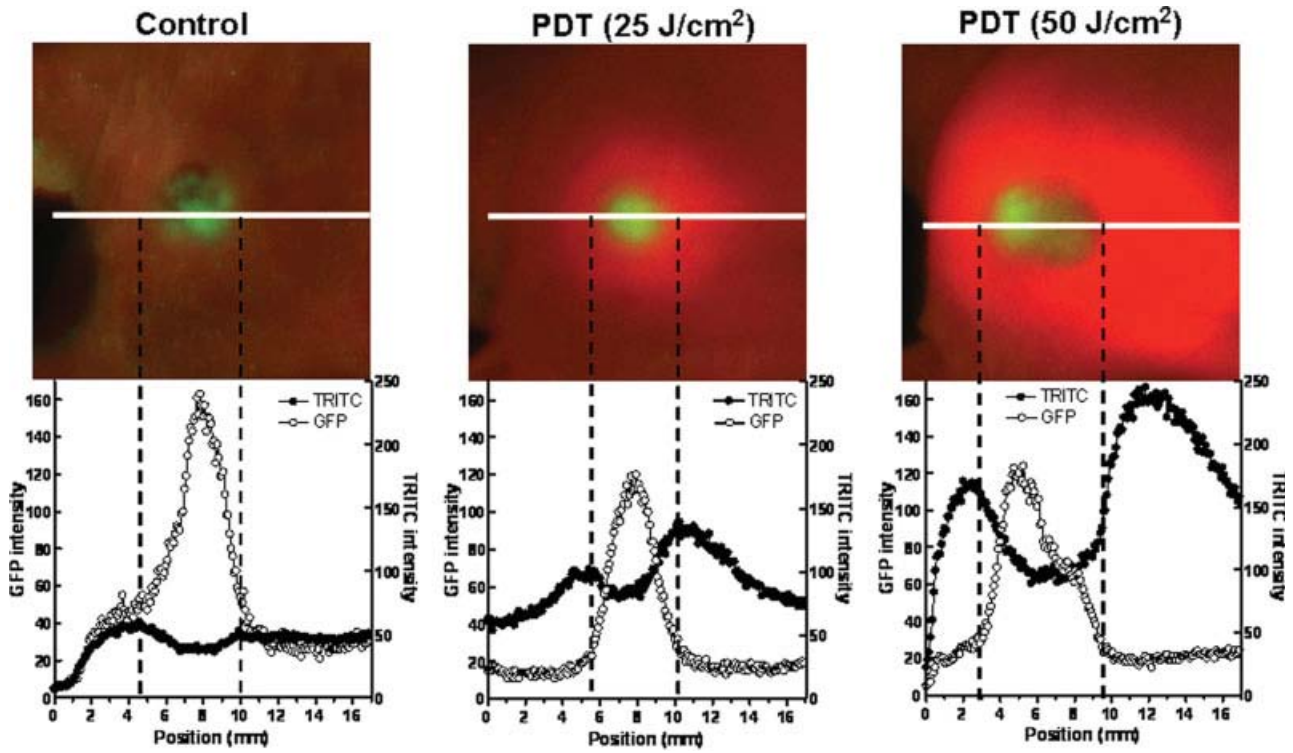

FIGURE 3 – *In vivo* fluorescence image analysis showing the TRITC-albumin accumulation in relation to tumor EGFP fluorescence intensity. The 4-hr-time-point images from Figure 1 were analyzed and shown here. A 17-mm line was drawn through the tumor tissue on each fluorescence image. Both TRITC-albumin and tumor EGFP fluorescence intensities were measured along the line and are shown in the figure. Dashed lines indicate the boundary of the tumor tissue. Note the opposite pattern between tumor TRITC-albumin accumulation and tumor EGFP fluorescence intensity profiles. [Color figure can be viewed in the online issue, which is available at www.interscience.wiley.com.]

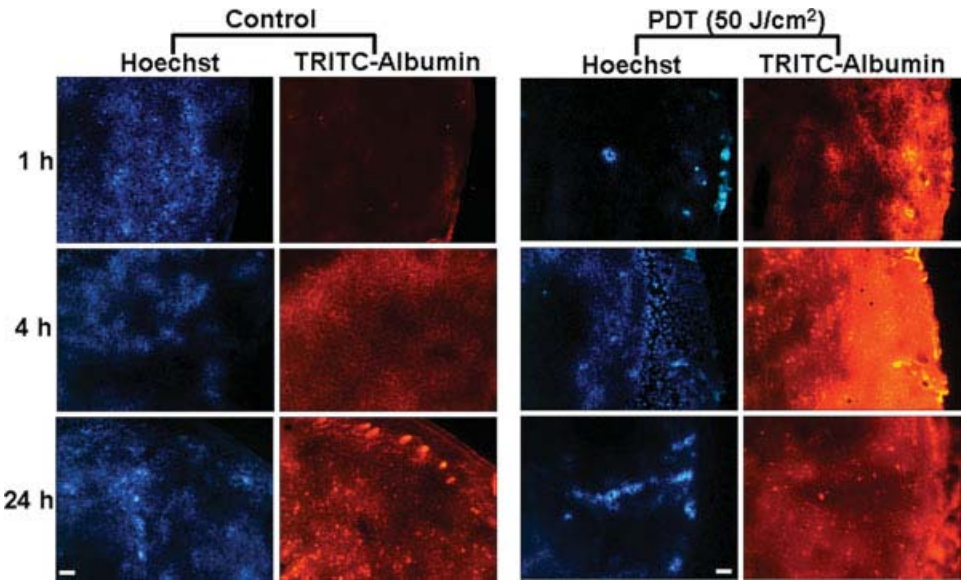

FIGURE 4 – *Ex vivo* fluorescence microscopy images showing the distribution of TRITC-albumin in relation to the functional blood vessels highlighted by Hoechst dye staining. The EGFP-MatLyLu tumors were treated with 50 J/cm^2 light at 15 min after i.v. injection of 0.25 mg/kg dose of verteporfin. Control tumors received no treatment. Immediately after treatment, tumor-bearing animals were i.v. injected with 20 mg/kg TRITC-albumin. Animals were euthanized at 1, 4 or 24 hr after injection of the TRITC-albumin. Hoechst dye (20 mg/kg) was i.v. injected at 1 min before euthanizing the animal. Frozen tumor sections from tissue samples were first imaged for Hoechst fluorescence and the same fields were then imaged for TRITC-albumin fluorescence. All images shown include the tumor periphery. Bars = 100 μm. [Color figure can be viewed in the online issue, which is available at www.interscience.wiley.com.]

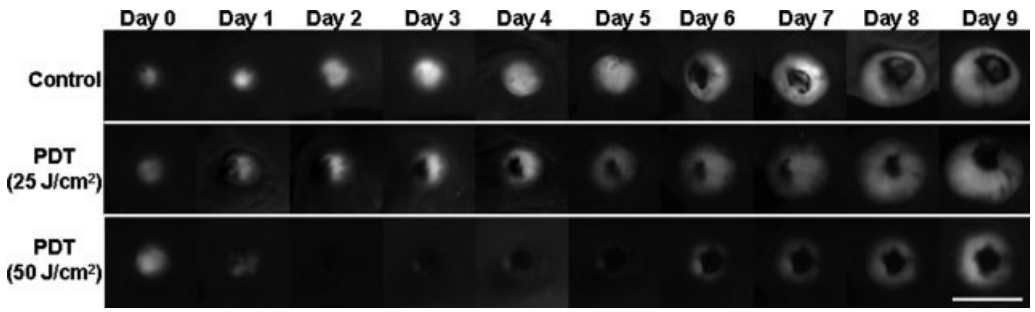

FIGURE 5 – *In vivo* tumor EGFP fluorescence images showing tumor response to vascular-targeting PDT with verteporfin. The EGFP-MatLyLu tumors were treated with 25 or 50 J/cm^2 light at 15 min after i.v. injection of 0.25 mg/kg dose of verteporfin. Tumor EGFP fluorescence was imaged daily for up to 9 days after treatment with a whole-body fluorescence imaging system as described in the Material and methods. Images at Day 0 were taken right before treatment. Control tumors received no treatment. Scale bar = 10 mm.

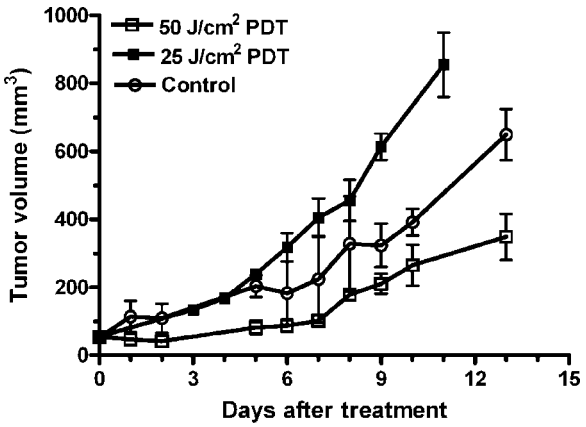

FIGURE 6 – Tumor volume changes after vascular-targeting PDT with verteporfin. The EGFP-MatLyLu tumors were treated with 25 or 50 J/cm^2 light at 15 min after i.v. injection of 0.25 mg/kg dose of verteporfin. Control tumors received no treatment. Tumor volume at Day 0 represented the starting volume right before the treatment.

blood vessels were mainly detected at the tumor periphery after PDT. In agreement with the macroscopic *in vivo* tumor imaging results, fluorescence microscopy also demonstrated a significant increase in the TRITC fluorescence intensity after PDT, especially in the tumor periphery.

Tumor response to vascular-targeting PDT was monitored noninvasively by whole body fluorescence imaging. The EGFP-MatLyLu tumors were imaged for EGFP fluorescence before and after treatments. Representative tumor EGFP fluorescence images are shown in Figure 5. Control tumors grew rapidly and exhibited central necrosis when tumor reached about 8–10 mm in diameter. Dead EGFP-MatLyLu tumor cells were unable to produce EGFP, causing dead tumor tissues to appear as dark areas in the EGFP fluorescence images. PDT with 25 J/cm^2 light dose induced a partial tumor necrosis, but this PDT condition failed to inhibit tumor growth (Fig. 5). In fact, tumor growth after this PDT treatment was even more rapid than control tumors and average tumor volume was nearly twice that of control tumors at 9 days after treatment (Fig. 6, $p < 0.01$). In contrast, the 50 J/cm^2 PDT effectively inhibited prostate tumor growth as indicated by a substantial decrease in EGFP fluorescence (Fig. 5) and average tumor volume (Fig. 6, $p < 0.01$ compared to the control tumor) after treatment. EGFP fluorescence was barely detectable at 2 days after PDT. But small EGFP fluorescent spots, indicating the existence of viable tumor cells, were often found at tumor edges several days after treatment and gradually grew in size which led to tumor recurrence. As shown in Figure 7, some viable tumor cells were clearly detected in tumor periphery at 48 hr after 50 J/cm^2 PDT.

Discussion

A whole-body animal fluorescence imaging system was used in this study to visualize noninvasively tumor response following PDT targeting of tumor blood vessels in an EGFP-expressing MatLyLu prostate tumor model. TRITC-albumin was used as a macromolecular probe to image tumor vascular barrier function (vascular permeability). The increase in the TRITC fluorescence intensity, caused by enhanced extravasation from blood vessels, is an indicator of vascular barrier disruption. Albumin has a plasma half-life of more than 24 hr and it was used to follow vascular permeability changes up to several hours after treatment.[22]

We found in the present study that vascular-targeting PDT increased vascular permeability in a dose-dependent manner, which is in agreement with our previous study and indicates that tumor vasculature is a primary target of PDT with verteporfin.[6] Importantly, our results demonstrate that the enhanced TRITC-albumin tumor uptake as a result of PDT-induced permeability increase was not homogeneous in tumor tissues. Both *in vivo* and *ex vivo* tumor imaging studies indicate that increase in TRITC-albumin extravasation was significantly higher in the peripheral tumor area than in the interior tumor area. Because the accumulation of a circulating molecule in tumor tissues is dependent upon the existence of functional blood vessels, the enhancement of TRITC-albumin accumulation in the tumor periphery is likely related to the predominant localization of functional blood vessels in peripheral tumor areas after vascular-targeting PDT. As shown in Figure 4, PDT was remarkably effective in inducing interior tumor blood vessel shutdown while some peripheral vessels were still functional up to 24 hr after PDT. Early closure of central tumor vessels limited the enhancement of TRITC-albumin in the tumor interior, whereas prolonged perfusion of some peripheral tumor vessels allowed more TRITC-albumin to continuously extravasate in the tumor periphery. We and others have previously reported that peripheral tumor vessels tend to maintain perfusion function after vascular-targeting PDT.[23–25] Our present results further demonstrate that continuous functioning of peripheral blood vessels, which had been permeabilized by PDT, led to preferential accumulation of circulating molecules in the tumor periphery.

The existence of functional blood vessels in the tumor periphery was associated with peripheral tumor cell survival after PDT. As shown in Figure 7, H&E staining indicated a rim of viable tumor cells in the tumor periphery at 48 hr after PDT in spite of extensive tumor necrosis. *In vivo* imaging of tumor EGFP fluorescence demonstrated that the survival of these peripheral tumor cells resulted in peripheral tumor recurrence (Fig. 5). Here we used EGFP as an indicator of tumor cell viability with the assumption that dead tumor cells are not able to synthesize EGFP and emit EGFP fluorescence. However, because EGFP has a half-life of more than 3 hr,[26] monitoring EGFP fluorescence shortly after treatment might not accurately report tumor cell viability. Sufficient time is needed for the degradation of EGFP synthesized

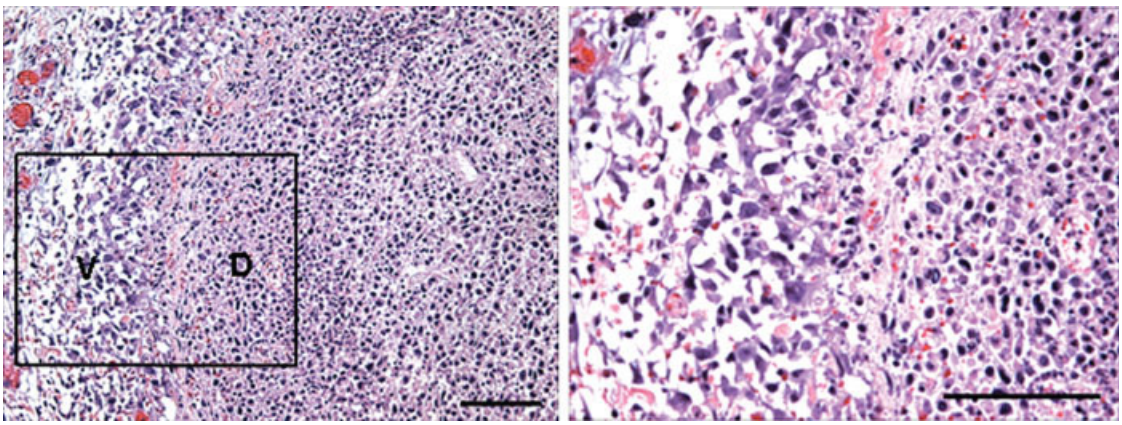

FIGURE 7 – H&E staining images showing the existence of viable tumor cells at the tumor periphery after vascular-targeting PDT with verteporfin. The EGFP-MatLyLu tumors were treated with 50 J/cm^2 light at 15 min after i.v. injection of 0.25 mg/kg dose of verteporfin. H&E staining of tumor sections taken at 48 hr after treatment showed wide spread tumor cell death and vascular damage. But a small number of viable tumor cells were detected at the tumor periphery. Part of the image on the left, highlighted in the box, is shown at a higher magnification on the right. The letters V and D indicate the viable tumor area and the dead tumor area, respectively. Bars = 100 μm. [Color figure can be viewed in the online issue, which is available at www.interscience.wiley.com.]

before treatment in order to use EGFP fluorescence to report cell viability. The observed decrease in EGFP fluorescence shortly after PDT in the present study was likely due to the oxidative degradation of EGFP during PDT rather than a real decrease in tumor cell viability. This was supported by the fact that there was little further decrease in EGFP fluorescence intensity over the following 5 hr period after PDT (Fig. 2*c*).

It is still not clear why peripheral tumor blood vessels react differently from interior blood vessels to vascular-targeting PDT. Understanding the mechanism behind this disparity in vascular response will help find ways to enhance the therapeutic effects of vascular-targeting PDT. Differences in vascular structure and function between tumor peripheral and interior blood vessels caused by morbid tumor pathobiology possibly contribute to such variations in vascular response. It is known that tumor tissues have higher tissue interstitial pressure than normal tissues because of leaky tumor blood vessels and poor lymphatic system function.[27,28] High tumor interstitial pressure is able to compress tumor vessels and lead to vessel collapse. Vessel compression and collapse are more severe in the tumor interior where tumor interstitial pressure is higher.[29,30] PDT has been shown to further increase tumor interstitial pressure as a result of enhancing vascular permeability.[31,32] Such an increase in tumor interstitial pressure will likely impose a greater compression on tumor blood vessels and cause vascular shutdown, especially in tumor interior areas. Moreover, we recently found that, compared to the interior tumor vessels, peripheral tumor blood vessels were generally larger and exhibited vascular lumen as well as more coverage of vascular pericytes and basement membrane.[33] Less mechanic compression together with more vessel supporting structures might make peripheral tumor vessels more resistant than the interior vessels to vessel closure induced by vascular-targeting PDT.

The survival of peripheral tumor cells as a consequence of disparity in vascular response between peripheral and interior blood vessels represents a therapeutic challenge for the vascular-targeting PDT. Several strategies can be adopted to eliminate or at least minimize surviving tumor cells at the tumor periphery. First of all, we could increase the PDT dose to determine whether a higher dose of vascular-targeting PDT will lead to the shutdown of both interior and peripheral tumor blood vessels, resulting in an increased tumor cure. Secondly, as combination therapies have been routinely used in cancer treatments, one approach of enhancing photodynamic vascular targeting effectiveness is to combine it with other cancer therapies. Combination therapies can be designed based on different targeting principles. Targeting both tumor vascular and cellular compartments by combining vascular-targeting PDT with a cancer cell-targeted therapy could be a promising strategy because the increased vascular permeability induced by PDT has been shown to enhance drug delivery.[6,34,35] Our present study further demonstrates that the enhancement of drug accumulation mainly occurred at the tumor periphery where tumor cell survival tends to occur after vascular-targeting PDT. Therefore, combining vascular-targeting PDT with other anticancer drug therapies will allow more anticancer agents to be preferentially deposited in the peripheral tumor area to kill tumor cells that otherwise might survive after PDT treatment.

In summary, we utilized *in vivo* animal fluorescence imaging combined with standard *ex vivo* tissue fluorescence microscopy to examine changes in vascular function and tumor cell viability after vascular-targeting PDT. Our results indicate that, although PDT causes an overall increase in vascular permeability, peripheral tumor blood vessels are somehow able to maintain perfusion function whereas interior blood vessels are shutdown shortly after PDT. Such a disparity in vascular response is conducive to peripheral tumor cell survival and also explains the preferential accumulation of circulating molecules in the tumor periphery. We are currently investigating the mechanisms underlying this response disparity and exploring therapeutic strategies that minimize the survival of peripheral tumor cells.

Acknowledgements

The authors gratefully acknowledge Dr. Tayyaba Hasan of the Wellman Center for Photomedicine for helpful discussions and QLT Inc. for providing verteporfin.

References

1. Dougherty TJ, Gomer CJ, Henderson BW, Jori G, Kessel D, Korbelik M, Moan J, Peng Q. Photodynamic therapy. J Natl Canc Inst 1998; 90:889–905.
2. Schmidt R. Photosensitized generation of singlet oxygen. Photochem Photobiol 2006;82:1161–77.
3. Chen B, Pogue BW, Hoopes PJ, Hasan T. Vascular and cellular targeting for photodynamic therapy. Crit Rev Eukaryot Gene Expr 2006;16:279–305.
4. Brown SB, Mellish KJ. Verteporfin: a milestone in opthalmology and photodynamic therapy. Expert Opin Pharmacother 2001;2:351–61.

5. Chen B, Pogue BW, Hoopes PJ, Hasan T. Combining vascular and cellular targeting regimens enhances the efficacy of photodynamic therapy. Int J Radiat Oncol Biol Phys 2005;61:1216–26.
6. Chen B, Pogue BW, Luna JM, Hardman RL, Hoopes PJ, Hasan T. Tumor vascular permeabilization by vascular-targeting photosensitization: effects, mechanism, and therapeutic implications. Clin Canc Res 2006;12:917–23.
7. Liu DL, Svanberg K, Wang I, Andersson-Engels S, Svanberg S. Laser Doppler perfusion imaging: new technique for determination of perfusion and reperfusion of splanchnic organs and tumor tissue. Laser Surg Med 1997;20:473–9.
8. Enejder AM, af Klinteberg C, Wang I, Andersson-Engels S, Bendsoe N, Svanberg S, Svanberg K. Blood perfusion studies on basal cell carcinomas in conjunction with photodynamic therapy and cryotherapy employing laser-Doppler perfusion imaging. Acta Derm Venereol 2000;80:19–23.
9. Yu G, Durduran T, Zhou C, Wang HW, Putt ME, Saunders HM, Sehgal CM, Glatstein E, Yodh AG, Busch TM. Noninvasive monitoring of murine tumor blood flow during and after photodynamic therapy provides early assessment of therapeutic efficacy. Clin Canc Res 2005;11:3543–52.
10. Kruijt B, de Bruijn HS, van der Ploeg-van den Heuvel A, Sterenborg HJ, Robinson DJ. Laser speckle imaging of dynamic changes in flow during photodynamic therapy. Laser Med Sci 2006;21:208–12.
11. Smith TK, Choi B, Ramirez-San-Juan JC, Nelson JS, Osann K, Kelly KM. Microvascular blood flow dynamics associated with photodynamic therapy, pulsed dye laser irradiation and combined regimens. Laser Surg Med 2006;38:532–9.
12. Aalders MC, Triesscheijn M, Ruevekamp M, de Bruin M, Baas P, Faber DJ, Stewart FA. Doppler optical coherence tomography to monitor the effect of photodynamic therapy on tissue morphology and perfusion. J Biomed Opt 2006;11:044011.
13. Ohlerth S, Laluhova D, Buchholz J, Roos M, Walt H, Kaser-Hotz B. Changes in vascularity and blood volume as a result of photodynamic therapy can be assessed with power Doppler ultrasonography. Laser Surg Med 2006;38:229–34.
14. Schmidt-Erfurth U, Niemeyer M, Geitzenauer W, Michels S. Time course and morphology of vascular effects associated with photodynamic therapy. Ophthalmology 2005;112:2061–9.
15. Zilberstein J, Schreiber S, Bloemers MC, Bendel P, Neeman M, Schechtman E, Kohen F, Scherz A, Salomon Y. Antivascular treatment of solid melanoma tumors with bacteriochlorophyll-serine-based photodynamic therapy. Photochem Photobiol 2001;73:257–66.
16. Seshadri M, Spernyak JA, Mazurchuk R, Camacho SH, Oseroff AR, Cheney RT, Bellnier DA. Tumor vascular response to photodynamic therapy and the antivascular agent 5,6-dimethylxanthenone-4-acetic acid: implications for combination therapy. Clin Canc Res 2005; 11:4241–50.
17. Yang M, Baranov E, Jiang P, Sun FX, Li XM, Li L, Hasegawa S, Bouvet M, Al-Tuwaijri M, Chishima T, Shimada H, Moossa AR, et al. Whole-body optical imaging of green fluorescent protein-expressing tumors and metastases. Proc Natl Acad Sci USA 2000;97:1206–11.
18. Hoffman RM. The multiple uses of fluorescent proteins to visualize cancer in vivo. Nat Rev Canc 2005;5:796–806.
19. Ntziachristos V. Fluorescence molecular imaging. Annu Rev Biomed Eng 2006;8:1–33.
20. Nguyen TH, Oberholzer J, Birraux J, Majno P, Morel P, Trono D. Highly efficient lentiviral vector-mediated transduction of nondividing, fully reimplantable primary hepatocytes. Mol Ther 2002;6:199–209.
21. Pogue BW, Gibbs SL, Chen B, Savellano M. Fluorescence imaging in vivo: raster scanned point-source imaging provides more accurate quantification than broad beam geometries. Technol Canc Res Treat 2004;3:15–21.
22. Matsushita S, Chuang VT, Kanazawa M, Tanase S, Kawai K, Maruyama T, Suenaga A, Otagiri M. Recombinant human serum albumin dimer has high blood circulation activity and low vascular permeability in comparison with native human serum albumin. Pharm Res 2006;23:882–91.
23. Chen B, Pogue BW, Goodwin IA, O'Hara JA, Wilmot CM, Hutchins JE, Hoopes PJ, Hasan T. Blood flow dynamics after photodynamic therapy with verteporfin in the RIF-1 tumor. Radiat Res 2003; 160:452–9.
24. Kurohane K, Tominaga A, Sato K, North JR, Namba Y, Oku N. Photodynamic therapy targeted to tumor-induced angiogenic vessels. Cancer Lett 2001;167:49–56.
25. Koudinova NV, Pinthus JH, Brandis A, Brenner O, Bendel P, Ramon J, Eshhar Z, Scherz A, Salomon Y. Photodynamic therapy with Pd-bacteriopheophorbide (TOOKAD): successful in vivo treatment of human prostatic small cell carcinoma xenografts. Int J Canc 2003; 104:782–9.
26. Li X, Zhao X, Fang Y, Jiang X, Duong T, Fan C, Huang CC, Kain SR. Generation of destabilized green fluorescent protein as a transcription reporter. J Biol Chem 1998;273:34970–5.
27. Fukumura D, Jain RK. Tumor microenvironment abnormalities: causes, consequences, and strategies to normalize. J Cell Biochem 2007;101:937–49.
28. Heldin CH, Rubin K, Pietras K, Ostman A. High interstitial fluid pressure - an obstacle in cancer therapy. Nat Rev Canc 2004;4:806–13.
29. Rofstad EK, Tunheim SH, Mathiesen B, Graff BA, Halsor EF, Nilsen K, Galappathi K. Pulmonary and lymph node metastasis is associated with primary tumor interstitial fluid pressure in human melanoma xenografts. Canc Res 2002;62:661–4.
30. Boucher Y, Jain RK. Microvascular pressure is the principal driving force for interstitial hypertension in solid tumors: implications for vascular collapse. Canc Res 1992;52:5110–14.
31. Fingar VH, Wieman TJ, Doak KW. Changes in tumor interstitial pressure induced by photodynamic therapy. Photochem Photobiol 1991; 53:763–8.
32. Leunig M, Goetz AE, Gamarra F, Zetterer G, Messmer K, Jain RK. Photodynamic therapy-induced alterations in interstitial fluid pressure, volume and water content of an amelanotic melanoma in the hamster. Br J Canc 1994;69:101–3.
33. Chen B, He C, de Witte P, Hoopes PJ, Hasan T, Pogue BW. Vascular targeting in photodynamic therapy. In: Hamblin MR, Mroz P, eds. Advances in photodynamic therapy: basic, translational and clinicaled. Norwood, MA: Artech House Inc (in press).
34. Snyder JW, Greco WR, Bellnier DA, Vaughan L, Henderson BW. Photodynamic therapy: a means to enhanced drug delivery to tumors. Canc Res 2003;63:8126–31.
35. Debefve E, Pegaz B, Ballini JP, Konan YN, van den Bergh H. Combination therapy using aspirin-enhanced photodynamic selective drug delivery. Vascul Pharmacol 2007;46:171–80.

CHAPTER 9

Vascular Targeting in Photodynamic Therapy

Bin Chen, Chong He, Peter de Witte, P. Jack Hoopes, Tayyaba Hasan, and Brian W. Pogue

9.1 Introduction

The mechanism of PDT in cancer treatment is complicated and evolves as our understanding of cancer biology and pharmacology progresses. It is now clear that PDT can either directly kill tumor cells or indirectly induce tumor cell death as a result of direct damage to tumor stroma [1]. Adequate and simultaneous deposition of a photosensitizer, light, and oxygen molecules in tumor cells will cause tumor cell death. However, this direct photocytotoxicity is often limited (generally less than 1-log) in tumor cell killing likely due to inadequate supply of photosensitizers, light, and/or oxygen in tumor tissues [2]. Tumor vasculature is an important target of PDT and this indirect tumor targeting mechanism is mainly responsible for the acute decrease of tumor burden after PDT with most photosensitizers [1]. Furthermore, PDT-induced inflammation as well as direct photosensitizing effects on immune cells may activate the body immune system and lead to the generation of tumor-specific immunity, which is important for maintaining long-term tumor control [3].

For most photosensitizers, vascular damage is the predominant PDT effect and primarily responsible for the final treatment outcome [1]. Because of this, vascular-targeting PDT has been developed to further potentiate vascular damage. In this chapter, we will focus on vascular targeting in PDT. This targeting mechanism has led to so far the most successful application of PDT and is showing great promise in cancer treatment as well. We will discuss photodynamic vascular targeting principle, mechanisms, challenges, and strategies to enhance its therapeutic outcome.

9.2 Tumor Vascular Targeting

It is well-known that solid tumors cannot grow larger than about 1 mm^3 without developing a vascular network [4]. This is because, similar to normal tissues, tumor tissues require a functional vascular system for the delivery of nutrients and the removal of metabolic waste. To sustain tumor growth, tumor tissues need to depend upon existing host vessels as well as develop new blood vessels for blood supply. Compared to the normal vasculature, tumor blood vessels exhibit significant abnor-

malities in vessel architecture (e.g., tortuousity, dilatation, irregular branching, and lack of pericyte and basement membrane coverage) and function (e.g., stagnant blood flow, increased vascular permeability) [5]. Although the mechanisms leading to tumor vessel structural and functional abnormalities are not well understood, the imbalance between pro- and antiangiogenic factors and mechanical compression generated by high tumor interstitial pressure and proliferating tumor cells have been suggested to be the major contributing factors [5]. The differences between tumor versus normal vasculature in the vessel molecular signature, structure, and function provide the basis for selective tumor vascular targeting.

Vascular targeting therapy can be divided into antiangiogenic therapy that inhibits the formation of new vessels and vascular disrupting therapy that targets the existing blood vessels [6]. The overall goal of tumor vascular targeting therapy is to selectively disrupt or modulate tumor vascular function for the therapeutic purposes without affecting much normal tissue functions. This modality can be used alone as monotherapy, but more often it is used in combination with other therapies in cancer treatment. Tumor vascular targeting strategy has several apparent advantages over the conventional tumor cellular targeting approach [4, 7]. First, vascular targets are readily accessible to the therapeutic agents delivered intravenously whereas tumor cellular targets are typically difficult to reach due to the existence of various physiological barriers. Second, vascular targeting is highly efficient and potent in tumor cell killing because, unlike tumor cell-targeted therapies, not all the endothelial cells are necessary to be targeted to disrupt tumor vascular function. Instead, damage to a single endothelial cell or a portion of blood vessel may induce catastrophic effect on tumor perfusion, resulting in killing thousands of tumor cells that are dependent upon that vessel for blood supply. Third, because endothelial cells are generally considered to be more genetically stable than tumor cells, the risk of acquiring drug resistance is usually low. These advantages render tumor vascular targeting a promising approach in current cancer therapy.

9.3 Principle of Photodynamic Vascular Targeting

Photodynamic vascular targeting is based on site-directed delivery of photosensitizing agents to the vascular system followed by light irradiation to induce site-specific vascular photosensitizing effects. Since vasculature-directed photosensitizer delivery can be achieved by passive or active means, photodynamic vascular targeting can be further divided into passive or active targeting approach [1]. The passive vasculature-directed photosensitizer delivery is primarily based on the innate photosensitizer pharmacokinetic property that plasma drug level is often high shortly after intravenous administration of a photosensitizer (Color Plate 4). As can be seen, fluorescence image of hypericin (a) and the corresponding H&E staining photograph (b) demonstrate the intravascular localization of hypericin at 30 minutes after i.v. injection of a 5-mg/kg dose of hypericin in the RIF-1 mouse tumor model. Vascular-targeting PDT with hypericin, (i.e., light treatment at 30 minutes after a 5-mg/kg dose of hypericin injection, caused vascular shutdown in central tumor areas). However, some tumor peripheral blood vessels were still functional, as indicated by the presence of Hoechst dye fluorescence (c), which was injected 1

minute before euthanizing the animal. The corresponding H&E staining image (d) confirmed the vessel histology. Vascular-targeting PDT with hypericin (i.e., light treatment at 30 minutes after a 1-mg/kg dose of hypericin injection), significantly inhibited the RIF tumor growth and its antitumor effect was further enhanced by subcutaneous injection of antiangiogenic drug TNP-470 at a dose of 30 mg/kg once every 2 days. Each group included 8 to 10 animals (Figure 9.1).

This time period when photosensitizer is mainly localized inside the vasculature provides a temporal window for the passive vascular targeting. Although the exact location of this temporal window is largely dependent on the plasma kinetics of individual photosensitizer, for most photosensitizers it typically occurs within 60 minutes after injection.

By contrast, active vascular-targeting PDT seeks to achieve vasculature-directed drug delivery by altering photosensitizer pharmacokinetic property through drug structure modification or drug formulation into a targeted delivery system [1]. A targeting moiety that has a high affinity to endothelial cell markers (e.g., integrins, VEGF receptors, tumor endothelial markers) or vessel supporting structures (e.g., fibronectin with ED-B domain) is often used in the photosensitizer modification. The resulting photosensitizer conjugates are expected to be selectively accumulated in the targeted blood vessels, leading to a site-specific photosensitization upon light activation.

9.4 Mechanisms of Photodynamic Vascular Targeting

Photodynamic vascular targeting therapy has been shown to produce reactive oxygen species intravascularly, in particular singlet oxygen, which is believed to be mainly responsible for the subsequent vessel structural and functional alterations [8]. The ultimate goal of vascular-targeting PDT in cancer therapy is to obtain maximal tumor cell killing by inducing tumor vascular shutdown. The mechanism of

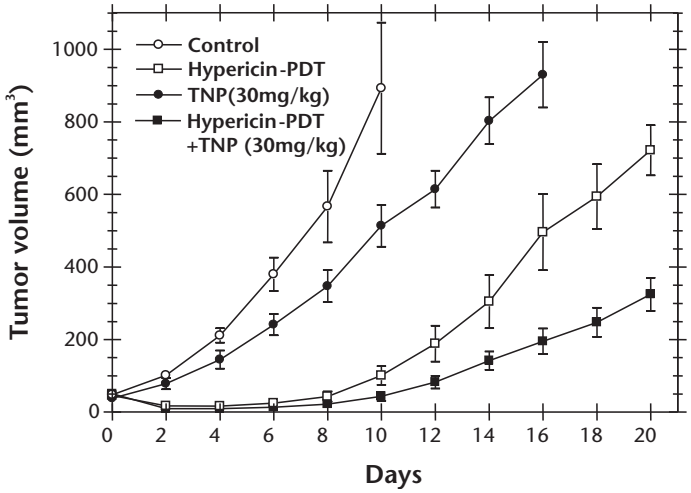

Figure 9.1 Tumor inhibition after vascular-targeting PDT with hypericin and antiangiogenic drug TNP-470.

PDT-induced vascular shutdown is complicated because it likely involves multiple targets in the blood cells and blood vessels, which are interweaved in complex cascades of events. Intravital fluorescence microscopic study demonstrates that microcirculation dysfunction after vascular-targeting PDT is induced by at least two vascular events, vessel occlusion induced by thrombus formation and vessel constriction/collapse caused by mechanic compression and vasoactive substances (Figure 9.2(a) and (b)).

Thrombus formation can be induced by photosensitizing damage to either blood cells or endothelial cells. It has been shown that PDT can cause platelet aggregation and thrombus formation by direct damage to the platelet and red blood cell membranes [9, 10]. Damage to the platelets may further stimulate the release of thromboxane, a vasoactive substance with potent vessel constriction and thrombus formation effects [11]. More often, PDT-induced damage to the blood cells is coupled with damage to the endothelial cells, which might explain why blood cell aggregation is often observed starting from the vessel wall. Since endothelium serves as an interface between blood and underneath tissue, loss of endothelial barrier as a result of vascular photosensitization exposes tissue extracellular matrix to the circulation, which activates platelets and polymorphonuclear leukocytes and induces blood cell adherence to the damaged endothelial cells. Thromboxane release as a result of platelet activation has been shown to contribute significantly to vessel constriction and thrombus formation, which can be inhibited by thromboxane inhibitors aspirin and indomethacin [12] or platelet depletion [11]. Endothelial cells also

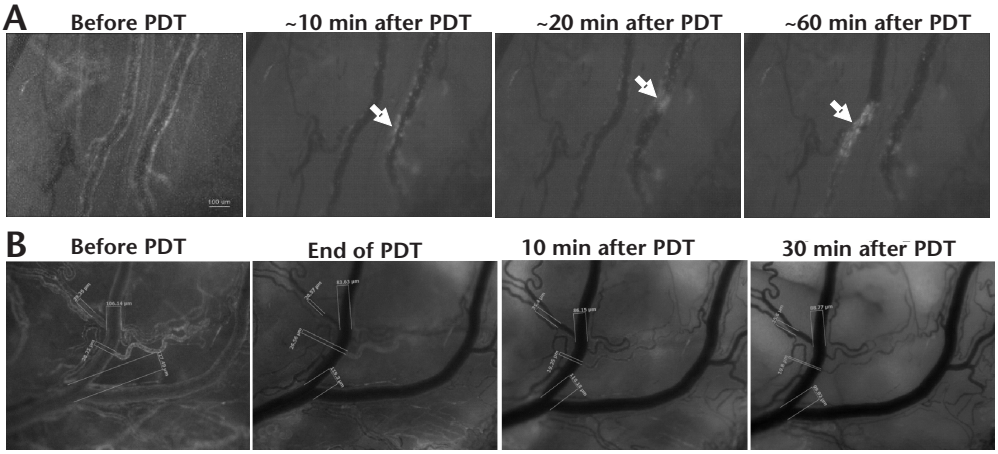

Figure 9.2 (a) Intravital fluorescence microscopic images showing intravascular localization of verteporfin and thrombus formation after vascular-targeting PDT in the orthotopic MatLyLu rat prostate tumor. Rat blood cells were labeled with fluorescent dye DiI and injected (i.v.) into the animals to highlight blood vessels. The MatLyLu tumors were treated with 50-J/cm^2 light (690 nm, at 50 mW/cm^2) at 15 minutes after i.v. injection of 0.25-mg/kg verteporfin to target tumor blood vessels. Blood cell adherence and thrombus formation, indicated by arrows, were clearly visible after vascular-targeting PDT. (b) Intravital fluorescence microscopic imaging of vascular permeability increase and vessel compression after vascular-targeting PDT with verteporfin. Animals were i.v. injected with 10-mg/kg 2,000-kDa FITC-dextran right before irradiation and imaged every 2 minutes for the FITC fluorescence during and after PDT. The images shown are right before PDT, immediately, 10 minutes, and 30 minutes after PDT. Sizes of some blood vessels are labeled on the images.

influence blood clotting balance by releasing von Willebrand factor that facilitates thrombus formation [13] and prostacyclin that inhibits thrombus formation and dilates blood vessels [14]. The net effect likely favors clot formation at least at early stage after vascular photosensitization. Blood clots formed inside vessel lumen cause obstruction to blood flow. However, blood vessels may resume perfusion because not all the clots are stable and some of them can be dissolved and dislodged possibly by body anticoagulants. Only the stable thrombi will finally occlude blood vessels and shut down vascular function. Inhibition of thrombus formation by heparin has been shown to delay PDT-induced blood flow stasis [15]. But it is not able to completely inhibit blood flow decrease, suggesting that thrombus formation is only partially responsible for the vascular damage induced by PDT.

As a spontaneous response to blood vessel damages, vessel constriction is often observed after vascular photosensitization, which also contributes to PDT-induced blood flow stasis (Figure 9.3).

Vessel constriction can be caused by the release of vasoactive substances such as thromboxane and leukotrienes [16]. However, a strong inducer of vessel constriction and even collapse in tumor tissues comes from the increase of interstitial fluid pressure [5]. It is well-established that tumor tissues generally have higher tissue interstitial pressure than the normal tissues because of leaky tumor blood vessels. The mechanic compression generated by high tumor interstitial pressure can collapse tumor blood vessel even without treatment and this is one of the mechanisms involved in acute hypoxia development in tumor tissues [17]. Such vessel compression/collapse effects are aggravated by PDT because PDT is able to cause vascular barrier disruption and therefore further increase tumor interstitial pressure [18, 19].

Since endothelial cells play a critical role in maintaining vascular barrier and perfusion functions, it is important to study how endothelial cells respond to photosensitization at cellular and molecular levels. Studies with different photosensitizers have shown that photosensitization of endothelial cells induces rapid microtubule

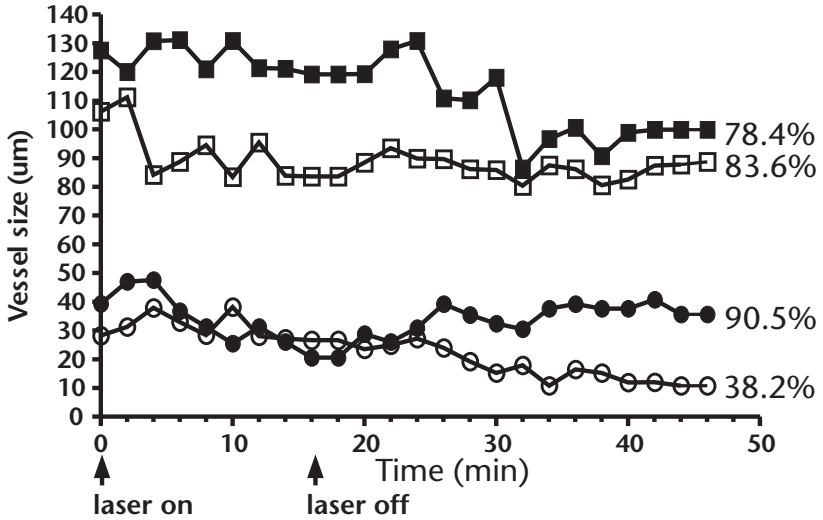

Figure 9.3 The change of blood vessel size during and after vascular-targeting PDT with verteporfin. Sizes of four blood vessels shown in Figure 9.2b were measured and the percentages over pretreatment sizes are shown.

depolymerization followed by stress fiber actin formation and cell rounding [20, 21].

Although it is not clear how microtubule damage results in endothelial cell shape change, microtubule depolymerization is believed to initiate subsequent vessel functional changes because endothelial cell barrier function is dependent on endothelial cell morphology regulated by cell cytoskeleton. Indeed, photosensitization-induced endothelial cell shape change has been shown to be correlated to the permeability increase [21]. Increase in cytosol calcium concentration has been suggested to be the cause of microtubule depolymerization [20]. However, direct photosensitizing damage to the microtubules cannot be ruled out. Vascular permeability increase has been observed in both animal and human studies shortly after PDT [16, 22], suggesting that this is an early event following endothelial cell damage (Figure 9.4).

The disruption of vascular barrier function will trigger the subsequent thrombus formation and vessel compression as described above.

The molecular mechanism involved in endothelial photosensitization is poorly studied. There are reports showing that photosensitization activates nuclear transcriptor NF-κB in endothelial cells through a reactive oxygen species-mediated mechanism [23, 24]. Since NF-κB is major regulator of inflammatory and immune reactions, its activation in endothelial cells plays an important role in vascular photosensitization-induced tumor destruction. Paradoxically, NF-κB activation can cause both tumor inhibition and stimulation [25]. Tumor inhibition is related to its role in enhancing gene expression of cytokines (IL-6, TNF-α), adhesion molecules (intercellular adhesion molecule-1, vascular cell adhesion molecule-1), and possibly heat shock proteins [24, 26]. As a result, vascular photosensitization treatment is able to stimulate blood cells, especially neutrophils adhesion to the endothelial cells, inducing vascular damages. On the other hand, tumor stimulation as a consequence of NF-κB activation is associated with the upregulation of cyclooxygenas-2 (COX-2), matrix metalloproteases (MMPs), and inhibitors of apoptosis [25]. Although there is no report demonstrating the upregulation of COX-2 and

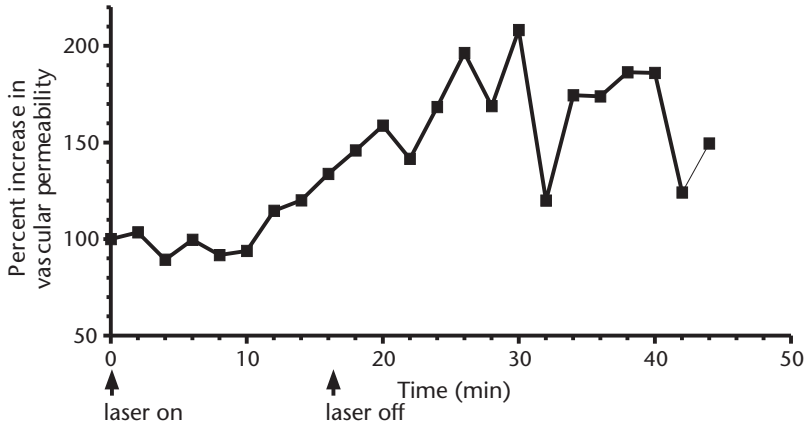

Figure 9.4 The change of vascular permeability during and after vascular-targeting PDT with verteporfin. Vascular permeability change was determined by measuring the 2,000-kDa FITC-dextran fluorescence intensity from the above intravital microscopic images Figure 9.2b, and normalizing the aftertreatment intensity values to the pretreatment value.

apoptosis inhibitors in endothelial cells, which has been shown in tumor cells, the induction of MMP-9 expression has been confirmed in endothelial cells after PDT, suggesting a role of NF-κB activation in endothelial resistance to photosensitization [25]. Interestingly, pretreatment of endothelial cells with PDT or other oxidative stress inducers has been shown to induce cell adaptation, resulting in the upregulation of heat shock protein and antioxidation enzymes through the p38 MARK pathway. This cellular adaptation to the oxidative stressors indeed renders endothelial cells' resistance to the subsequent treatment [27].

9.5 Therapeutic Challenges of Photodynamic Vascular Targeting

Although vascular-targeting PDT is able to induce extensive tumor vascular shutdown, and consequently, tumor cell death, functional blood vessels are typically detected at tumor peripheral areas following noncurative treatments. The existence of these functional blood vessels can lead to tumor recurrence, which is often observed starting from the peripheral tumor area [28, 29]. Figure 9.5 shows representative tumor fluorescence images after verteporfin-PDT.

In this experiment, we used a lentivirus-transduced MatLyLu prostate tumor cell line that permanently expresses EGFP. The EGFP-MatLyLu tumors were imaged noninvasively for the EGFP fluorescence before and after PDT by using a whole-body fluorescence imaging system. Because dead EGFP-MatLyLu tumor cells were not able to produce EGFP, dead tumor tissues would appear as dark areas and only viable tumor tissues could be visible on tumor EGFP fluorescence images. Control tumors grew rapidly and generally exhibited central necrosis when a tumor reached about 8 to 10 mm in diameter. The 50-J/cm^2 PDT was effective in eradicating tumor tissue and little EGFP fluorescence was detected by 2 days after PDT. However, small EGFP fluorescent spots, indicating the existence of viable tumor cells, were detected at tumor edges several days after treatment. Peripheral viable tumor tissues were found growing rapidly, leading to tumor recurrence.

It is still not clear why tumor peripheral and central blood vessels react differently to the vascular photosensitization. It is hypothesized that such a variation in vascular response is likely related to the differences in tumor interstitial pressure and the structure of blood vessels in tumor central versus peripheral areas. Because

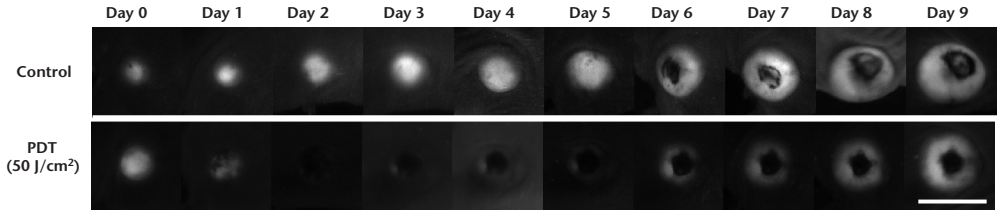

Figure 9.5 Noninvasive fluorescence imaging of tumor response after vascular-targeting PDT with verteporfin. The EGFP-MatLyLu tumors were imaged with a whole-body fluorescence imaging system before and after the vascular-targeting PDT, showing tumor recurrence starting from 3 days after treatment. Images of control tumor receiving no treatment are also shown for comparison. Bar=10 mm.

the tumor central area generally has a higher interstitial pressure than the peripheral area, central blood vessels are more likely to collapse than the peripheral vessels as a result of higher mechanic compression [30, 31]. Moreover, peripheral tumor blood vessels are generally found to be larger and have more vessel supporting structures such as pericytes than the central tumor vessels (Figure 9.6).

Collectively, less tumor interstitial pressure together with more vessel supporting structures might make peripheral tumor vessels more resistant to the vessel compression/collapse imposed by PDT-induced tumor interstitial pressure elevation. Survival of these peripheral blood vessels after vascular photosensitization provides a chance of survival to the tumor cells supported by these vessels.

To maintain tissue integrity and function, biological systems develop sets of well-balanced repairing and adaptive mechanisms to deal with various internal and external damages. Through complicated and often redundant signaling cascades, cells are able to survive nonfatal damages by stimulating cell growth, tissue angiogenesis, and remodeling. Unfortunately, tumor endothelial and tumor cells can hijack these spontaneous responses to obtain their own survival after subcurative treatments, leading to disease recurrence. As mentioned above, photosensitization activates p38 MAPK survival signaling in endothelial cells [27]. The activation of p38 MARK is able to further induce the upregulation of COX-2, which catalyzes the conversion of arachidonic acid to prostaglandins (PGs) [32, 33]. PGs, especially PGE2, have been shown to enhance cell motility, adhesion, and survival, and stimulate tumor angiogenesis by inducing VEGF release. Furthermore, elevated VEGF release can also be obtained via HIF-1-mediated signaling pathway activated by PDT-induced tissue hypoxia [34, 35]. Through the activation of these self-repairing and surviving pathways, tumor endothelial and tumor cells actually create a favorable microenvironment to maintain their survival and growth. It is not unusual to observe that tumor cells after subcurative PDT treatments are actually becoming

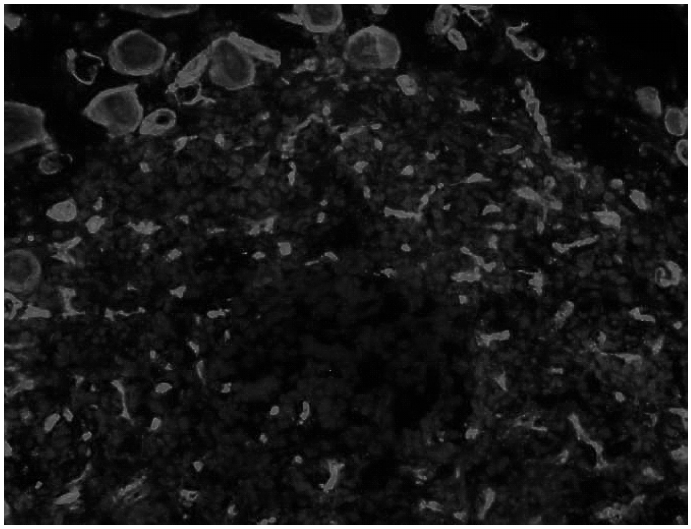

Figure 9.6 Immunohistochemical staining showing the difference in vessel morphology and structure between tumor peripheral and central blood vessels. Blood vessel pericyte marker α-small muscle actin (α-SMA) staining indicates that peripheral vessels are generally bigger and have better pericyte coverage than central vessels. Note the existence of central necrosis.

more aggressive [35, 36]. In the end, noncurative treatments might unintentionally select a small population of cells that are good at manipulating normal physiological pathways to survive therapeutic stressors. Therefore, how to target cell survival signals and adaptation mechanisms represents a major therapeutic challenge for not only photodynamic vascular targeting, but also all other cancer therapies.

9.6 Current Status of Photodynamic Vascular Targeting

Passive vascular-targeting PDT provides an effective way of targeting blood vessels and has been successfully translated into clinical application for diseases characterized by the overproliferation of blood vessels. Based on this mechanism, verteporfin is currently being used for the treatment of age-related macular degeneration (AMD) and more photosensitizers such as tin ethyletiopurpurin (SnET2, Purlytin) and lutetium texaphyrin (Lu-Tex, Optrin) are under clinical trials for AMD. Quite a few photosensitizers have also been evaluated for cancer treatment based on this passive targeting mechanism [1]. Among these photosensitizes, Tookad is at the forefront in the development pipeline. Currently, Tookad is in a phase I/II clinical trial for locally recurrent prostate cancer after radiation therapy [37]. Although limited in the number of studies, active vascular-targeting PDT is being pursued actively for the treatment of cancer and noncancer diseases. Promising results have been obtained from several studies of conjugating photosensitizers to the blood vessel-homing peptides [38–42].

9.7 Strategies to Enhance Photodynamic Vascular Targeting

As combination therapy has been routinely used in cancer treatment, one approach of enhancing photodynamic vascular targeting efficacy is to combine it with other cancer therapies. Combination therapies can be designed based on several different targeting principles. Targeting both tumor vascular and cellular compartments by combining photodynamic vascular targeting therapy with a cancer cell-targeted therapy has been demonstrated to be an effective strategy. For instance, more than additive antitumor effects have been obtained from most early studies exploring the combination of PDT and cancer chemotherapy [43, 44]. Recently, PDT itself has been studied for targeting tumor blood vessels or tumor cells, and enhanced therapeutic effects have been reported from studies with combined PDT regimens that target both tumor compartments. These dual targeting PDT treatments include PDT using a vascular-targeting photosensitizer Photofrin in combination with PDT using a cellular-targeting photosensitizer 5-aminolevulinic acid (5-ALA) [45], PDT regimen based on photosensitizer dose fractionation protocol so that light can be delivered when photosensitizer has been deposited in both vascular and cellular compartments [46], and sequential combination of a cancer cell-targeted PDT followed by a blood vessel-targeted PDT [28].

Although the mechanisms responsible for such enhanced antitumor effects are still not clear, spatial cooperation in tumor cell killing between vascular-targeting PDT and cancer cell-targeted therapies possibly plays a role here. As mentioned

above, vascular-targeting PDT is especially effective in inducing central tumor cell death. Cancer cell-targeted therapies however mainly kill peripheral PDT tumor cells because most anticancer agents, including photosensitizers, tend to accumulate more at the tumor periphery presumably because of better perfusion at tumor peripheral areas [47, 48]. Thus, cancer cell-targeted therapies may complement vascular-targeting PDT in reducing some peripheral tumor cells that are otherwise not able to be killed by vascular-targeting PDT. The other mechanism possibly involved in the therapeutic enhancement is that both conventional and vascular-targeting PDT treatments have been shown to improve drug delivery to tumor tissues as a result of PDT-induced vascular permeability increase [21, 49]. Interestingly, we have found that such an enhancement in tumor drug delivery caused by vascular-targeting PDT is actually more pronounced in the tumor peripheral area than in the tumor central area (observation not yet published). The overall increase of the anticancer agent in the tumor tissue, tumor peripheral areas in particular, after vascular-targeting PDT may also account for the improved antitumor effect.

The other important combination strategy is to target the surviving and repairing pathways that tumor endothelial cells as well as tumor cells depend on to maintain their survival after vascular-targeting PDT. An example in this case is the combination of vascular-targeting PDT with antiangiogenic therapy. PDT treatments have been found to stimulate angiogenesis and tumor growth by inducing VEGF upregulation [34, 35]. Depending on the photosensitizer, the type of tumor model, and treatment conditions, the elevation of VEGF can be caused by hypoxia-induced HIF-1 activation [34], COX-2 overexpression [33, 50] and p38 MAPK activation [35]. Thus, combined treatments of PDT with VEGF antibody bevacizumab [51], antiangiogenic drug TNP-470 [52] or COX-2 inhibitor [50] have all been shown to enhance the therapeutic effects. As our understanding regarding tumor/endothelial cell adaptation to therapeutic stressors increases, more such rationale-designed combination regimens will be designed to target crucial cellular and molecular surviving pathways, leading to a synergistic treatment outcome.

9.8 Summary and Conclusions

Vascular damage is the most important mechanism involved in PDT-mediated tumor eradication. Vascular-targeting PDT is designed to further strengthen this vascular photosensitization effect by site-directed delivery of photosensitizing agents to the vascular targets. Being so far the most successful PDT regimen, vascular-targeting PDT has been used clinically in the management of AMD and is showing great promise in cancer treatment as well. However, spatial heterogeneity in the vascular response and tumor/endothelial cell adaptation to the oxidative and hypoxic stressors often result in tumor recurrence. Therefore, a combination therapy with modalities complementary to the vascular-targeting PDT in tumor cell killing or treatments targeting cell surviving and adaptive signaling pathways often shows better results than vascular-targeting PDT alone. These combination regimens should be further evaluated in the clinic. Equally important, we need to further understand the mechanism of vascular-targeting PDT at tissue, cellular, and molecular levels. It is obvious that 100% tumor cure can be achieved in preclinical animal

tumor models with photodynamic vascular targeting therapies. The question is whether it is possible to deliver such curative, rather than subcurative, vascular-targeting PDT to the patients, and how.

Acknowledgment

This work was supported by Department of Defense (DOD) Prostate Cancer Research Grant W81XWH-06-1-0148. The authors would like to gratefully acknowledge QLT Inc. for providing verteporfin.

References

[1] Chen, B., et al., "Vascular and cellular targeting for photodynamic therapy," *Crit Rev Eukaryot Gene Expr*, Vol. 16, 2006, pp. 279–305.

[2] Henderson, B. W., and Dougherty, T. J., "How does photodynamic therapy work?," *Photochem Photobiol*, Vol. 55, 1992, pp. 145–157.

[3] Canti, G., De Simone, A., and Korbelik, M., "Photodynamic therapy and the immune system in experimental oncology," *Photochem Photobiol Sci*, Vol. 1, 2002, pp. 79–80.

[4] Siemann, D. W., Chaplin, D. J., and Horsman, M. R., "Vascular-targeting therapies for treatment of malignant disease," *Cancer*, Vol. 100, 2004, pp. 2491–2499.

[5] Fukumura, D., and Jain, R. K., "Tumor microenvironment abnormalities: causes, consequences, and strategies to normalize," *J Cell Biochem*, Vol. 101, 2007, pp. 937–949.

[6] Siemann, D. W., et al., "Differentiation and definition of vascular-targeted therapies," *Clin Cancer Res*, Vol. 11, 2005, pp. 416–420.

[7] Thorpe, P. E., "Vascular targeting agents as cancer therapeutics," *Clin Cancer Res*, Vol. 10, 2004, pp. 415–427.

[8] Gross, S., et al., "Monitoring photodynamic therapy of solid tumors online by BOLD-contrast MRI," Nat Med, Vol. 9, 2003, pp. 1327–1331.

[9] Fingar, V. H., Wieman, T. J., and Haydon, P. S., "The effects of thrombocytopenia on vessel stasis and macromolecular leakage after photodynamic therapy using photofrin," *Photochem Photobiol*, Vol. 66, 1997, pp. 513–517.

[10] Ben-Hur, E., et al., "Photodynamic treatment of red blood cell concentrates for virus inactivation enhances red blood cell aggregation: protection with antioxidants," *Photochem Photobiol*, Vol. 66, 1997, pp. 509–512.

[11] Fingar, V. H., Wieman, T. J., and Doak, K. W., "Role of thromboxane and prostacyclin release on photodynamic therapy-induced tumor destruction," *Cancer Res*, Vol. 50, 1990, pp. 2599–2603.

[12] Reed, M. W., et al., "The microvascular effects of photodynamic therapy: evidence for a possible role of cyclooxygenase products," *Photochem Photobiol*, Vol. 50, 1989, pp. 419–423.

[13] Foster, T. H., et al., "Photosensitized release of von Willebrand factor from cultured human endothelial cells," *Cancer Res*, Vol. 51, 1991, pp. 3261–3266.

[14] Henderson, B. W., et al., "Effects of photodynamic treatment of platelets or endothelial cells in vitro on platelet aggregation," *Photochem Photobiol*, Vol. 56, 1992, pp. 513–521.

[15] Dolmans, D. E., et al., "Vascular accumulation of a novel photosensitizer, MV6401, causes selective thrombosis in tumor vessels after photodynamic therapy," *Cancer Res*, Vol. 62, 2002, pp. 2151–2156.

[16] Fingar, V. H., "Vascular effects of photodynamic therapy," *J Clin Laser Med Surg*, Vol. 14, 1996, pp. 323–328.

[17] Vaupel, P., and Mayer, A., "Hypoxia in cancer: significance and impact on clinical outcome," *Cancer Metastasis Rev*, Vol. 26, 2007, pp. 225–239.

[18] Fingar, V. H., Wieman, T. J., and Doak, K. W., "Changes in tumor interstitial pressure induced by photodynamic therapy," *Photochem Photobiol*, Vol. 53, 1991, pp. 763–768.

[19] Leunig, M., et al., "Photodynamic therapy-induced alterations in interstitial fluid pressure, volume and water content of an amelanotic melanoma in the hamster," *Br J Cancer*, Vol. 69, 1994, pp. 101-103.

[20] Sporn, L. A., and Foster, T. H., "Photofrin and light induces microtubule depolymerization in cultured human endothelial cells," *Cancer Res*, Vol. 52, 1992, pp. 3443–3448.

[21] Chen, B., et al., "Tumor vascular permeabilization by vascular-targeting photosensitization: effects, mechanism, and therapeutic implications," *Clin Cancer Res*, Vol. 12, 2006, pp. 917–923.

[22] Schmidt-Erfurth, U., et al., "Time course and morphology of vascular effects associated with photodynamic therapy," *Ophthalmology*, Vol. 112, 2005, pp. 2061–2069.

[23] Volanti, C., Matroule, J. Y., and Piette, J., "Involvement of oxidative stress in NF-kappaB activation in endothelial cells treated by photodynamic therapy," *Photochem Photobiol*, Vol. 75, 2002, pp. 36–45.

[24] Volanti, C., et al., "Downregulation of ICAM-1 and VCAM-1 expression in endothelial cells treated by photodynamic therapy," *Oncogene*, Vol. 23, 2004, pp. 8649–8658.

[25] Matroule, J. Y., Volanti, C., and Piette, J., "NF-kappaB in photodynamic therapy: discrepancies of a master regulator," *Photochem Photobiol*, Vol. 82, 2006, pp. 1241–1246.

[26] Korbelik, M., Sun, J., and Cecic, I., "Photodynamic therapy-induced cell surface expression and release of heat shock proteins: relevance for tumor response," *Cancer Res*, Vol. 65, 2005, pp. 1018–1026.

[27] Plaks, V., et al., "Homologous adaptation to oxidative stress induced by the photosensitized Pd-bacteriochlorophyll derivative (WST11) in cultured endothelial cells," *J Biol Chem*, Vol. 279, 2004, pp. 45713–45720.

[28] Chen, B., et al., "Combining vascular and cellular targeting regimens enhances the efficacy of photodynamic therapy," *Int J Radiat Oncol Biol Phys*, Vol. 61, 2005, pp. 1216–1226.

[29] Chen, B., Roskams, T., and de Witte, P. A., "Antivascular tumor eradication by hypericin-mediated photodynamic therapy," *Photochem Photobiol*, Vol. 76, 2002, pp. 509–513.

[30] Boucher, Y., and Jain, R. K., "Microvascular pressure is the principal driving force for interstitial hypertension in solid tumors: implications for vascular collapse," *Cancer Res*, Vol. 52, 1992, pp. 5110–5114.

[31] Rofstad, E. K., et al., "Pulmonary and lymph node metastasis is associated with primary tumor interstitial fluid pressure in human melanoma xenografts," *Cancer Res*, Vol. 62, 2002, pp. 661–664.

[32] Hendrickx, N., et al., "Up-regulation of cyclooxygenase-2 and apoptosis resistance by p38 MAPK in hypericin-mediated photodynamic therapy of human cancer cells," *J Biol Chem*, Vol. 278, 2003, pp. 52231–52239.

[33] Hendrickx, N., et al., "Targeted inhibition of p38alpha MAPK suppresses tumor-associated endothelial cell migration in response to hypericin-based photodynamic therapy," *Biochem Biophys Res Commun*, Vol. 337, 2005, pp. 928–935.

[34] Ferrario, A., et al., "Antiangiogenic treatment enhances photodynamic therapy responsiveness in a mouse mammary carcinoma," *Cancer Res*, Vol. 60, 2000, pp. 4066–4069.

[35] Solban, N., et al., "Mechanistic investigation and implications of photodynamic therapy induction of vascular endothelial growth factor in prostate cancer," *Cancer Res*, Vol. 66, 2006, pp. 5633–5640.

[36] Momma, T., et al., "Photodynamic therapy of orthotopic prostate cancer with benzoporphyrin derivative: local control and distant metastasis," *Cancer Res*, Vol. 58, 1998, pp. 5425–5431.

[37] Pinthus, J. H., et al., "Photodynamic therapy for urological malignancies: past to current approaches," *J Urol*, Vol. 175, 2006, pp. 1201–1207.

[38] Birchler, M., et al., "Selective targeting and photocoagulation of ocular angiogenesis mediated by a phage-derived human antibody fragment," *Nat Biotechnol*, Vol. 17, 1999, pp. 984–988.

[39] Tirand, L., et al., "A peptide competing with VEGF165 binding on neuropilin-1 mediates targeting of a chlorin-type photosensitizer and potentiates its photodynamic activity in human endothelial cells," *J Control Release*, Vol. 111, 2006, pp. 153–164.

[40] Ichikawa, K., et al., "Antiangiogenic photodynamic therapy (PDT) by using long-circulating liposomes modified with peptide specific to angiogenic vessels," *Biochim Biophys Acta*, Vol. 1669, 2005, pp. 69–74.

[41] Reddy, G. R., et al., "Vascular targeted nanoparticles for imaging and treatment of brain tumors," *Clin Cancer Res*, Vol. 12, 2006, pp. 6677–6686.

[42] Frochot, C., et al., "Interest of RGD-containing linear or cyclic peptide targeted tetraphenylchlorin as novel photosensitizers for selective photodynamic activity," *Bioorg Chem*, Vol. 35, 2007, pp. 205–220.

[43] Streckyte, G., et al., "Effects of photodynamic therapy in combination with Adriamycin," *Cancer Lett*, Vol. 146, 1999, pp. 73–86.

[44] Ma, L. W., et al., "Enhanced antitumour effect of photodynamic therapy by microtubule inhibitors," *Cancer Lett,* Vol. 109, 1996, pp. 129–139.

[45] Peng, Q., et al., "Antitumor effect of 5-aminolevulinic acid-mediated photodynamic therapy can be enhanced by the use of a low dose of photofrin in human tumor xenografts," *Cancer Res*, Vol. 61, 2001, pp. 5824–5832.

[46] Dolmans, D. E., et al., "Targeting tumor vasculature and cancer cells in orthotopic breast tumor by fractionated photosensitizer dosing photodynamic therapy," *Cancer Res*, Vol. 62, 2002, pp. 4289–4294.

[47] Jain, R. K., "Delivery of molecular medicine to solid tumors: lessons from in vivo imaging of gene expression and function," *J Control Release*, Vol. 74, 2001, pp. 7–25.

[48] Pogue, B. W., et al., "Analysis of sampling volume and tissue heterogeneity on the in vivo detection of fluorescence," *J Biomed Opt*, Vol. 10, 2005, pp. 41206.

[49] Snyder, J. W., et al., "Photodynamic therapy: a means to enhanced drug delivery to tumors," *Cancer Res*, Vol. 63, 2003, pp. 8126–8131.

[50] Ferrario, A., et al., "Cyclooxygenase-2 inhibitor treatment enhances photodynamic therapy-mediated tumor response," *Cancer Res*, Vol. 62, 2002, pp. 3956–3961.

[51] Ferrario, A., and Gomer, C. J., "Avastin enhances photodynamic therapy treatment of Kaposi's sarcoma in a mouse tumor model," *J Environ Pathol Toxicol Oncol*, Vol. 25, 2006, pp. 251–259.

[52] Kosharskyy, B., et al., "A mechanism-based combination therapy reduces local tumor growth and metastasis in an orthotopic model of prostate cancer," *Cancer Res*, Vol. 66, 2006, pp. 10953–10958.

Combination of vascular targeting PDT with combretastatin A4 phosphate

Chong He, Babasola Fateye, Bin Chen*
[a] Department of Pharmaceutical Sciences, Philadelphia College of Pharmacy, University of the Sciences in Philadelphia, Philadelphia, PA, USA 19104

ABSTRACT

Tumor vasculature is an attractive target for cancer therapy due to its accessibility to blood-borne therapeutic agents and the dependence of tumor cells on a functional blood supply for survival and growth. Vascular targeting photodynamic therapy (vPDT) is a novel modality based on the selective laser light activation of photosensitizers localized inside tumor vasculature to shutdown tumor vascular function. Although this vascular targeting therapy is showing great promise for cancer treatment, tumor recurrence has been observed in both preclinical and clinical studies. In this study, we intend to enhance the therapeutic outcome of vascular targeting PDT by combining it with combretastatin A4 phosphate (CA4P), a blood flow inhibitor. We found that the combination of CA4P and vPDT significantly increased endothelial cell apoptosis than each single therapy. Western blot analysis suggests that myosin light chain kinase (MLCK) is a common target of CA4P and vPDT. In a PC-3 prostate tumor model, we found that CA4P was able to greatly enhance tumor response to vPDT. These results demonstrate that CA4P and vPDT can be combined to enhance the therapeutic effect.

Keywords: photodynamic therapy (PDT), tumor vascular targeting, verteporfin, combretastatin, endothelial cells, myosin light chain kinase (MLCK)

1. INTRODUCTION

Photodynamic therapy (PDT) is an established cancer treatment modality, which involves the combination of a photosensitizing compound, light with a wavelength matching the absorption of photosensitizer, and oxygen molecules [1]. Upon absorption of light, photosensitizer molecules are activated from the ground state to the triplet state, which then reacts with oxygen molecules and produces highly reactive oxygen species, mainly singlet oxygen, to induce oxidative damage to the target cells. Currently, PDT is being offered for the treatment of various types of cancer including lung, skin, gastrointestinal tract, head and neck and urological cancers [2] and non-cancer diseases such as age-related macular degeneration (AMD), atherosclerosis, viral or bacterial infections [3]. The mechanism of tumor destruction induced by PDT is complicated, which involves a combined effect of direct photocytotoxicity, vascular damage and immune reactions [2].

To preferentially target blood vessels, vascular targeting PDT (vPDT) is developed based on site-directed delivery of photosensitizing agents to the vascular system, which induces selective vascular functional disruption following light irradiation. Since vasculature-directed photosensitizer delivery can be achieved by either passive or active means, photodynamic vascular targeting can be further divided into passive or active targeting approach [4]. The passive vascular targeting PDT is primarily based on the innate photosensitizer pharmacokinetic property that plasma drug concentration is often high shortly after intravenous administration of a photosensitizer. The time period when photosensitizer is mainly localized within the vasculature provides a temporal window for targeting blood vessels. By contrast, active vascular-targeting PDT seeks to achieve vasculature-directed drug delivery by altering photosensitizer pharmacokinetic property through photosensitizer structure modification or drug formulation into a targeted delivery system [4]. A targeting moiety that has a high affinity to endothelial cell markers or other vessel supporting structures is often used in the photosensitizer modification. The resulting photosensitizer conjugates or delivery system are expected to be selectively accumulated in the targeted blood vessels, leading to a site-specific photosensitization upon light activation.

*b.chen@usp.edu; phone 1 215 596-7481; fax 1 215 895-1161

Liposomal photosensitizer verteporfin (benzoporphyrin derivative monoacid ring A) has been approved by FDA for the treatment of age-related macular degeneration (AMD). We have been using verteporfin to target tumor vasculature. This

is based on the finding that verteporfin is predominantly localized within tumor blood vessels at 15 min after i.v. injection [5], and light delivered at this time induces preferential tumor vascular damage [6]. Effects of verteporfin-PDT on tumor vasculature include vascular permeability increase, thrombus formation and blood flow reduction [6, 7]. The goal of tumor vascular targeting is to induce vascular shutdown, which causes tumor cell death by tissue ischemia [8]. By analyzing tumor blood vessels with different diameter and velocity to vPDT, we found a strong correlation between blood cell velocity and the time taken to reach vascular shutdown after vPDT, suggesting that blood vessels with higher flow rate are more resistant to vPDT-induced vascular shutdown [6]. Based on this result, we hypothesize that tumor vascular response to vPDT can be further enhanced by a pretreatment that decreases tumor blood flow rate. To test this hypothesis, we choose a vascular disrupting agent combretastatin A4 phosphate (CA4P) to modulate tumor blood flow rate to determine whether CA4P in combination with vPDT will enhance tumor response.

2. MATERIALS & METHODS

2.1. Drugs. Verteporfin (benzoporphyrin derivative (BPD) in a lipid-formulation) was obtained from QLT Inc. (Vancouver, Canada) as a gift. A stock saline solution of verteporfin was reconstituted according to the manufacturer's instructions and stored at 4°C in the dark. Vascular disrupting agent combretastatin A4 phosphate (CA4P) was provided by OXiGENE Inc. (Waltham, MA) as a gift. CA4P was dissolved in normal saline and stored at 4°C in the dark.

2.2. Cell culture. SVEC4-10 mouse endothelial cells and PC-3 human prostate cancer cells, both from American Type Culture Collection (Manassas, VA), were maintained in RPMI 1640 with glutamine (Mediatech, Herndon, VA) supplemented with 10% fetal bovine serum (Hyclone, Logan, UT) and 100 units/mL penicillin/streptomycin (Mediatech) at 37°C in a 5% CO_2 incubator.

2.3. Tumor model. Human PC-3 prostate cancer model in male athymic nude mice (NCR, nu/nu) was used in this study. Prostate tumors were induced by subcutaneous injection of about 1 x 10^6 PC-3 cells (in 0.05 ml PBS) in the flank region. PC-3 tumors were used for experiments at 30-35 days after implantation when they reached 5-7 mm in diameter.

2.4. PDT treatment. A diode laser system (High Power Devices Inc., North Brunswick, NJ) with 690 nm wavelength was used for the irradiation of SVEC4-10 cells and PC-3 tumors. The laser was coupled to an optical fiber with 600 μm core diameter for light delivery. A microlens was connected to the end of fiber to achieve homogeneous irradiation. SVEC4-10 cells were incubated with different doses of verteporfin for 15 minutes and exposed to 5 mW/cm^2 intensity of light for 100 seconds. Light intensity was measured by an optical power meter (Thorlabs, Inc., North Newton, NJ). The PC-3 tumors were exposed to external illumination with an irradiance of 50 mW/cm^2 for 800 or 1000 seconds, resulting in a total light dose of 40 or 50 J/cm^2, respectively. Light treatment was performed at 15 min after the injection of verteporfin. Animals were anesthetized with i.p. injection of a mixture of ketamine (120 mg/kg) and xylazine (12 mg/kg) during treatment.

2.5. Cytotoxicity assay. Cytotoxicity after different treatments was determined by CellTiter 96 Aqueous Non-Radioactive Cell Proliferation Assay (Promega), which is based on the conversion of tetrazolium compound into water soluble formazan by dehydrogenase enzymes found in metabolically active cells. SVEC4-10 cells were seeded at a density of 5.0 x 10^3 per well in 96 well plates and allowed to adhere overnight. Cells were then treated with CA4P alone, verteporfin-PDT alone or the combination of CA4P and verteporfin-PDT. For the combination therapy, CA4P was added to the wells at 15-20 min before PDT. At 24h after treatments, the absorbance of each well at the wavelength of 492nm was measured with a microplate reader. Cell viability was estimated by normalizing the absorbance of treated wells to that of control wells. Each experimental condition was assessed in duplicate and experiment was repeated at least 3 times.

2.6. Western blotting analysis. SVEC4-10 cells with about 80% confluence were treated with CA4P alone, verteporfin-PDT alone or the combination of CA4P and verteporfin-PDT. At 24h after treatment, cells were washed thrice with PBS and then lysed on ice with 1X RIPA lysis buffer supplemented with PMSF (1mM), N-ethylmaleimide (2 mM), Pepstatin A (1 μg/ml), NaF (1 mM), $NaPP_i$ (10 μg/ml) and $NaVO_3$ (1mM). Denatured cell lysates were separated by sodium dodecyl sulphate polyacrylamide gel electrophoresis (SDS-PAGE) and then electrophoretically transferred to polyvinylidene fluoride (PVDF) membranes (Millipore). The blots were first incubated with anti-myosin light chain kinase [pS^{1760}], anti-poly ADP ribose polymerase-1 (PARP-1) or anti-glyceraldehyde 3 phosphate dehydrogenase (GAPDH) primary antibody, followed by incubation with horseradish peroxidase-conjugated secondary antibody. After incubating the blots with SuperSignal West Dura extended duration substrate (Thermo Scientific), the immunoreactive bands were visualized and captured with UVP imaging system.

2.7. Tumor regrowth assay. Three dimensional tumor sizes were measured regularly after treatment by caliper, and the tumor volume was calculated using formula $\pi/6 \times$ tumor length $\times$ tumor width $\times$ tumor height. Tumor cure was defined as tumor free for 40 days after treatment. In case of treatment groups where tumor cure was observed, tumor response was presented as Kaplan-Meier curve where the percentage of tumor free animals was plotted against the day after treatment.

2.8. Statistical analysis. Students' two-tailed t-test was used to calculate statistical differences between 2 experimental groups. Log-rank analysis was used to analyze Kaplan-Meier curve. Statistical significance carried out using GraphPad software (GraphPad, San Diego, CA) was accepted at $p < 0.05$.

3. RESULTS & DISCUSSION

CA4P is vascular disrupting agent that is currently under clinical trial for cancer treatment [9]. It has been shown that CA4P is able to induce endothelial cell microtubule depolymerization, thereby causing endothelial cell morphological changes and cell death [10]. In tumor models, CA4P is able to induce rapid blood flow reduction and even vascular shutdown in a dose-dependent manner. However, it has been known that single injection of CA4P is hardly able to achieve significant long-term tumor growth inhibition, suggesting the recovery of tumor perfusion after treatment [11]. Here we intend to determine whether the combination of CA4P and vPDT can enhance tumor response.

We first determined whether the combination therapy led to an enhanced cytotoxicity to endothelial cells. SVEC4-10 mouse endothelial cells were exposed to various concentrations of CA4P for 24h and the cytotoxicity was assessed. Fig 1A indicates that CA4P induces a dose-dependent cytotoxicity in SVEC4-10 cells. CA4P at 6.25 nM induced almost no cell death. We chose this dose for the subsequent combination experiments. Fig 1B shows cytotoxicity profiles of verteporfin-PDT only and the combination of CA4P (6.25 nM) and PDT. It can be seen clearly that pretreatment of SVEC4-10 cells with a low dose of CA4P with little cytotoxicity significantly enhances cytotoxicity of PDT.

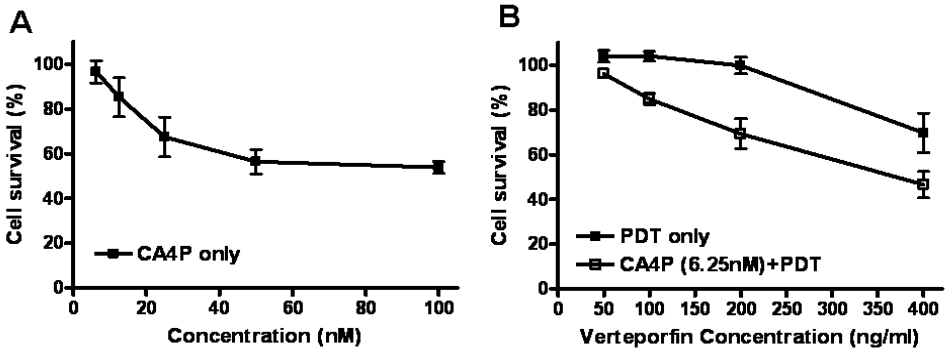

Fig. 1. Effects of CA4P alone, verteporfin-PDT alone and the combination of CA4P and verteporfin-PDT on the survival of SVEC4-10 endothelial cells. **(A)** SVEC4-10 cell survival at 24h after treatment with different doses of CA4P alone. **(B)** SVEC4-10 cell survival at 24h after treatment with verteporfin-PDT alone and the combination of CA4P and verteporfin-PDT. For PDT treatments, cells were incubated with different doses of verteporfin for 15 min followed by 5 mW/cm^2 light treatment for 100 sec. For the combination treatments, 6.25 nM CA4P was added to medium 15-20 min before light treatments. Cell cytotoxicity was determined by CellTiter 96 Aqueous Non-Radioactive Cell Proliferation Assay.

We continued to use western blot to examine the effects of CA4P alone, verteporfin-PDT alone and the combination of CA4P and verteporfin-PDT on endothelial cell death. The cleavage of PARP, a hallmark of cell apoptosis, was determined at 24h after treatment. No significant PARP cleavage was observed after treatment with 6.25 and 25 nM of CA4P (Fig 2). PDT with 400 ng/ml, but not 200 ng/ml, verteporfin induced significant PARP cleave. This result is in agreement with previous reports indicating that verteporfin-PDT induces endothelial cell apoptosis [12, 13]. Importantly, we found that the combination of CA4P and verteporfin-PDT induced more endothelial cell apoptosis, as demonstrated by more PARP cleavage. This enhanced cytotoxicity also can be seen in the change of phosphorylated myosin light chain kinase (p-MLCK) after treatments. P-MLCK has been shown to be important for cell viability by maintaining cell attachment to the substrate [14]. We recently demonstrated that PDT with verteporfin induced a rapid down regulation of p-

MLCK, which partially contributes to PDT-induced cell death (Submitted for publication). As shown in Fig 2, significant down regulation of p-MLCK was observed after PDT alone treatment and p-MLCK bands were barely visible after the combination therapy. Our western blot study indicates that pretreatment of endothelial cells with non-toxic low dose of CA4P significantly synergizes PDT-induced cytotoxicity by inducing more apoptosis.

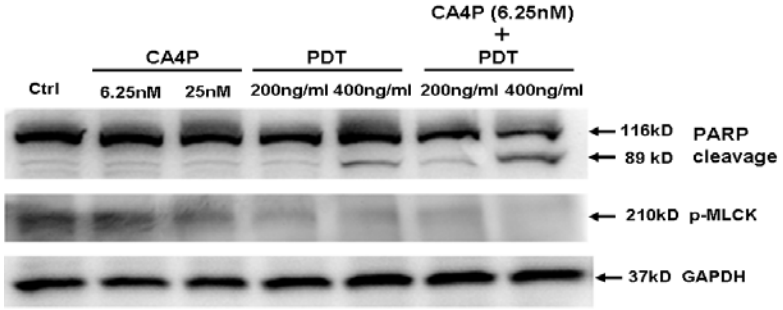

Fig. 2. Western blot analysis of effects of CA4P alone, verteporfin-PDT alone and the combination of CA4P and verteporfin-PDT on PARP cleavage and p-MLCK in SVEC4-10 endothelial cells. SVEC4-10 cells were treated as indicated in the figure. Cells were lysed at 24h after treatment and subjected to western blot analysis as described in the Materials & Methods.

Tumor response to CA4P alone, verteporfin-PDT alone and the combination of CA4P and verteporfin-PDT was assessed in the PC-3 prostate tumor model. As indicated in Fig 3A, neither CA4P treatment alone at the dose of 100 mg/kg nor PDT treatment alone with verteporfin dose of 0.25 mg/kg and light dose of 50 J/cm^2 was able to inhibit tumor growth. However, tumor inhibition became significant when these two sub-lethal treatments were combined. PDT treatment with verteporfin dose of 0.5 mg/kg and light dose of 40 J/cm^2 induced almost 40% tumor cure at 40 days after treatment. Injection of 100 mg/kg dose of CA4P, which was not effective in inhibiting tumor growth, led to 100% tumor cure at 40 days after treatment. These results clearly demonstrated that the combination of CA4P and vascular targeting PDT significantly enhanced tumor response.

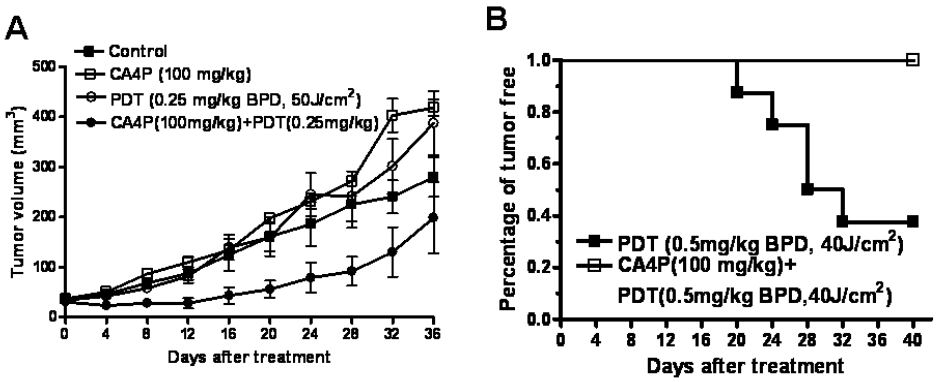

Fig. 3. Effects of CA4P alone, verteporfin-PDT alone and the combination of CA4P and verteporfin-PDT on tumor growth in the PC-3 prostate tumor model. **(A)** Tumor volume as a function of time after i.p. injection of CA4P (100 mg/kg) only, PDT alone with 50 J/cm^2 light treatment at 15 min after i.v. injection of 0.25 dose of verteporfin, and the combination of CA4P (100 mg/kg, i.p.) and PDT with 50 J/cm^2 light treatment at 15 min after i.v. injection of 0.25. Control tumors received no treatment. **(B)** Kaplan-Meier curve showing the percentage of tumor free animals at different time after treatment. In all the combination treatments, CA4P was i.p. injected at about 20 min before light treatment.

In this study, we presented some preliminary results clearly demonstrating that the combination of vascular disrupting agent CA4P and vascular targeting PDT with verteporfin enhanced more endothelial cell killing in vitro and tumor growth inhibition in vivo. However, the mechanism leading to this synergistic effect is still not known. It is possible that the synergistic interaction between these two treatments occurs at both cellular and tissue levels. Our in vitro study indicated that both CA4P and PDT caused down regulation of p-MLCK. Since endothelial cell survival is dependent upon MLCK function, inhibition of MLCK by both CA4P and PDT might lead to enhanced cell killing. More importantly, we believe that the interaction between CA4P and vascular targeting occurs at the tissue level. As mentioned previously, vascular response to vPDT is dependent upon blood vessel flow rate. Pretreatment with CA4P will likely decrease blood flow rate, which makes them more sensitive to the subsequent vPDT treatment. We are currently determining blood flow dynamics after each single treatment and the combination treatments to assess whether the combination therapy leads to more vascular shutdown.

4. CONCLUSIONS

The present study examines the possibility of combining vascular disrupting agent CA4P and vascular targeting PDT with verteporfin to enhance tumor response. Our preliminary results demonstrated that the combination of CA4P and vPDT significantly enhance endothelial cell killing in vitro and tumor response in vivo.

REFERENCES

[1] Dougherty TJ, Gomer CJ, Henderson BW, Jori G, Kessel D, Korbelik M, et al. Photodynamic therapy. *J Natl Cancer Inst* 1998;90(12):889-905.

[2] Dolmans DE, Fukumura D, Jain RK. Photodynamic therapy for cancer. *Nat Rev Cancer* 2003;3(5):380-7.

[3] Detty MR, Gibson SL, Wagner SJ. Current clinical and preclinical photosensitizers for use in photodynamic therapy. *J Med Chem* 2004;47(16):3897-915.

[4] Chen B, Pogue BW, Hoopes PJ, Hasan T. Vascular and cellular targeting for photodynamic therapy. *Crit Rev Eukaryot Gene Expr* 2006;16(4):279-305.

[5] Chen B, Pogue BW, Hoopes PJ, Hasan T. Combining vascular and cellular targeting regimens enhances the efficacy of photodynamic therapy. *Int J Radiat Oncol Biol Phys* 2005;61(4):1216-26.

[6] He C, Agharkar P, Chen B. Intravital microscopic analysis of vascular perfusion and macromolecule extravasation after photodynamic vascular targeting therapy. *Pharm Res* 2008;25(8):1873-80.

[7] Chen B, Pogue BW, Luna JM, Hardman RL, Hoopes PJ, Hasan T. Tumor vascular permeabilization by vascular-targeting photosensitization: effects, mechanism, and therapeutic implications. *Clin Cancer Res* 2006;12(3):917-23.

[8] Brekken RA, Li C, Kumar S. Strategies for vascular targeting in tumors. *Int J Cancer* 2002;100(2):123-30.

[9] Tozer GM, Kanthou C, Baguley BC. Disrupting tumour blood vessels. *Nat Rev Cancer* 2005;5(6):423-35.

[10] Kanthou C, Greco O, Stratford A, Cook I, Knight R, Benzakour O, et al. The tubulin-binding agent combretastatin A-4-phosphate arrests endothelial cells in mitosis and induces mitotic cell death. *Am J Pathol* 2004;165(4):1401-11.

[11] Tozer GM, Kanthou C, Lewis G, Prise VE, Vojnovic B, Hill SA. Tumour vascular disrupting agents: combating treatment resistance. *Br J Radiol* 2008;81 Spec No 1:S12-20.

[12] Granville DJ, Levy JG, Hunt DW. Photodynamic therapy induces caspase-3 activation in HL-60 cells. *Cell Death Differ* 1997;4(7):623-8.

[13] Peng TI, Chang CJ, Guo MJ, Wang YH, Yu JS, Wu HY, et al. Mitochondrion-targeted photosensitizer enhances the photodynamic effect-induced mitochondrial dysfunction and apoptosis. *Ann N Y Acad Sci* 2005;1042:419-28.
[14] Fazal F, Gu L, Ihnatovych I, Han Y, Hu W, Antic N, et al. Inhibiting myosin light chain kinase induces apoptosis in vitro and in vivo. *Mol Cell Biol* 2005;25(14):6259-66.

Myosin light chain kinase as a target of verteporfin-PDT in microvascular endothelial cells.

Running title: MLCK as a target of verteporfin-PDT

Priyanka Agharkar[1], Anastasia Jancina[1], Bin Chen[1*]

[1]Department of Pharmaceutical Sciences, Philadelphia College of Pharmacy, University of the Sciences in Philadelphia, Philadelphia, PA 19104

***Corresponding author:** Bin Chen, PhD., Department of Pharmaceutical Sciences, Philadelphia College of Pharmacy, University of the Sciences in Philadelphia, 600 South 43rd Street, Philadelphia, PA 19104. Tel: 215-596-7481; Fax: 215-895-1161; Email: b.chen@usp.edu.

Key words: photodynamic therapy (PDT), verteporfin, cytoskeleton, myosin light chain kinase (MLCK), endothelial cells

Abstract

Vascular targeting photodynamic therapy (vPDT) is an anti-cancer treatment regimen designed to cause selective and rapid shutdown of the tumor blood vessels which ultimately results in tumor necrosis due to ischemia and extensive hemorrhage. Here we decided to elucidate the causative factors responsible for morphological and functional changes in endothelial cells lining the tumor vasculature following vPDT. By using an in vitro model system consisting of SV40 infected mouse endothelial cells (SVEC4-10) and verteporfin as the photosensitizer, we found that within minutes of treatment with verteporfin PDT, increase in reactive oxygen species production preceded rise in calcium levels. The dose- and time- dependant studies using verteporfin PDT revealed morphological alterations characterized by cell contraction and formation of blebbing morphology. Besides this, we investigated changes in the cytoskeletal protein, myosin light chain kinase and its downstream target myosin light chain II. We found that PDT caused an increase in phosphorylated myosin light chain (MLC), but this event was independent of its upstream modulator, myosin light chain kinase (MLCK) as it was found to be inactivated shortly after PDT. To further investigate the significance of this finding, we performed combination studies of PDT with ML-7 (an MLCK inhibitor) or tumor necrosis factor α (TNFα), an inducer of MLCK. Here we report for the first time that, verteporfin-PDT in combination with ML7 has a more than additive toxic effect on endothelial cells.

Introduction

Photodynamic therapy (PDT) is a minimally invasive therapeutic modality approved for treatment of several types of cancer and non-neoplastic diseases. PDT using the second generation photosensitizer, verteporfin (the lipid formulation of benzoporphyrin derivative monoacid ring A - BPD-MA) is reported to affect the microvasculature of tumor tissue as well as tumor cells. Verteporfin has been approved in 44 countries, including Europe, U.S. and Canada for the treatment of age related macular degeneration, which is caused by a growth of abnormal blood vessels under the central part of the retina or macula. Besides causing direct photocytotoxicity to tumor cells, PDT also induces substantial vascular damage, which contributes significantly to the final treatment outcome. Vascular PDT (vPDT) involves a whole host of signaling cascades, which results in increased vascular permeability and blood flow stasis, ultimately leading to vascular shutdown and tumor necrosis. In order to realize the full potential of vPDT, it is important to explore its effects on vascular function at a molecular level [1, 2, 3].

Till now it is clear that the PDT involves the production of reactive oxygen species which is the central factor for causing tumor cytotoxicity [4]. The formation of reactive oxygen species occurs due to the interaction between the photosensitizer and light in the presence of molecular oxygen. Among the members of reactive oxygen species, singlet oxygen ($^1O_2$), generated due to the photosensitization reaction has unique features as it is the only ROS that is an electronically excited state. As the diffusion radius of $^1O_2$ in water is only about 220nm (after three lifetimes), in a typical PDT setting, it is desirable if the photosensitized singlet oxygen formation occurs at target sub-cellular structures, so as to achieve maximum damage upon illumination [5]. The vascular meshwork surrounding the tumor is a vulnerable to oxidant stress, as at higher concentrations, it is known to impair endothelial barrier function, thereby increasing vascular permeability, and ultimately vascular collapse which is the strategy of vPDT, as this starves the tumor of its nutrient and oxygen supply. Oxidative stress is selective and has specific sub-cellular targets like the actin filament network, actin binding proteins like filamin, intracellular calcium stores [6, 7, 8], molecular chaperones such as glucose regulated protein-78 (Grp78) and heat shock protein 60 (Hsp60) [7]. How oxidative stress translates into cell survival, morphological alterations and apoptosis or necrosis is poorly understood. In this study we investigated the production of ROS by using the molecular probe CM-H_2DCFDA. Our results clearly indicate a robust release of ROS within seconds of verteporfin-PDT treatment as compared to verteporfin only or light only treated cells. ROS produced within cells in this manner, is likely to be the triggering event for multiple effects, in this case leading to impaired endothelial barrier function and cell death.

Free calcium is one of the most versatile and ubiquitous secondary messengers and has been implicated in several signaling processes. Knowing that verteporfin-PDT not only generates ROS but also impacts the regulation of the mitochondria, it is therefore conceivable that calcium homeostasis could be affected. An increase in intracellular calcium levels has been shown to be an early event in the apoptotic pathway [9, 10]. In

order to improve our understanding of the complex interactions between PDT and changes in endothelial cell behavior, we monitored calcium levels after verteporfin-PDT treatment and also modulated calcium release by using $CaCl_2$ or BAPTA. The results suggest that both extracellular and intracellular calcium sources contribute to increases in calcium levels after PDT.

Vascular endothelial cells perform a very critical function by forming a selective barrier between the blood and the surrounding tissues, which is compromised after PDT treatment [1, 2, 17]. In nonmuscle cells, phosphorylation of myosin light chain (MLC) at position serine 19 correlates with changes in shape and stress fiber formation which can lead to barrier dysfunction and increased permeability due to formation of gaps between the cells. It is well established that the phosphorylation of MLC is largely determined by the balance of activities of MLCK and myosin phosphatase [14, 15, 16]. MLC, besides being an important parameter in maintaining endothelial barrier function, represents the complexity of this process as multiple signaling molecules like Ca^{+2}-calmodulin, and protein kinases (CaMKII, PAK, ZIP kinase and MAPK) have been shown to modulate this protein [12].
In vertebrates, myosin light chain kinase (MLCK) exists in two isoforms which are the products of a single genetic locus: a short isoform (108kDa) which is ubiquitous in all adult tissues, with highest amounts in smooth muscle cells (SMC) and a long isoform (210kDa) which is predominantly expressed in SMC and adult cells of non-muscular lineage [11, 12, 14]. MLCK seems to bear a promiscuous nature, since it can participate in the actomyosin contractile response in the cells; it may be involved in the assembly of the microtubular network and also function in the motility response of cells [13]. We investigated the effect of PDT on MLCK and MLC in SVEC4-10 cells and our results show that PDT immediately induces dephosphorylation of MLCK, but the levels of phosphorylated MLC increased significantly above control levels. Furthermore, by using ML7, which is an MLCK inhibitor we found that combination treatment of ML7 with PDT is extremely toxic to endothelial cells and that the levels of phosphorylated MLC correlate with the amount of insult subjected to cells. Our data suggests that MLCK has a unique function involving cell survival and cell death.

The actin cytoskeleton appears to play a critical role in the regulation of the cell's response to apoptotic signals [18]. Now knowing that verteporfin-PDT induces dose and time dependant changes in endothelial cell morphology, we decided to characterize the apoptotic response after PDT. Cleavage of caspase-3 and poly ADP ribose (PARP-1) are classic markers of apoptosis [19, 20], and numerous reports suggest that apoptosis is the major and rapid form of cell death following PDT [7,8, 9, 21]. Of course factors like the choice of photosensitizer and cell line majorly influence the final mode of cell death, as a variety of sub-cellular photosensitizer (PS) localizations and PS induced mechanisms of cellular damage have been reported in different cell lines. We provide evidence that verteporfin PDT induces a dose and time dependant increase in both caspase-3 and PARP-1 cleavage. And when ML-7 was combined with our standard PDT protocol, it further induced caspase-3 and PARP-1 cleavage as compared to TNFα with PDT or PDT alone. In all, we have characterized the early developments occurring at a molecular

level and investigated the behavior of MLCK and MLC in endothelial cells after verteporfin-PDT treatment.

Materials and Methods

Photosensitizer: Verteporfin (benzoporphyrin derivative in a lipid formulation) was obtained from QLT, Inc., as a gift (Vancouver, Canada). A stock solution of verteporfin was reconstituted according to the manufacturer's instructions and stored at 4°C in the dark.

Cell culture: Mouse endothelial cells SVEC4-10 (American Type Culture Collection, Manassas, VA) were maintained in RPMI 1640 with glutamine (Mediatech, Herndon, VA) supplemented with 10% fetal bovine serum (Hyclone, Logan, UT) and 100 units/mL penicillin/streptomycin (Mediatech) at 37°C in a 5% CO_2 incubator.

Photodynamic therapy treatments: A diode laser system (Applied Optronics, South Plainfield, NJ) with 690nm wavelength was used throughout this study for the irradiation of in vitro cultured cells. The light was delivered through an optical fiber (140-Am core diameter). For the in vitro study, SVEC4-10 cells were incubated with 100ng/ml of verteporfin (this dose was used for most of the experiments, unless specified) for 15 minutes and exposed to 5 mW/cm^2 intensity of light for 100 seconds. Light intensity was measured by an optical power meter (Thorlabs, Inc., North Newton, NJ).

Time-lapse microscopy: Briefly, ~2500 cells were plated in 96 well plates. Once cells were confluent, phase contrast images were obtained with a Hamamatsu ORCA-AG CCD monochrome camera connected to a Leica DMI6000B inverted fluorescence microscope and recorded using Simple PCI software (Compix Inc, Cranberry, PA). For assessment of PDT effects, cells were incubated (5% CO_2, 37^{o}C) with verteporfin for 15 minutes in medium containing 2% FBS, after which the cells were irradiated for 100 seconds. Immediately after this, a microscopic field was selected and recorded for at least 40 minutes. Image slices were obtained using NIH Image J Software. At least three experiments were performed for each treatment.

Measurement of intracellular reactive oxygen species: The intracellular ROS production was detected using non-fluorescent compound CM-H_2DCFDA (Invitrogen Corporation, USA). Upon crossing the membrane, the compound undergoes deacetylation by intracellular esterases producing the non-fluorescent CMH_2DCF, which quantitatively reacts with oxygen species inside the cell to produce the highly fluorescent dye CM-DCF. This compound remains trapped within the cell. Confluent cells in 96 well plates were incubated at 37^{o}C for 45 minutes with phosphate buffered saline (PBS) containing 3uM CM-H_2DCFDA in darkness. After washings with PBS, cells were incubated for 15 minutes with 100ng BPD in PBS. Right after this, a microscopic field was selected using a Leica DMI6000B inverted fluorescence microscope with appropriate filter sets for FITC (excitation: 480/40 nm; emission: 527/30 nm) followed by irradiation with red light (690nm) for 100 seconds and visualized during light treatment at the speed of one frame every 4 seconds up to 4-5 minutes. Images were captured with a Hamamatsu ORCA-AG CCD monochrome camera. Image acquisition with appropriate filter setup was controlled by SimplePCI software (Compix Inc, Cranberry, PA). All the following image analyses were performed with the SimplePCI and NIH ImageJ software packages. Approximately 20 cells were assessed for each experiment. At least three

experiments were performed for each treatment. The normalized percentage change in fluorescence intensity (8 bit) for each experiment was recorded and plotted.

Measurement of intracellular Ca^{2}: SVEC 4-10 cells were plated into 96 well plates and cultured to a confluent monolayer. Medium was removed and cells were rinsed twice with phosphate buffered saline. Cells were incubated at 37°C in PBS containing 4mM green fluorescent calcium indicator, fluo4 AM (Invitrogen) for 1h, after which cells were washed twice with PBS followed by 15 minutes incubation with 100ng/ml verteporfin in PBS. The cells were then irradiated with red light (690nm) for 100 seconds and visualized during light treatment at the speed of one frame every 4 seconds up to 4-5 minutes using a Leica DMI6000B inverted fluorescence microscope with appropriate filter sets for FITC channel (excitation: 480/40 nm; emission: 527/30 nm). Images were captured with a Hamamatsu ORCA-AG CCD monochrome camera and image acquisition with appropriate filter setup was controlled by SimplePCI software (Compix Inc, Cranberry, PA). Image analyses were performed with the SimplePCI and NIH ImageJ software packages. Along with photodynamic therapy treatment, some wells were also incubated with PBS containing $CaCl_2$ or BAPTA (Sigma-Aldrich Co.) or verteporfin alone. Approximately 20 cells were assessed for each experiment. At least three experiments were performed for each treatment. The normalized percentage change in fluorescence intensity (8 bit) for each experiment was calculated and plotted.

Cellular cytotoxicity assay: Briefly, SVEC4-10 cells were seeded at a density of 5.0 x 10^{3}/100ul in medium containing 2% FBS in 96 well plates and allowed to adhere overnight. After 24h, cultures were re-fed with fresh media containing various concentrations of ML7 (Sigma) alone, tumor necrosis factor α (Sigma) alone, ML7 in combination with verteporfin-PDT and tumor necrosis factor α (TNF α) in combination with verteporfin-PDT and some wells contained medium without cells, serving as a background. The 96 well plate was then incubated for 24h at 37°C. The number of living cells was measured using an MTS assay. (Celltiter 96 Aqueous MTS, Promega, USA). This colorimetric assay is based on the principle of conversion of yellow colored MTS to aqueous soluble red formazan produced by metabolically active cells. The MTS solution was added to each well and the cells were incubated for 4h at 37°C after which absorbance was measured using a microplate reader at a wavelength of 492nm. Each condition was assessed in duplicates and statistical analysis was performed on data obtained from 3 independent experiments.

Western blotting: Confluent monolayers were obtained by plating cells at a density of 4.0 x 10^{5} /cm^{2} for 3 days. Cells were used between the first and eighth passages. Microvascular endothelial cells (SVEC4-10 cells) were switched from medium containing10% FBS to medium containing 2% FBS on the day of treatment so as to keep the method consistent with the rest of the experiments included in this study. At different time points after photodynamic therapy treatments, the drug containing medium was removed and cells were subsequently washed thrice with PBS and lysed with 1X RIPA lysis buffer on ice. Insoluble material was removed by centrifugation at 15,000 x g for 15 minutes at 4°C. Denatured cell lysates were separated by sodium dodecyl sulphate polyacrylamide gel electrophoresis (SDS-PAGE) and were electrophoretically transferred to polyvinylidene fluoride (PVDF) membranes (Millipore). Membranes were blocked in SuperBlock Blocking buffer 37535 (Pierce) for 1 hr at room temperature. The blots were incubated with anti-smooth muscle myosin light chain kinase [pS^{1760}] phospho-specific

(Invitrogen) (1:250), anti-myosin light chain kinase clone K36 (Sigma) (1:1000), anti-phosphorylated myosin light chain serine 19 (Santa Cruz Biotechnology, Santa Cruz, CA) (1:250), anti-myosin light chain 2 (Cell Signaling) (1:500), anti-caspase3 (Cell Signaling) (1:500), anti-poly ADP ribose (Cell Signaling) (1:500), anti-glyceraldehyde 3 phosphate dehydrogenase (Santa Cruz) (1:1000) in 3% BSA in 1X TBST solution overnight at 4°C. After washes in 1X TBST solution, the blots were incubated with horseradish peroxidase-conjugated goat anti-rabbit IgG antibody (1:1000) or anti-mouse IgG antibody (1:1000) for 90 minutes at room temperature and finally after subsequent washings; the immunoreactive bands were visualized with SuperSignal West Dura Extended duration substrate (ThermoScientific) or ECL (Amersham Biosciences) according to manufacture instructions and exposure to Amersham Hyperfilm ECL. Band intensities were quantified by densitometry and expressed as mean area density using NIH ImageJ software.

Statistical analysis: Students' two-tailed t-test was used to calculate statistical differences between 2 groups and the significance was accepted at $p < 0.05$. Statistical analysis was carried out using GraphPad Prizm 4.0 software (GraphPad, San Diego, CA). All experiments were repeated at least three times to ensure reproducibility.

Results

Verteporfin-PDT induces morphological alterations, ROS generation and changes in intracellular Ca^{2+} concentration in endothelial cells

The cytoskeleton provides the basic infrastructure for regulating cellular shape, rigidity and motility in all cells. Additionally, the endothelial cytoskeleton maintains vascular homeostasis by controlling barrier integrity and permeability changes. Figure 1 shows that untreated control SVEC4-10 cells represent the characteristic flat and polygonal morphology throughout the imaging period. Whereas with 100ng verteporfin-PDT treatment we found that after 20 minutes some cells show a rounded appearance and they stay contracted till 40 minutes. No apparent apoptotic phenotype was observed at this point in time. After 20 minutes of 200ng verteporfin-PDT treatment, loss of flat morphology due to condensation and retraction was seen, thereby leaving gaps between the cells, which remain attached to one another by thin processes, and at 40 minutes some cells fragmented into multiple protrusions (or blebs), which is characteristic of an apoptotic event. PDT treatment using 400ng verteporfin caused a strikingly apoptotic phenotype, as after 20 minutes cells shed their elongated endothelial shape; contact with neighboring cells is interrupted and at 40 minutes most cells finally dissociate into apoptotic bodies. These morphological modifications are crucial during the course of apoptosis. This data shows that PDT treatment mainly causes dose and time dependant increase in apoptotic cell death.

We next evaluated the intracellular ROS formation by fluorescence microscopy in SVEC4-10 cells after verteporfin-PDT by detecting the conversion of non fluorescent compound CM-H_2DCFDA to highly fluorescent dye CM-DCF, which forms after reacting with oxygen species inside the cell. The PDT treated cells showed a rapid and intense generation of ROS within the first minute of red light irradiation followed by a gradual decrease up to 4 minutes. Along with the standard PDT protocol, we included three separate controls to confirm that maximum release of ROS occurred only when

photosensitized cells were irradiated with red light. Our results clearly show that incubating cells with the same verteporfin dose but no irradiation, or irradiation alone without verteporfin, resulted in little or no increase in fluorescence respectively. Likewise even non-photosensitized control cells without irradiation did not generate fluorescence. This result verifies that PDT using verteporfin is capable of causing an immediate and strong production of ROS in endothelial cells.
Changes in $[Ca^{2+}]_i$ during PDT were measured and visualized by fluorescence microscopy using flou4 AM as an indicator. Imaging analysis revealed that verteporfin-PDT alone caused an increase in $[Ca^{2+}]_i$ which then attained a steady phase with elevated $[Ca^{2+}]_i$ levels (Figure 3). This suggests that in the absence of an external calcium source, the surge of Ca^{2+} levels comes from an intracellular calcium store such as the endoplasmic reticulum, mitochondria or other calcium storing cellular organelles. This elevation was inhibited when cells were pre-incubated with intracellular calcium chelator BAPTA, although chelation was not able to entirely abrogate calcium release. Conversely, pre-incubation of cells with $CaCl_2$ followed by PDT treatment, resulted in a higher increase in calcium levels as compared to both verteporfin-PDT alone or verteporfin-PDT with BAPTA. As far as the two controls included in this experiment are concerned, treatment with the same verteporfin dose lacking irradiation had little effect on $[Ca^{2+}]_i$ levels and untreated control cells showed no increase in $[Ca^{2+}]_i$ levels. This indicates that PDT induced rise of $[Ca^{2+}]_i$ in the absence of any extracellular calcium is attributed majorly to internal calcium stores.

PDT induces dephosphorylation of MLCK but upregulates phosphorylated MLC levels
Based on our first phase of experimental findings which show that PDT disrupts cellular homeostasis by triggering the release of potential signaling molecules like ROS and Ca^{2+}, we hypothesized that PDT induced endothelial cell morphological change could involve the activation of cytoskeletal contraction regulating protein such as myosin light chain kinase (MLCK). We focused on the effects of verteporfin-PDT on the longer isoform of MLCK (or endothelial MLCK) which is predominantly found in non muscle cells and is known to preferably phosphorylate its downstream target MLC on the Ser-19 site [12].

Overall, the results (Figure 4A) show a decrease in phosphorylated MLCK after PDT, especially for 100ng and 200ng verteporfin at both 1hr and 4hr, though it appears as if cells try to recover from PDT induced damage by upregulating MLCK at 24hr. This recovery could be attributed to MLCK acting as a survival signal. Conversely, the failure to recover which was seen for 400ng 24hr is likely due to increased cell death at this dose and time point. A dose dependant decrease in total MLCK suggests that a progressive increase in protein damage and possibly DNA damage occurs in PDT treated SVEC4-10 cells. An important observation which could provide clues as to why we see MLCK dephosphorylation is that this event coincides with accumulation of caspase-3 cleavage product (Figure 5). Also, a concomitant increase in PARP-1 cleavage product was also found (Figure 5). In control non-PDT treated cells low basal levels of MLC phosphorylation was detected which is in accordance with their elongated morphology (Figure 4B). For all verteporfin doses and time points after PDT an increase in phosphorylated MLC was observed over control levels. This suggests that phosphorylation of MLC is a crucial event occurring in progressively contracting or

blebbing cells; because there is a marked increase in phosphorylated MLC levels in 400ng – 4hr as compared to 100ng – 4hr or 200ng – 4hr. A transient decline in levels of phosphorylated MLC was seen at 200ng-4hr and 24hr, but the levels were still more than control. Also, there is no significant further increase in phosphorylated MLC at 400ng-24hr as compared to 400ng-4hr, which means that cells have reached their maximum ability to phosphorylate this protein, probably because after 24hr, a large population of cells would be in the final stages of cell death. The total levels of MLC remain unaffected for the most part except at 24 hr time points for 100ng and 200ng verteporfin-PDT, an increase in total MLC was observed, suggesting that 24hr allows sufficient time for significant resynthesis of this protein. A decline in total MLC levels was seen for 400ng verteporfin-PDT, possibly because a large population of cells are damaged at this point in time. The data provides evidence that MLC phosphorylation is independent of MLCK phosphorylation and that apoptotic cell blebbing is characterized by an increase in phosphorylation of MLC.

PDT in combination with ML7 is severely toxic to endothelial cells

Owing to the unexpected effect of PDT on MLCK, we extended our studies to investigate whether maintenance of MLCK was important for cell survival after verteporfin-PDT. By using three different doses of ML7 (an MLCK inhibitor which is known to inhibit endothelial MLCK by interacting with the catalytic and myosin binding domain of the enzyme) in combination with a single verteporfin-PDT dose, we have shown for the first time that ML-7 in combination with PDT, especially 20uM ML-7 with PDT certainly displayed the most dramatic toxic effect (approximately 90% cell death) on endothelial cells as compared to any other treatment included in this experiment (Figure 6). We used TNF α, which is known to induce MLCK [40], as a comparative measure so as to determine whether induction of MLCK would confer protection to endothelial cells. Our results indicate that TNF α alone (10ng, 20ng and 40ng) caused approximately 10% cell death and TNF α (10ng, 20ng and 40ng) in combination with PDT (approximately 25% cell death) did not cause any significant increase in endothelial cell death as compared to PDT alone.

In Figure 7A and Figure 7B, when only TNFα (20ng and 40ng) was added, we observed an expected increase in phosphorylated MLCK and MLC levels as compared to control. This linkage is in agreement with many studies [40, 41]. But when verteporfin-PDT was combined with TNFα (20ng or 40ng) the levels of phosphorylated MLCK reduced as compared to TNFα treatment alone. Also, an increase in levels of phosphorylated MLC (Figure 7B) and increases in caspase-3 and PARP-1 cleavage products (Figure 8) was seen for this combination treatment as compared to TNFα treatment alone. These western blot results (Figure 8) are in line with the cytotoxicity results (Figure 6) confirming the finding that combination treatment of TNFα with PDT causes more endothelial cell apoptosis as compared to cells treated with TNFα alone.

10uM ML7 with PDT treatment which caused approximately 50% cell death (Figure 6) resulted in a slight reduction in levels of phosphorylated MLCK (Figure 7A) and a greater increase in phosphorylated MLC levels (Figure 7B) as compared to 10uM ML7 only treated cells which caused approximately 10% cell death (Figure 6). The increase in phosphorylated MLC seen for 10uM ML7 with PDT indicates that cells need to phosphorylate MLC to remain contracted or maintain 'blebbed' morphology. Overall a

greater decrease in phosphorylated MLCK levels was noticed with the ML7-PDT combination protocol as compared to ML7 treatment alone (Figure 7A) which suggests that MLCK plays a role in cell survival. 20uM ML7 with PDT resulted in acute cytotoxicity as compared to 20uM ML7 treatment alone (Figure 6) and it was only for this particular combination condition that we did not see an increase of phosphorylated MLC levels (Figure 7B). This can be attributed to the enhanced cell death induced by this treatment, which explains the sharp decline in phosphorylated MLC. As seen in Figure 8, the combination treatment of ML7 (10uM and 20uM) with PDT resulted in both caspase-3 and PARP-1 cleavage as compared to ML7 treatment alone (10uM and 20uM). Lack of caspase-3 cleavage but concomitant accumulation PARP-1 cleavage product for 20uM with PDT implies that ML7 does activate the apoptotic pathway but indicates a possible involvement of other caspases.

Discussion

It has been well established that PDT damages the tumor vasculature and interrupts endothelial cell homeostasis by causing vessel constriction and disrupting endothelial barrier function, which then progresses to hemorrhage and release of clotting factors finally resulting in thrombus formation and blood flow stasis [2, 22, 23, 24]. Considering that this mode of vascular targeting plays a big role in determining the final treatment outcome, a detailed map of signaling events leading to the aforementioned endothelial cell modifications has not yet been elucidated. Since most reports indicate that changes in cell morphology is one of the earliest events after PDT mediated damage [21-25], presumably leading to vessel constriction, we decided to decipher the molecular effects of PDT and the resultant changes in endothelial cell morphology particularly involving the major cytoskeletal protein MLCK.

The data presented in this study demonstrate that progressive damage to endothelial cells using increasing verteporfin doses (as seen in Figure 1) indicates the enhanced sensitivity of these cells to increase in PDT mediated insult. A quick change in morphology characterized by cell rounding and blebbing and especially higher doses causing apoptotic protrusions was seen. These morphological aberrations correlate with in vivo findings showing that vascular-PDT can either be exploited to enhance drug delivery to tumors due to the pronounced endothelial gap formation thereby increasing vascular permeability [24, 28] or specifically target the tumor vasculature itself using combination therapies [2, 29].

Next, we decided to characterize the release of ROS and calcium in endothelial cells. We found that verteporfin-PDT lead to rapid increases in ROS production in endothelial cells (Figure 2). Peak ROS formation was achieved during the fist minute of red light irradiation itself, indicating that this event is the earliest tangible outcome after PDT. The choice of dose and photosensitizer has been shown to affect the extent and mode of cell death which correlated with the amounts of ROS production [26, 27]. This indicates that by manipulating the amounts of ROS produced, it could be possible to optimize and predict PDT efficiency [4]. Besides ROS being an important parameter involved with PDT, calcium has also been shown to be another contributor in the signaling mechanisms

related to PDT [9, 30]. Our findings clearly indicate that release of ROS occurs before calcium release (Figure 2 and Figure 3). PDT induced calcium release has been shown before in various cell lines utilizing several photosensitizers [8, 9, 30, 31]. Our results confirm that in SVEC4-10 cells, a rise in intracellular calcium occurs after PDT and a further increase in calcium levels was seen with PDT in the presence of extracellular calcium (Figure 3). When we used BAPTA, which is an intracellular calcium chelator, we found that increasing the concentration of BAPTA affected endothelial cell morphology, indicating that cells were stressed due to high amounts of BAPTA. Due to this effect, we decided not to further increase BAPTA concentration. Hence the concentration we used was presumably not sufficient enough to chelate the intracellular calcium, accounting for the slight increase in calcium release after PDT. But this increase was much less as compared to the other two conditions using PDT with $CaCl_2$ and PDT alone, which means that calcium release after PDT comes majorly from intracellular sources.

Alterations in calcium homeostasis along with intracellular production of ROS are the main effects caused by PDT, both of which are responsible for setting off a chain of signaling events leading to multiple outcomes in a single cell ranging from cell survival to cell death. The early signs of a cell's response to toxic stressors are identified by changes in its morphology, and since we found dramatic cytoskeletal modifications in endothelial cells with increasing doses of PDT (Figure 1), we decided to further investigate the morphology associated response. The events related to cytoskeletal changes after verteporfin-PDT involving MLCK has not been studied before. To our knowledge, our report is the first to demonstrate a disassociation between phosphorylation of MLCK and phosphorylation of MLC after verteporfin-PDT. However, we also found that the decrease in phosphorylated MLCK levels correlated with the accumulation of caspase-3 cleavage product (Figure 4 and Figure 5). Petrache et al [32] demonstrated that in bovine pulmonary artery endothelial cells, both MLCK isoforms serve as targets for caspase-3 cleavage, thereby uncovering a critical role of MLCK in apoptotic signaling. A similar study also reported that caspase-3 cleaves myosin heavy chain and vimentin, the latter being an intermediate filaments (IF's) protein [33]. Likewise several cytoskeletal proteins have been identified as substrates for caspase-3. These events are responsible for cytoskeletal dysfunction and remodeling during the course of apoptosis [18]. Furthermore, a dose dependent increase in cytotoxicity was found for all ML7 doses (5uM, 10uM and 20uM) in combination with PDT as compared to ML7 treatment alone (5uM, 10uM and 20uM) (Figure 6). On the contrary, inducing MLCK by using TNFα or the combination treatment of verteporfin-PDT with TNFα, did not generate the cell death profile which was observed with 20uM ML7 alone or 20uM ML7 with PDT. Inhibition of MLCK expression via antisense techniques has been reported to cause cell rounding and decreased cell proliferation [34]. Also, the maintenance of MLCK has been shown to play an important role in cell survival [35]. In all, our study reveals that MLCK is clearly downregulated after verteporfin-PDT and that combination therapy of PDT and ML7, which aims at further inhibition of MLCK, caused a pronounced enhancement in cytotoxicity of SVEC4-10 cells, which strongly suggests that this protein plays an important role in endothelial cell survival.

We also found that irrespective of MLCK dephosphorylation, its downstream target MLC was phosphorylated in a dose and time dependant fashion after verteporfin-PDT. Although MLCK induced MLC phosphorylation has been largely implicated in cell contraction, there exists conflicting reports in literature regarding the phosphorylation state of both these proteins during the apoptotic response [36, 37, 38, 39]. This signifies the cell specific nature of physiological responses to various drugs. Our phase imaging studies (Figure 1) which clearly show progressive rounding, contraction and blebbing of endothelial cells match with the enhanced MLC phosphorylation (Figure 4B), which leads us to conclude that MLC is not only needed for cells to contract at lower verteporfin doses but is also essential to maintain the blebbing state of the cell at higher doses (400ng verteporfin), where the strongest increase in MLC phosphorylation over control was observed. But once cells were subjected to the most toxic combination of 20uM ML7 with PDT, MLC phosphorylation levels decreased significantly (Figure 7B), which means that with exceedingly harsh treatment, endothelial cells loose their ability to phosphorylate MLC. We therefore conclude that phosphorylation of MLC, besides being a mandatory outcome following PDT induced cellular stress, is indeed a transient, time dependent and characteristic event during endothelial cell apoptosis mediated by verteporfin-PDT.

Lack of phosphorylation of MLCK in our study leads us to speculate the possible involvement of Rho kinase which is also known to indirectly phosphorylate MLC at the Ser 19 site by inhibiting myosin phosphatase [15]. Further validation of this particular criterion may lead to a better understanding as to why cells depend on multiple kinases to phosphorylate a single protein. In summary we have characterized molecular effectors like ROS and calcium, which are released shortly after verteporfin PDT treatment in endothelial cells. Besides we have shown how alterations in MLCK affect cell survival and also demonstrated the significance of MLC phosphorylation in endothelial cell apoptosis after verteporfin-PDT. It is important to investigate how vascular PDT orchestrates microvascular damage at the molecular level such that future work in this field may lead to the discovery of novel targets which will help strategize combination therapies to treat cancer.

References

1. Bin Chen, Curtis Crane, Chong He, David Gondek, Priyanka Agharkar, Mark Savellano, P. Jack Hoopes, Brian W. Pogue et al. Disparity between prostate tumor interior versus peripheral vasculature in response to verteporfin mediated vascular targeting therapy. Int. J. Cancer 2008,123:695-701

2. Chen B, Pogue BW, Hoopes PJ, Hasan T. Vascular and cellular targeting for photodynamic therapy. Crit Rev Eukaryot Gene Expr 2006,16:279-305

3. Bin Chen, Chong He, Peter de Witte, P. Jack Hoopes, Tayyaba Hasan and Brian W. Pogue. Vascular targeting in photodynamic therapy Book Chapter 9; 179-191.

4. Junkoh Yamamoto, Seiji Yamamoto, Toru Hirano, Shaoyi Li, Massayo Koide, Eiji Kohno, Mitsuo Okada, Chikanori Inenaga, Tsutomu Tokuyama, Naoki Yokota, Susumu Terakawa and Hiroki Namba. Monitoring of singlet oxygen is useful for

predicting the photodynamic effects in the treatment for experimental glioma. Cancer Therapy: Preclinical 2006,12(23):7132-7139

5. Robert W. Redmond and Irene E. Kochevar. Spatially resolved cellular responses to singlet oxygen. Photochemistry and Photobiology 2006,82:1178-1186

6. Hazel Lum and Kenneth A. Roebuck. Oxidant stress and endothelial cell dysfunction. Am J Physiol Cell Physiol 2001,280:719-741

7. B Magi, A Ettorre, S Liberatori, L Bini, M Andreassi, S Frosali, P Neri, V Pallini and A Di Stefano. Selectivity of protein carbonylation in the apoptotic response to oxidative stress associated with photodynamic therapy: a cell and proteomic investigation. Cell Death and Differentiation 2004,11:842-852

8. Zhongbing Lu, Yi Tao, Zhixiang Zhou, Junjing Zhang, Cong Li, Lingcheng Ou, Baolu Zhao. Mitochondrial reactive oxygen species and nitric oxide-mediated cancer cell apoptosis in 2-butylamino-2-demethoxyhypocrellin B photodynamic treatement. Free Radical Biology and Medicine 2006,41:1590-1605

9. Angelika Ruck, Klaus Heckelsmiller, Roland Kaufmann, Nili Grossman, Elke Haseroth and Nermin Akgun. Light induced apoptosis involves a defined sequence of cytoplasmic and nuclear calcium release in $AlPcS_4$-photosensitized rat bladder RR1022 epithelial cells. Photochemistry and Photobiology 2000,72(2):210-216

10. Scott A. Oakes, Joseph T. Opferman, Tullio Pozzan, Stanley J. Korsmeyer, Luca Scorrano. Regulation of endoplasmic reticulum Ca^{2+} dynamics by proapoptotic BCL-2 family members. Biochemical Pharmacology 2003,66:1335-1340

11. Patrick Olhmann, Angela Tesse, Cecile Loichot, Hantamalala Ralay Ranaivo, Gerald Roul, Claude Phillipe, D. Martin Watterson, Jacques Haiech, Ramaroson Adriantsitohaina. Deletion of MLCK 210 induces subtle changes in vascular reactivity but does not affect cardiac function. Am J Physiol Heart Circ Physiol 2005,58:H2342-H2349

12. T. Borbiev, J. G. N. Garcia and A. D Verin. Role of phosphorylation of myosin and actin binding proteins in thrombin induced permeability of endothelial cells. Russian Journal of Bioorganic chemistry 2003,29:464-470

13. Dmitry S. Kudryashov, Olga V. Stepanova, Elena L. Vilitkevich, Tatyana A. Nikonenko, Elena S. Nadezhdina, Nina A. Shanina, Thomas J. Lukas, Linda J. Van Eldik, D. Martin Watterson, and Vladimir P. Shirinsky. Myosin light chain kinase (210 kDa) is a potential cytoskeleton integrator through its unique N-terminal domain. Experimental Cell Research 2004,298:407-417

14. Kristine E. Kamm and James T. Stull. Dedicated myosin light chain kinases with diverse cellular functions. The Journal of Biological Chemistry 2001,276(7):4527–4530

15. Michael Sebbagh, Claire Renvoize, Jocelyne Hamelin, Nicole Riche, Jacques Bertoglio and Jacqueline Breard. Caspase-3 mediated cleavage of ROCK I induces MLC phosphorylation and apoptotic membrane blebbing. Nature Cell Biology 2001,3(4):345-52.

16. Hazel Lum and Asrar B. Malik. Mechanisms of increased endothelial permeability. Can. J. Physiol. Pharmacol 1996,74;787-800

17. Gianfranco Bazzoni and Elisabetta Dejana. Endothelial cell to cell junctions: Molecular organization and role in vascular homeostasis. Physiol Rev. 2004,84;869-901.

18. Jacqueline Breard et al. Cytoskeleton and apoptosis. Biochemical Pharmacology, 2008.

19. Douglas Green and Guido Kroemer. The central executioners of apoptosis: caspases or mitochondria? Trends in Cell biology 1999,8(7);267-271

20. C. Soldani and A. I. Scovassi. Poly(ADP-ribose) polymerase-1 cleavage during apoptosis: An update Apoptosis 2002; **7**: 321–328

21. Brett W. Engbrecht, Chandrakala Menon, Alexander V. Kachur, Stephen M. Hahn and Douglas L. Fraker. Photofrin mediated PDT induces vascular occlusion and apoptosis in a human sarcoma xenograft model. Cancer research 1999,59:4334-4342

22. Thomas H. Foster, Melissa C. Primavera, Victor J. Marder, Russell Hilf and Lee Ann Sporn. Photosensitized release of von Willebrand factor from cultured human endothelial cells. Cancer Research 1991;51:3261-3266

23. Victor H. Fingar, T. Jeffery Wieman, Sandra A. Wiehle and Patricia B. Cerrito. The role of microvascular damage in photodynamic therapy: The effect of treatment on vessel constriction, permeability, and leukocyte adhesion. Cancer Research 1992;52:4914-4921

24. Bin Chen, Brian Pogue, Jorge M. Luna, Tayyaba Hasan et al. Tumor vascular permeabilization by vascular targeting photosensitization: Effects, Mechanisms and therapeutic implications. Clin Cancer Res 2006;12(3):917-923

25. Reed MW, Wieman TJ, Schuschke DA, Tseng MT and Miller FN. A comparison of the effects of photodynamic therapy on normal and tumor blood vessels in the rat microcirculation. Radiat Res 1989;119(3):542-52

26. Sonja Radakovic-Fijan, Klemens Rappersberger, Adrian Tanew, Herbert Honigsmann and Bernhard Ortel. Ultrastructural Changes in PAM cells after PDT with delta ALA induced porphyrins or photosan. The Journal of Investigative Dermatology 1999;112:264-270

27. H. Kolarova, R. Bajgar, K. Tomankova, P. Nevrelova and J. Mosinger. Comparison of sensitizers by detecting reactive oxygen species after photodynamic reaction in vitro. Toxicology in Vitro 2007;21:1287-1291

28. John W. Sydner, William R. Green, David A. Bellnier, Lurine Vaughan and Barbara Henderson. Photodynamic Therapy: A means to enhanced drug delivery to tumors. Cancer Research 2003;63:8126-8131

29. Sarika Verma, Gregory M. Watt, Zhiming Mai and Tayyaba Hasan. Strategies for enhanced photodynamic therapy effects. Photochemistry and Photobiology. 2007;83:996-1005.

30. Zheng JH, Shi D, Zhao Y and Chen ZL. Role of calcium signal and protective mechanism of colon cancer cell line SW480 in response to 5-aminolevulinic acid-photodynamic therapy. Ai Zheng 2006;25(6):683-8

31. Xin Hong, Feng Jiang, Steven N. Kalkanis, Zheng Gang Zhang, Xuepeng Zhang, Xuguang Zheng, Hao Jiang and Michael Chopp. Intracellular free calcium mediates glioma cell detachment and cytotoxicity after photodynamic therapy. Lasers Med Sci 2009 Feb 7

32. Irina Petrache, Konstantin Birukov, Ari L. Zaiman, Michael T. Crow, Haiteng Deng, Raj Wadgaonkar, Lewis H. Romer and Joe G. N. Garcia. Caspase dependant cleavage of MLCK is involved in TNF alpha mediated bovine pulmonary endothelial cell apoptosis. The FASEB Journal 2003;17:407-416

33. N. Suarez-Huerta, R. Lecocq, R. Mosselmans, P. Galand, J. E. Dumont and B. Robaye. Myosin heavy chain degradation during apoptosis in endothelial cells. Cell Prolif 2000;33:101-114

34. Michael O. Shoemaker, Wai Lau, Rebecca L. Shattuck, Ann P. Kwiatkowski, Paul E. Matrisian, Luis Guerra-Santos, Emily Wilson, Thomas J. Lukas, Linda J. Van Eldik, and D. Martin Watterson. Use of DNA sequence and mutant analyses and antisense oligodeoxynucleotides to examine the molecular basis of nonmuscle myosin light chain kinase autoinhibition, calmodulin recognition, and activity. The Journal of Cell Biology, 1990;111:1107-1125

35. Laureen E. Connell and David M. Helfman. Myosin light chain kinase plays a role in the regulation of epithelial cell survival. Journal of Cell Science 2005;119:2269-2281

36. Jason C. Mills, Nicole L. Stone, Joseph Erhardt, and Randall N. Pittman. Apoptotic membrane blebbing is regulated by myosin light chain phosphorylation. The Journal of Cell Biology, 1998;140(3):627–636

37. Daniel R. Croft, Mathew L. Coleman, Shuixing Li, David Robertson, Teresa Sullivan, Colin L. Stewart and Michael F. Olson. Actin-myosin–based contraction is responsible for apoptotic nuclear disintegration. The Journal of Cell Biology, 2005;168(2):245–255

38. Fabeha Fazal, Lianzhi Gu, Ivanna Ihnatovych, YooJeong Han, WenYang Hu, Nenad Antic, Fernando Carreira, James F. Blomquist, Thomas J. Hope, David S. Ucker, and Primal de Lanerolle. Inhibiting myosin light chain kinase induces apoptosis in vitro and in vivo. Molecular and cellular biology, 2005;25(14):6259–6266

39. Lian-Zhi Gu, Wen-Yang Hu, Nenad Antic, Rajendra Mehta, Jerrold R. Turner and Primal de Lanerolle. Inhibiting myosin light chain kinase retards the growth of mammary and prostate cancer cells. European Journal of Cancer, 2006;42:948-957

40. Stephanie A. Blair, Sunanda V. Kane, Daniel R. Clayburgh and Jerrold R. Turner. Epithelial myosin light chain kinase activity expression and activity are upregulated in inflammatory bowel disease. Laboratory Investigation, 2006;86:191-201

41. Thomas Y. Ma, Michel A. Boivin, Dongmei Ye, Ali Pedram and Hamid M. Said. Mechanism of TNF-a modulation of Caco-2 intestinal epithelial tight junction barrier: role of myosin light chain kinase protein expression. Am J Physiol Gastrointest Liver Physiol 2005;288:422-430.

Legend

Figure 1. Changes in morphology of endothelial cells treated with PDT were observed using phase contrast microscopy. SVEC4-10 cells were grown in 96-well plates and incubated with the indicated concentrations of verteporfin for 15 minutes followed by 100 second red light illumination (690nm). Time lapse series of phase micrographs for each of the four indicated treatments were taken once every minute for a total duration of 40 minutes. Each panel shows a representative endothelial cell monolayer for the indicated time points from three experiments. Control cells show the typical shape of adherent SVEC4-10 cells. 100ng/ml verteporfin treated cells appear similar to control cells but some show a rounded morphology after 20 minutes. 200ng/ml verteporfin treated cells show more pronounced rounding and onset of blebbing. Almost all cells

show blebbing morphology after 20 minutes and some undergo apoptosis within 40 minutes of 400ng/ml verteporfin-PDT. Scale bar = 40um.

Figure 2. Verteporfin-PDT significantly induces formation of intracellular ROS. All conditions included in this experiment were carried out on confluent SVEC4-10 cells and each indicated treatment condition was carried out in PBS only. The rate of ROS production was calculated from appropriate selection of regions of interest (ROI's) of cells for the entire imaging period. Data represent normalized average of total CM-DCF fluorescence expressed as a percentage of fluorescence before irradiation. Each value represents mean ± S.E. from 3 independent experiments.

Figure 3. Increase in intracellular calcium levels as a function of time after verteporfin-PDT. All conditions included in this experiment were carried out on confluent SVEC4-10 cells and in PBS only in order to avoid the interference of external calcium sources. Cells were incubated with BAPTA (40uM) for 1h prior to verteporfin treatment. $CaCl_2$ (0.1ng/ml) solution was added along with verteporfin during the 15 minute incubation period. Suitable regions of interest were chosen from the first field obtained at zero time. Keeping these ROI's constant throughout the image stack the rate of calcium release was calculated for the total imaging period. Values represent normalized change in fluorescence intensity expressed as percentage of fluorescence before photodynamic treatment. Each value represents mean ± S.E. from 3 independent experiments.

Figure 4. Phosphorylation of MLC is independent of MLCK phosphorylation after verteporfin-PDT. SVEC4-10 cells were either left untreated (control) or incubated with the indicated doses of verteporfin for 15 minutes followed by 100 s of red light irradiation (690nm) and then lysed in RIPA buffer after 1h, 4h and 24h as shown. A: Total cell lysate was used for Western blotting. After detecting phosphorylated MLCK the blot was stripped with Restore Western Blot Stripping Buffer (Pierce, Rockford, IL) according to the manufacture instructions and reprobed for total MLCK. B: The bands from *A* were quantified by scanning densitometry and the ratio of phosphorylated MLCK to total MLCK was calculated. Bars represent mean densitometric values (mean ± S.E.) from three independent experiments. C: Similar experiments were performed as described in *A* where MLC phosphorylated at Ser19 and total MLC were detected. D. Band quantification method was same as *B*. Ratio of phosphorylated MLC (Ser19) to total MLC was calculated and represented as bars (mean ± S.E.) from three independent experiments. $*P < 0.05$ vs. control. *A and C* are representative Western blots.

Figure 5. Verteporfin-PDT induces a time and dose dependent increase in caspase-3 and PARP-1 cleavage. Western blots of whole cell lysates from untreated (control) and verteporfin-PDT treated (100ng/ml, 200ng/ml and 400ng/ml) SVEC4-10 cells for the indicated time points showed A: Cleavage of caspase-3 progressively increases after PDT. B: Similar trend found in *A* is also observed for cleavage of PARP-1 C: Glyceraldehyde-3-phosphate dehydrogenase (GAPDH) represents the loading control.

Figure 6. Analysis of SVEC4-10 cell survival after photodynamic therapy utilizing verteporfin (100ng/ml) in combination with the indicated doses of either ML7 or TNFα.

Cell viability was determined by measuring the activity of living cells using MTS as described in materials and methods. The total yield of the MTS product by the control untreated cells was set as 100%. Values represent mean ± S.E. from 3 independents experiments. $^{+++}P < 0.05$ vs. ML7 5uM with PDT; $^{++}P < 0.05$ vs. ML7 10uM with PDT; $^{+}P < 0.05$ vs. ML7 20uM with PDT; $^{***}P < 0.05$ vs. TNFα 10ng with PDT $^{**}P < 0.05$ vs. TNFα 20ng with PDT and $^{*}P < 0.05$ vs. TNFα 40ng with PDT.

Figure 7. Changes in phosphorylated MLCK and phosphorylated MLC levels after verteporfin-PDT in combination with either ML7 or TNFα in endothelial cells. SVEC4-10 cells were left untreated (control) or treated with only 100ng verteporfin-PDT only or treated with the indicated doses of ML7 or TNFα alone or pre-treated with the indicated doses of ML7 (30 min) or TNFα (1h) following treatment with 100ng/ml verteporfin-PDT. Whole cell lysates were obtained after 24h. The rest of the method involving detection and quantification was the same as previously explained for Figure 4. $^{\#}P < 0.05$ vs. control; $^{+}P < 0.05$ vs. ML7 10uM with PDT and $^{++}P < 0.05$ vs. ML7 20uM with PDT; $^{**}P < 0.05$ vs. TNFα 20ng with PDT and $^{*}P < 0.05$ vs. TNFα 40ng with PDT.

Figure 8. Effects of combination treatment involving either ML7 or TNFα with verteporfin-PDT on the apoptotic response in SVEC4-10 cells. Total cell lysates were obtained after 24h lysis of the indicated treatments and doses. A: Significant capsase-3 cleavage was observed for only those treatment conditions involving PDT. B: PARP-1 cleavage was seen for all treatment conditions involving PDT and also for 20uM ML7 only. C: GAPDH serves as a loading control.